

**STUDY ON ENHANCED PHOTOCURRENT PROPERTIES  
AT DYE/GOLD NANOPARTICLES LOADED  $\text{TiO}_2$  THIN FILMS  
ON METALLIC GRATINGS**

**HATHAITHIP NINSONTI**

**DOCTORAL PROGRAM IN ELECTRICAL AND INFORMATION ENGINEERING  
GRADUATE SCHOOL OF SCIENCE AND TECHNOLOGY  
NIIGATA UNIVERSITY**

## **ACKNOWLEDGEMENT**

First of all, I would like to thank to Assoc. Prof. Dr. Sukon Phanichphant and Assoc. Prof. Dr. Akira Baba for their kind supervision, helpful guidance, corrections and support throughout the course of this research project.

I would also like to thank, Prof. Dr. Kazunai Shinbo, Prof. Dr. Keizo Kato and Prof. Dr. Futao Kaneko from Niigata University, Japan for their help, advice and useful suggestions during doing a research in Japan. I am thankful for Dr. Wiyong Kangwansupamonkon for his helpful advice and allowing to use the characterization facilities.

My gratitude go to Asst. Prof. Dr. Natda Wetchakun and Asst. Prof. Dr. Sangraee Sriwichai from Chiang Mai University, Thailand for their kindness, valuable guidance.

Special thanks would go directly to a Grant-in-Aid for Scientific Research (C) (25390051) from the Japan Society for the Promotion of Science (JSPS). I would like to thank the Global Circus Program from Graduate School of Science and Technology Niigata University, the Thailand Research Fund, The Royal Golden Jubilee Ph.D. Program (PHD/0358/2551), Ministry of Science and Technology, through its program of Center of Excellence Network, Thailand.

I am thankful for center for transdisciplinary research niigata university, Niigata, Japan and the Department of Chemistry, Faculty of Science, Chiang Mai University, Chiang Mai, Thailand

Finally, I would also like to thank my family, friends and all members of the center for transdisciplinary research niigata university, Niigata, Japan for their helps and warm friendship.

Hathaithip Ninsonti

## ABSTRACT

Dye-sensitized solar cells (DSSCs) are attractive organic-based solar cells on account of their high efficiency and low cost. Many studies on DSSCs have been reported. In this research, DSSC was improved by using an effect of Au-loaded titanium dioxide (Au-loaded TiO<sub>2</sub>). The Au-loaded TiO<sub>2</sub> nanopowders were synthesized by the modified sol–gel method together with the impregnation method. Anatase phase of TiO<sub>2</sub> was obtained in all samples with an average particle size of 20 nm. For the enhancement of DSSCs study, DSSCs composed of the Au grating/Au-loaded TiO<sub>2</sub>/TMPyP-SCC LbL (20 bilayers)/ electrolyte/ITO substrates were fabricated. Au-loaded TiO<sub>2</sub> films were deposited by electrophoretic deposition. TMPyP and SCC were used as photo-absorbing dyes and were prepared by LbL deposition. The fabricated cells were irradiated with visible light at various incident angles with SP excitation (p-pol.) and without surface plasmon excitation (s-pol.). The results showed that up to a 7.5-fold increase in the short-circuit photocurrent can be obtained by combining Au-loaded TiO<sub>2</sub> with grating-coupled surface plasmon excitation in the cells.

For further application on solid-state dye-sensitized solar cell (ss-DSSCs), the fabrication of a grating structure formed by a solid-state electrolyte layer on a dye-TiO<sub>2</sub> film by the nanoimprinting technique using a polydimethylsiloxane (PDMS) stamp and its application in photoelectric conversion devices are described. The PDMS grating pattern was imprinted from blu-ray disc recordable. A silver electrode was deposited on the patterned solid-state electrolyte layers. Surface plasmon

resonance (SPR) excitation was observed in the fabricated solar cells by irradiation with white light. The photoelectric conversion properties were measured to study the effect of the two types of SPR excitations, i.e., the propagating surface plasmon on the Ag grating surface and the localized surface plasmon from the Au nanoparticles on TiO<sub>2</sub>.

# CONTENTS

	<b>Page</b>
Acknowledgements	iii
Abstract	v
List of Figures	xi
List of Tables	xiv
Chapter 1 Introduction	1
1.1 Titanium dioxide (TiO <sub>2</sub> )	3
1.2 Dry-sensitized solar cell (DSSCs)	6
1.2.1 Dye-sensitized solar cells (DSSCs) system	7
1.2.2 Type of DSSCs	9
1.3 Surface plasmons	12
1.4 Gold	15
1.5 Preparation techniques of nanoparticles	17
1.5.1 Sol-gel method	17
1.5.2 Impregnation method	20
1.6 Characterization techniques	21
1.7 Research objectives	29
Reference	30

## CONTENTS (CONTINUED)

	<b>Page</b>
Chapter 2 Enhanced photocurrent properties of dye/Au-loaded TiO <sub>2</sub> films by grating-coupled surface plasmon excitation	39
2.1 Literature review	41
2.2 Material	49
2.3 Instruments	51
2.4 Experimental	52
2.4.1 Synthesis of unloaded TiO <sub>2</sub> by the modified sol-gel method	52
2.4.2 Preparation of Au-loaded TiO <sub>2</sub> by the impregnation method	53
2.4.3 Preparation Au grating substrate	53
2.4.4 Indium Tin Oxide (ITO) glass substrate cleaning	54
2.4.5 Fabrication and characterization of dye/TiO <sub>2</sub> films and dye/Au-loaded TiO <sub>2</sub> films	54
2.5 Results and discussion	57
2.5.1 Surface morphology of the fabricated thin film on Au grating substrate	57
2.5.2 White light-SPR measurements	58
2.5.3 Short-circuit photocurrent measurements	59

## CONTENTS (CONTINUED)

	<b>Page</b>
2.5.4 The enhancement of short-circuit photocurrent	66
2.6 Conclusions	69
Reference	70
Chapter 3 Enhanced photocurrent generation at a spiro-OMeTAD/AuNPs-TiO <sub>2</sub> interface with grating-coupled surface plasmon excitation	79
3.1 Literature review	80
3.2 Materials	84
3.3 Instruments	86
3.4 Experimental	87
3.4.1 Preparation of 1 mM gold nanoparticles	87
3.4.2 Preparation of BD-Rs grating master template	87
3.4.3 Preparation of PDMS grating mold	88
3.4.4 Indium Tin Oxide (ITO) glass substrate cleaning	89
3.4.5 Fabrication of the grating pattern on the solid-state electrolyte/TiO <sub>2</sub> or solid-state electrolyte/Au-TiO <sub>2</sub> films	89
3.4.6 Surface plasmon resonance measurements	92
3.4.7 Characterization of the fabricated solid-state dye-sensitized solar cells	93
3.5 Results and discussion	93



## CONTENTS (CONTINUED)

	<b>Page</b>
3.5.1 Atomic force microscopy images of the imprinted grating pattern	93
3.5.2 White light-SPR measurements	95
3.5.3 Short-circuit photocurrent measurements	96
3.6 Conclusions	99
Reference	100
Chapter 4 Conclusion	105
Appendix	108
Curriculum vitae	112

## LIST OF FIGURES

		<b>Page</b>
Figure 1.1	The crystal structure of rutile TiO <sub>2</sub>	4
Figure 1.2	The crystal structure of anatase TiO <sub>2</sub>	4
Figure 1.3	The crystal structure of brookite TiO <sub>2</sub>	5
Figure 1.4	Theory of process and energy level scheme of the dye-sensitized TiO <sub>2</sub> solar cell	7
Figure 1.5	Grating-coupled surface plasmon	13
Figure 1.6	Schematic illustration of the LSPR excitation by metallic nanoparticles and the formation of an electric dipole on a metallic nanoparticle	15
Figure 1.7	Schematic diagram of the beam-specimen interaction in (a) a thick specimen and (b) a thin specimen	24
Figure 1.8	Schematic diagram of the layout of a scanning electron microscope	26
Figure 1.9	Schematic diagram showing a secondary electron detector and a solid-state backscattered electron detector together with typical images	27
Figure 2.1	Scheme of the modified sol-gel method	52
Figure 2.2	Au vacuum evaporation.	53
Figure 2.3	Preparation of Au-TiO <sub>2</sub> film by electrophoretic deposition method.	54
Figure 2.4	Preparation of Au-TiO <sub>2</sub> film by electrophoretic deposition method.	55
Figure 2.5	Scheme of fabricated dye-sensitized solar cells (DSSCs).	56
Figure 2.6	AFM image of (a) BD-R grating and (b) the fabricated 1.0 at% Au-TiO <sub>2</sub> thin film on Au grating substrate (Film thickness = 30 nm)	57
Figure 2.7	SPR reflectivity curves for the fabricated DSSC measured at fixed incident angles of 20–50°.	58

## LIST OF FIGURES (CONTINUED)

		<b>Page</b>
Figure 2.8	Short-circuit photocurrent properties of the DSSC composed of Au grating/Au-TiO <sub>2</sub> /TMPyP-SCC LbL (20 bilayers)/electrolyte/ITO substrate upon irradiation of visible light with surface plasmon excitation (p-pol.) and without SP excitation (s-pol.).	59
Figure 2.9	Short-circuit photocurrents of the DSSC composed of the Au grating/Au-TiO <sub>2</sub> /TMPyP-SCC LbL (20 bilayers)/ electrolyte/ITO substrate upon irradiation with visible light at various incident angles with SP excitation (p-pol.) and without SP excitation (s-pol.) by using unloaded TiO <sub>2</sub> at incident angles of 0–35°.	61
Figure 2.10	Short-circuit photocurrents of the DSSC composed of the Au grating/Au-TiO <sub>2</sub> /TMPyP-SCC LbL (20 bilayers)/ electrolyte/ITO substrate upon irradiation with visible light at various incident angles with SP excitation (p-pol.) and without SP excitation (s-pol.) by using 0.25 mol% Au-TiO <sub>2</sub> at incident angles of 0–35°.	61
Figure 2.11	Short-circuit photocurrents of the DSSC composed of the Au grating/Au-TiO <sub>2</sub> /TMPyP-SCC LbL (20 bilayers)/ electrolyte/ITO substrate upon irradiation with visible light at various incident angles with SP excitation (p-pol.) and without SP excitation (s-pol.) by using 1.00 mol% Au-TiO <sub>2</sub> at incident angles of 0–35°.	62
Figure 2.12	Enhanced photocurrent factor as a function of the incident light angle. Here the enhancement factor is the ratio of the measured current in each sample to the current with unloaded TiO <sub>2</sub> and without propagating SP excitation.	67

## LIST OF FIGURES (CONTINUED)

	<b>Page</b>
Figure 3.1	AFM image of BD-Rs grating master template. 88
Figure 3.2	Scheme of PDMS grating mold preparation. 89
Figure 3.3	Schematic illustration for fabricating the grating pattern of Ag/spiro-OMeTAD. 91
Figure 3.4	The silver electrode deposited by the vacuum evaporation method on the spiro-OMeTAD layer. 92
Figure 3.5	Fabricated dye-sensitized solar cells (DSSCs). 93
Figure 3.6	AFM images of grating patterned PDMS mold (a), imprinted spiro-OMeTAD on the N-719/TiO <sub>2</sub> /ITO/glass substrate (b), and Ag/spiro-OMeTAD on the N-719/TiO <sub>2</sub> /ITO/glass substrate (c). 94
Figure 3.7	SPR reflectivity curves for the Ag/spiro-OMeTAD (imprinted grating)/N-719/TiO <sub>2</sub> /ITO-glass measured at fixed incident angles of 20°–60°. 95
Figure 3.8	Current density vs. voltage (J–V) curves for Ag/spiro-OMeTAD (imprinted grating)/N-719/TiO <sub>2</sub> /ITO-glass and Ag/spiro-OMeTAD (without imprinting) /N-719/TiO <sub>2</sub> /ITO-glass. 96
Figure 3.9	Short-circuit photocurrent properties upon irradiation with solar light: Ag/spiro-OMeTAD (imprinted grating)/N-719/Au-TiO <sub>2</sub> /ITO-glass, Ag/spiro-OMeTAD (imprinted grating)/N-719/TiO <sub>2</sub> /ITO-glass, and Ag/spiro-OMeTAD (without imprinting)/N-719/TiO <sub>2</sub> /ITO- glass. 98

## LIST OF TABLES

		<b>Page</b>
Table 1.1	The crystal structure of brookite TiO <sub>2</sub>	5
Table 1.2	Properties of gold	16
Table 2.1	Chemical, molecular weight, purity and company	49
Table 2.2	Instruments, model and company	51
Table 2.3	Short-circuit photocurrents of the DSSC composed of the Au grating/TiO <sub>2</sub> /TMPyP-SCC LbL (20 bilayers)/electrolyte/ITO substrate upon irradiation with visible light at various incident angles with SP excitation (p-pol.) and without SP excitation (s-pol.)	63
Table 2.4	Short-circuit photocurrents of the DSSC composed of the Au grating/0.25 mol% Au-TiO <sub>2</sub> /TMPyP-SCC LbL (20 bilayers)/electrolyte/ITO substrate upon irradiation with visible light at various incident angles with SP excitation (p-pol.) and without SP excitation (s-pol.)	64
Table 2.5	Short-circuit photocurrents of the DSSC composed of the Au grating/1.00 mol% Au-TiO <sub>2</sub> /TMPyP-SCC LbL (20 bilayers)/electrolyte/ITO substrate upon irradiation with visible light at various incident angles with SP excitation (p-pol.) and without SP excitation (s-pol.)	65
Table 2.6	Enhanced photocurrent factor, as a function of the incident light angle, of the fabricated DSSC	68
Table 3.1	Chemical, molecular weight, purity and company.	84
Table 3.2	Instruments, model and company.	86
Table 3.3	Photovoltaic performance of Ag/spiro-OMeTAD (imprinted grating)/N-719/TiO <sub>2</sub> /ITO-glass and Ag/spiro-OMeTAD (without imprinting)/N-719/TiO <sub>2</sub> /ITO-glass.	97

## CHAPTER 2

### **Enhanced photocurrent properties of dye/Au-loaded TiO<sub>2</sub> films by grating-coupled surface plasmon excitation**

Nowadays, renewable energy has been widely studied due to an increase in energy demand in the world. There are various renewable energy technologies such as photocatalytic oxidation, adsorption/separation processing, solar cells, fuel cells, and biofuels. Solar cell is found to be the most extremely sustainable option in terms of its availability and massive potential. Currently, numerous studies on dye-sensitized solar cells (DSSCs) have been reported due to their high efficiency performance and low cost of materials [1–4]. In 1991, O'Regan and Grätzel first reported a high conversion efficiency DSSCs [5]. After that, several studies on dye-sensitized solar cells (DSSCs) have been reported [6–13]. Catalyst materials are used in the solar cell for renewable energy options. In the photoanode of DSSCs, a monolayer of sensitized organic dye molecules covered with covalent bond on anatase TiO<sub>2</sub> film is commonly used [14]. Titanium dioxide (TiO<sub>2</sub>) is one of the most popular material for dye-sensitized solar cells (DSSCs) because of its chemical stability, nontoxicity, good electrical properties and inexpensiveness [1–4]. There are three crystal structures of TiO<sub>2</sub> consist of anatase, rutile and brookite. The anatase TiO<sub>2</sub> is used as dye-sensitized solar cells material since it has band gap energy of 3.2 eV of which the absorption thresholds correspond to 380 nm, which is easy for photon–electron transfer under solar light irradiation [3].

Surface plasmon (SP) excitation is an attractive method for enhancing the performance of DSSCs because the active thin film can absorb more light from the increased optical field [6–8]. Propagating SP is an SP excitation technique that can occur on a grating structure [15, 16]. Baba *et al.* [17] have previously reported that the short-circuit photocurrent in organic solar cells can be increased by using grating-coupled SP excitations in which a Blu-ray disc recordable (BD-R) is used as a grating substrate. Another method to increase light harvesting by light scattering and localized surface plasmon properties of DSSCs, metal nanoparticles were used [9]. Furthermore, metal nanoparticles have the scattering property which could enlarge its possibility of

exciting dye molecule. More electrons to be injected into  $\text{TiO}_2$  conduction band due to the increased absorption in the dye. Therefore, the photocurrent and photo efficiency of the device could be improved [9]. When metal nanoparticles were excited by the incident light, a collective oscillation of electron in metal nanoparticles will take place, this phenomena called localized surface plasmon. It could enhance the electric field on photoanode of DSSCs in order to enlarge the optical absorption. Consequently, it has been extensively used to improve the DSSCs performance [6–9]. In addition, metal nanoparticles could perform as electron acceptor from the photo-excited metal oxide semiconductor. Therefore, electron transfer rate could be enhanced and the increasing of photocurrent was found [6, 18, 19]. Au is a metal nanoparticle that have several advantages such as high conductivity, chemical and thermal stability [19]. Au is widely added to the metal oxide semiconductor to increase the photocurrent property of the DSSCs [20, 21]. Au is known to be the most effective catalyst among various kind of metal nanoparticles that could notably improve dye sensitized solar cells by surface plasmon resonance effect [22, 23]. It could be effectively used to enlarge photocurrent of dye sensitized solar cells. For these reason, Au nanoparticles were chosen to induce light scattering and localized surface plasmon excitation for the improvement of DSSCs performance.

$\text{TiO}_2$  nanoparticles could be synthesized by several techniques such as precipitation technique [24–26], solvothermal technique [27–30], sol-gel technique [31–35], spray pyrolysis [10–13] and microwave technique [36–38]. Sol-gel technique consists of 2 major reactions, hydrolysis and condensation [31–35, 39–42]. In the previous work [43], the preparation of  $\text{TiO}_2$  by the modified sol-gel technique using cellophane membrane to reduce the diffusion rates of reactants in hydrolysis and condensation steps was studied. This preparation technique had many advantages such as good reproducibility, good ability to obtain  $\text{TiO}_2$  in nano-sized scale and good production for high purity products [41, 42].

In this research,  $\text{TiO}_2$  and Au-loaded  $\text{TiO}_2$  nanoparticles were synthesized by the modified sol-gel technique and coupling the modified sol-gel with impregnation technique respectively. The obtained nanoparticles were used to enhance DSSCs

performance. Dye/Au-loaded TiO<sub>2</sub> films were fabricated on a Au grating surface to couple with surface plasmon resonance (SPR) to further enhance the photocurrent in DSSCs.

## 2.1 Literature review

Enhanced efficiency of dye-sensitized solar cells by high surface area anatase-TiO<sub>2</sub>-modified P25 paste was studied by Pan *et al.* [44] Two major problems are to improve the conversion efficiency and the stability of dye-sensitized solar cells (DSSCs). In addition, reduction of the manufacturing cost of DSSCs and large-scale manufacture are also very significant factors. For a raw material used in DSSCs fabrication, commercial P25 would be used for large-scale manufacture of TiO<sub>2</sub> paste with uncomplicated preparation process. However, there are several disadvantages for P25 such as the low surface area of P25 powder and the poor connectivity among particles in film using convention P25 paste without modification. In the report, a simple modified method by adding high surface area anatase TiO<sub>2</sub> into pure P25 paste was introduced. The photoelectric conversion properties of DSSCs based on these photo-electrodes were investigated. The results confirmed that the open-circuit voltage, the fill factor and the energy conversion efficiency of the modified electrode were increased. It was found that the modified P25 films had fast electron transportation and a slow charge recombination. It could be concluded that through adding the anatase TiO<sub>2</sub> nanoparticles to the P25 paste with high surface area, it could not only improve the particles connectivity among inside the films, but also enhance the DSSCs efficiency.

Dhas *et al.* [45] synthesized thin anatase TiO<sub>2</sub> nanoleaves (NLs) with high surface area (~93 m<sup>2</sup>/g) by the hydrothermal method and dye-sensitized solar cells (DSSC) prepared using such NLs were compared with TiO<sub>2</sub> nanoparticles synthesized by the hydrothermal method and the Degussa P25 powder. The NLs-based DSSCs showed enhancement of 16% and 24% in the total conversion efficiency over the cells prepared with NPs and P25 respectively. It was found that, the highest enhancement in the conversion efficiency (~35%) is achieved for cells using a 50:50 (wt/wt) mixture of



NLs and NPs. In this case the dye loading was found to be >50% higher than the case of NP films. Furthermore, the DC resistance of diffusion of  $I_3^-$  in electrolyte (as revealed by the electrochemical impedance spectroscopy) was significantly lower than the NP film case, other cell parameters being nominally comparable.

Plasmonic metal nanoparticles was studied by Kawawaki *et al.* [46] It is known that plasmonic metal nanoparticles could work as light-harvesting materials that could improve photocurrents of photovoltaic cells and reaction rates of photocatalysts. The properties were expected to enhance the energy conversion efficiency and to decrease the thickness of a light-absorbing layer and costs for materials. They studied the plasmonic improvement of dye-sensitized photocurrents by Au nanoparticle ensembles with different particle densities to investigate the effects of interparticle plasmon coupling on the photocurrent enhancement. The coupling effects permit improvement in a longer wavelength region. The best particle size for the improvement by coupled nanoparticles was 100 nm. However, that for isolated nanoparticles, best particle size was 40 nm due to the plasmon coupling effect more important for larger nanoparticles. Moreover, it was found that theoretical calculations reproduced those results.

The development of  $TiO_2/Au$  (or  $TiO_2/Ag$ ) composite particles, which most likely have the plasmon resonance effect, on FTO-glass (Fluorine doped tin oxide,  $SnO_2:F$ ) substrate of the working electrode of a dye-sensitized solar cell (DSSC) was studied by Chou *et al.* [47] The dry particle coating procedure was used to coat the surfaces of  $TiO_2$  particle with nano-sized Au (or Ag) powder particles. A film of  $TiO_2/Au$  (or  $TiO_2/Ag$ ) composite particles was deposited on the FTO-glass substrate of the working electrode, and it was then sintered in a high-temperature oven. The working electrode coated with a  $TiO_2/Au$  (or  $TiO_2/Ag$ ) thin film was kept immersed in a solution of N-719 (Ruthenium) dye for 12 h. Moreover, a thin film of platinum was deposited on the FTO-glass substrate of the counter electrode. Finally, the DSSC was fabricated, and the short-circuit photocurrent; the open-circuit photovoltage, and the power conversion efficiency  $\eta$  of DSSC were investigated using a home-made I-V measurement system. This study also investigated the effects of the mass ratio of  $TiO_2$  to Au (or Ag), and the period of dry coating on the power conversion efficiency  $\eta$  of the DSSC. If the period of dry

coating was sufficient, the power conversion efficiency  $\eta$  of the DSSC with TiO<sub>2</sub>/Au (or TiO<sub>2</sub>/Ag) composite particles increased with increase in the percentage of Au (or Ag) in the composite particles. Most essentially, this study showed that the power conversion efficiency  $\eta$  of the DSSC with a film of TiO<sub>2</sub>/Au (or TiO<sub>2</sub>/Ag) on the working electrode was always more than that of the conventional DSSC because of the Schottky barrier, which was probably produced in the TiO<sub>2</sub>/Au (or TiO<sub>2</sub>/Ag) composite particles.

Muduli *et al.*[18] showed that anatase TiO<sub>2</sub> nanoparticles decorated with gold nanoparticles were prepared by the hydrothermal route by using mixed precursor and controlled conditions. From the result, diffused reflectance spectra (DRS) exposed that besides the expected TiO<sub>2</sub> interband absorption below 360 nm gold surface plasmon feature occurs near 564 nm. It was shown that the dye sensitized solar cells fabricated using TiO<sub>2</sub>-Au plasmonic nanocomposite yielded greater photovoltaic property with conversion efficiency (CE) of ~6% (no light harvesting), current density (JSC) of ~13.2 mA/cm<sup>2</sup>, open circuit voltage ( $V_{oc}$ ) of ~0.74 V and fill factor ( $FF$ ) 0.61; significantly enhanced than that with only TiO<sub>2</sub> nanoparticles (CE ~ 5%,  $J_{SC}$  ~ 12.6 mA/cm<sup>2</sup>,  $V_{oc}$  ~ 0.70 V,  $FF$  ~ 0.56).

Mesoporous TiO<sub>2</sub> with extremely crystalline anatase phase and high surface area is a assuring material for energy and environmental application [48]. Huang *et al.* [48] showed that a novel and simple method for rapid synthesis of mesoporous TiO<sub>2</sub> through the microwave-assisted hydrothermal method using stable and water-soluble titanium citrate complexes as the starting material was improved the properties of TiO<sub>2</sub>. For the characterization, SEM, TEM, XRD, UV-vis spectroscopy, BET surface area analysis, and TGA/DTA were employed to investigate the physicochemical properties of mesoporous TiO<sub>2</sub> in terms of morphology, crystallization, optical property, surface area, and thermal behavior, respectively. Results proved that the synthesized TiO<sub>2</sub> contained mainly anatase phase with crystallite size of 5.0–8.6 nm with various hydrothermal temperatures and durations ranging from 150 to 180°C and from 30 to 120 min, respectively. The specific surface areas of the TiO<sub>2</sub> nanocrystals were found to be 217–323 m<sup>2</sup> g<sup>-1</sup> with the pore diameter of 5.8–6.9 nm, obviously showing the mesoporous characteristics of the hydrothermal TiO<sub>2</sub> nanocrystals. The mesoporous nanocrystals

synthesized at 180°C were then selected to prepare the TiO<sub>2</sub> photoelectrode using screen-printing deposition technique. The MW180–120-based TiO<sub>2</sub> photoanode revealed a good capability on photocurrent conversion and the conversion efficiency was in the range 4.8–7.1%, depending on active area and film thickness. Furthermore, the overall conversion efficiency of the DSSC with active area of 1 cm<sup>2</sup> and organic solvent electrolyte decreased slightly from 4.8% to 4.3% after being kept for more than 490 h, indicative the long-term stability of the DSSC use in their study.

Ding *et al.* [15] had improved a one-step direct imprinting process for application of plasmonic silver nanodome arrays in the back reflectors of solid-state dye-sensitized solar cells (ss-DSSCs). The imprinting process is low-cost and scalable, and allows accurate control over the characteristic size and periodicity. The resulting nanodome array significantly improves the light absorption of ss-DSSCs through light scattering and combination to propagating surface plasmon polariton modes. The short-circuit photocurrent ( $J_{sc}$ ) was enhanced by 16% for ss-DSSCs prepared with Z907 dye and by 12% for ss-DSSCs prepared with C220 dye. The enhancement in photocurrent resulted from an EQE improvement over a broad wavelength range, which is corresponding to simulation results. This process was a resultant to the development of new dyes, and the results show that even cells with strong-absorbing organic dyes could promote from the plasmonic nanodome array. They mentioned that, such design of plasmonic back reflectors which consisted of sub-wavelength size metallic structures was not restricted to dye-sensitized solar cells; it could possibly be applied to any thin-film solar cell materials structure with active layer thickness on the scale of 0.5–10 μm, such as amorphous silicon, CdTe and Cu(In,Ga)Se<sub>2</sub>.

Deepa *et al.*[6] showed that the photoelectrode of Eosin-Y sensitized DSSC was improved by loading Au-nanoparticles to increase the power conversion efficiency via scattering from surface plasmon polaritons. Effect of Au nanoparticle size on conversion efficiency was studied in DSSC for the first effect by varying the particle size from 20 to 94 nm. For this investigation, it was found that, the conversion efficiency was highly varying on the size of the Au nanoparticles. For larger Au particles, the efficiency was found to be increased because of constructive interference

between the transmitted and scattered waves from the Au nanoparticle whereas for smaller Au particles, the efficiency decreased due to destructive interference. Moreover, a decrease in the  $V_{oc}$  was observed in common, because of the negative shifting of the  $TiO_2$  Fermi level on the adsorption of Au nanoparticle. This shift was irrelevant for larger particles. When using 94 nm size particles, the conversion efficiency was doubled from 0.74% to 1.52%. This investigation pointed towards the application of the scattering effect of metal nanoparticle to improve the conversion efficiency in DSSCs.

Ghaffari *et al.* [49] studied the deposition of Au nano particles (NPs) on vertically grown  $TiO_2$  nanorod arrays on FTO substrate by the hydrothermal process. Metal nanoparticles were applied onto the surface of  $TiO_2$  nanorods via photochemical reduction procedure under ultraviolet irradiation. To characterize the as-prepared Au/ $TiO_2$  nanorod composites, X-ray diffraction (XRD), electron microscopy (FESEM), transmission electron microscopy (TEM) and X-ray photoelectron spectroscopy (XPS) investigation were employed. Current density–voltage ( $J$ – $V$ ) measurements were acquired from a two-electrode sandwich type cell. Au nanoparticles could support the electron–hole separation by attracting photoelectrons. Furthermore, loading of Au nanoparticles to the  $TiO_2$  nanorod extensively enhanced the fill factor and  $J_{sc}$  (short circuit current density). The utilization of Au NPs  $TiO_2$  nanorods in improving the performance of DSSCs was promising.

Jung *et al.* [50] reported that  $TiO_2$  nanoparticle-based dye sensitized solar cells (DSSCs) have an interesting significant level of scientific and technological attract for their ability as inexpensively viable photovoltaic devices. Even though DSSCs have numerous advantages such as material abundance, a short energy payback period, constant power output, and compatibility with flexible applications, there are still a number of interest that hold back large scale commercial production. Critical factors determining the potential of DSSCs implicate energy conversion efficiency, long-term stability, and manufacture cost. Permanent development of their long-term stability proposed that state-of-the-art DSSCs would be operated for more than 20 years without a significant reduction in DSSCs performance. However, key questions remain in consider to energy conversion efficiency developments and the reduction of material

cost. In this attitude, the present state of the field and the continuing attempt to concentrate on the supplies of DSSCs are summarized with opinions on the future of DSSCs.

Beck *et al.* [51] reported that effective light controlling was necessary in retaining high efficiencies as photovoltaic devices become thinner. They suggested a simple and effective method of improving light trapping in solar cells with absorber layers by modification localized surface plasmons in arrays of Ag nanoparticles. By redshifting the surface plasmon resonances by up to 200 nm, through the improvement of the local dielectric environment of the particles, they could enhance the optical absorption in an underlying Si wafer fivefold at a wavelength of 1100 nm and an increase the external quantum efficiency of thin Si solar cells by a factor of 2.3 at this wavelength where transmission losses are prevalent. Furthermore, they could avoid absorption losses below the resonance wavelength due to interference effects, while still allowing long wavelength light to be coupled into the cell by positioning the nanoparticles on the rear of the solar cells. Moreover, they also investigated numerical simulations to support the experimental result. It was found that, the fraction of light backscattered into the cell by nanoparticles located on the rear was comparable to the forward scattering effects of particles on the front. The researchers mentioned that this method was appropriate for use in large-scale photovoltaic devices fabrication.

Silver nanoparticle doped TiO<sub>2</sub> nanofiber dye sensitized solar cells was reported by Li *et al.* [52]. Silver nanoparticle doped TiO<sub>2</sub> nanofibers synthesized by the electrospinning method was employed as the photoanode to assemble dye sensitized solar cells. The result showed that the nanoparticle doped solar cells had a significantly improved photocurrent density resulting in a 25% increased conversion efficiency compared to undoped solar cells. They mentioned that the enhancement of the photovoltaic property was attributed to two factors: (1) the enlarged light harvesting efficiency attributable to the plasmon enhanced optical absorption induced by Ag nanoparticles, and (2) the enhanced electron collection efficiency due to faster electron transport in the Ag doped TiO<sub>2</sub> nanofiber photoanode. In this experiment, a dye sensitized solar cell with a photoanode of Ag nanoparticle doped TiO<sub>2</sub> nanofibers was

fabricated and investigated. It was found that the short circuit current density of the Ag doped DSSC sample was increase by 26% resulting in a conversion efficiency improvement of 25% when compared with the undoped DSSC sample. Increase optical absorption due to the Ag plasmon effect and a faster electron transport in the Ag doped TiO<sub>2</sub> nanofiber photoanode were found to be the two effects that provide the enhanced performance of the DSSC. Whereas the electron life time was found to be half of that in the undoped DSSC sample, while the electron dispersion length in the doped sample was still 30% higher than in the undoped sample, which confirmed that the Ag doped sample had effectively better electron collection efficiency compared to the undoped sample.

Derkacs *et al.* [53] reported the performance improvement of InP/InGaAsP quantum-well solar cells by using nanoparticle-induced light scattering. The combination of metal or dielectric nanoparticles above the quantum-well solar cell device was revealed to couple normally incident light into lateral optical propagation paths, with optical confinement due to the refractive index difference between the quantum-well layers and nearby material. With minimum optimization, short-circuit current density improved of 12.9% and 7.3% and power conversion efficiency improved of 17% and 1% was investigated for silica and Au nanoparticles, respectively.

Enhanced semiconductor optical absorption via surface plasmon excitation in metal nanoparticles was studied by Schaadt *et al.* [54] Surface plasmon resonances in metallic nanoparticles are studied for a multiplicity of applications because of the great electromagnetic field improvement that occurs in the vicinity of the metal surface. The resonance wavelength depends on the size, shape, and local dielectric environment of the metal nanoparticle. They deposited Au nanoparticles on the semiconductor surface and investigated an enhancement of optical absorption and photocurrent in a semiconductor by means of the excitation of surface plasmon resonances in spherical Au nanoparticles. The absorption of semiconductor increased due to the increased photocurrent response in Si p-n junction diodes over wavelength ranges that corresponded strongly to the nanoparticle plasmon resonance wavelengths as determined by the investigation of extinction spectra. These studies led to many

applications for the enhancement of the device's performance such as photodetectors, imaging arrays, and photovoltaics.

Lim *et al.* studied [55] photocurrent spectroscopy of optical absorption enhancement in silicon photodiodes via scattering from surface plasmon polaritons in gold nanoparticles. Experimental characterization and finite-element mathematical simulations of the electromagnetic interaction between Au nanoparticles deposited on a Si p-n junction photodiode and incident electromagnetic plane waves had been investigated as a function of wavelength. Au nanoparticles deposited on a Si p-n junction photodiode was found to lead to enlarged electromagnetic field amplitude within the semiconductor, and therefore improved photocurrent response, over a broad range of wavelengths extending upward from the nanoparticle surface plasmon polariton resonance wavelength. At shorter wavelengths, a reduction in electromagnetic field amplitude and a corresponding decrease in photocurrent response in the semiconductor are observed. Numerical simulations reveal that these different behaviors are a consequence of a shift in the phase of the nanoparticle polarizability near the surface plasmon polariton wavelength, leading to interference effects within the semiconductor that vary strongly with wavelength. These observations had substantial implications for the optimization of device structures in which surface plasmon polariton resonances in metallic nanoparticles were exploited to engineer the performance of semiconductor photodetectors and related devices.

## 2.2 Materials

**Table 2.1** Chemical, molecular weight, purity and company

<b>Chemical</b>	<b>Molecular weight</b>	<b>Purity</b>	<b>Company</b>
Ethanol absolute (C <sub>2</sub> H <sub>5</sub> OH)	46.08	100% v/v	Ajax
Ammonia (NH <sub>3</sub> )	17	25% v/v	Merck
Ethanol absolute (C <sub>2</sub> H <sub>5</sub> OH)	46.08	100% v/v	Ajax
Formic acid (HCOOH)	46.02	90%	Ajax
Gold chloride hydrate (H(AuCl <sub>4</sub> ).H <sub>2</sub> O)	393.83	49% of gold	Electron Microscopy Science
Nitric acid (HNO <sub>3</sub> )	63.01	65% v/v	Merck
Oxalic acid (C <sub>2</sub> H <sub>2</sub> O <sub>4</sub> ·2H <sub>2</sub> O)	126.07	98%	Aldrich
Perchloric acid(HClO <sub>4</sub> )	100.47	70%	Ajax



**Table 2.1 (cont.)** Chemical, molecular weight, purity and company

<b>Chemical</b>	<b>Molecular weight</b>	<b>Purity</b>	<b>Company</b>
Ethanol absolute (C <sub>2</sub> H <sub>5</sub> OH)	46.08	100% v/v	Ajax
1-Octadecanethiol ((CH <sub>3</sub> (CH <sub>2</sub> ) <sub>17</sub> SH),	286.56	98%	Aldrich
5,10,15,20-Tetrakis (1- methyl-4-pyridinio) porphyrin tetra(p- toluenesulfonate) (C <sub>72</sub> H <sub>66</sub> N <sub>8</sub> O <sub>12</sub> S <sub>4</sub> , TMPyP)	1363.60	97%	Aldrich
Sodium copper chlorophyllin (C <sub>34</sub> H <sub>31</sub> CuN <sub>4</sub> Na <sub>3</sub> O <sub>6</sub> , SCC)	724.15	99%	Aldrich
Ferrous sulfate heptahydrate (FeSO <sub>4</sub> .7H <sub>2</sub> O)	278.01	99.99%	Aldrich
sodium sulfate (Na <sub>2</sub> SO <sub>4</sub> )	142.04	99.99%	Aldrich

## 2.3 Instruments

**Table 2.2** Instruments, model and company

<b>Instruments</b>	<b>Model</b>	<b>Company</b>
Ultrasonic bath	D-78224 Transonic Digitals	Elma
Oven	Memmert 70	Memmert
Atomic force microscope (AFM)	SPM-9600	SHIMADZU
Potentiostat set	HZ-5000	Hokuto Denko Ltd.
Solar simulator (AM1.5)	HAL-C100	Asahi Spectra
Scanning electron microscope (SEM)	JSM6335F	JEOL
UV-vis spectrophotometer (UV-vis)	V-650	Jasco
Spin coater	1H-D3	Misaka
UV/Ozone Cleaning Equipment	ASM401N	ASUMI GIKEN Limited
Imprint machine	AH-1T	AS ONE

## 2.4 Experimental

### 2.4.1 Synthesis of unloaded TiO<sub>2</sub> by the modified sol-gel method

Titanium dioxide (TiO<sub>2</sub>) nanoparticles were synthesized by the modified sol-gel method as mentioned in the previous researches [43, 56]. Titanium tetraisopropoxide (Ti[OCH(CH<sub>3</sub>)<sub>2</sub>]<sub>4</sub>), absolute ethanol and ammonia were used as the starting materials. The solution of titanium tetraisopropoxide in absolute ethanol was loaded into cellophane membrane pouch and placed in solution containing absolute ethanol, deionized water and ammonia. The solutions inside and outside the cellophane pouch were kept constant stirring at 70–80 °C for 1 h. After the dialysis process was completed, the mixture solution in the pouch was centrifuged at 7500 rpm for 10 min and then dried in an oven at 60°C for 24 h. The white powders then were calcined at 400 °C for 3 h. Then, unloaded TiO<sub>2</sub> nanoparticles were obtained. The scheme of the modified sol-gel method is shown in Figure 2.1.

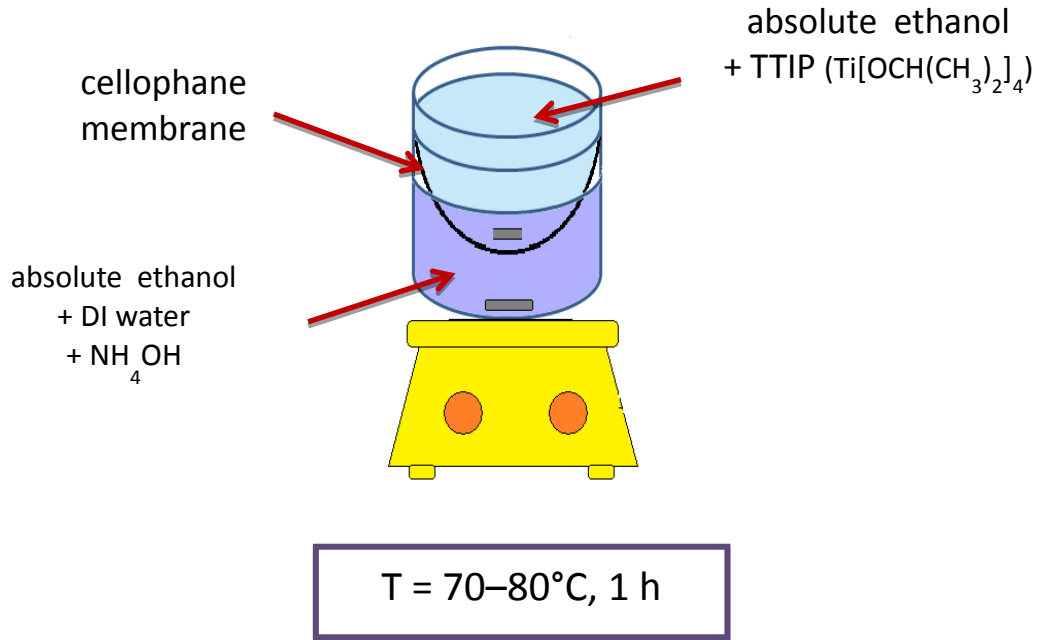


**Figure 2.1** Scheme of the modified sol-gel method [43, 56].

### 2.4.2 Preparation of Au-loaded TiO<sub>2</sub> by the impregnation method

Au-loaded TiO<sub>2</sub> nanopowders were prepared by the impregnation method as mentioned in the previous researches [43, 56]. Appropriate amounts of gold(III) chloride hydrate ((H(AuCl<sub>4</sub>)).H<sub>2</sub>O, Electron Microscopy Science) in absolute ethanol were added to unloaded TiO<sub>2</sub> nanopowders to obtain Au-loading levels of 0.25 and 1.00 mol%. Then, the samples were dried at 60°C for 24 h and calcined at 400°C for 3 h. Finally, 0.25 and 1.00 mol% Au-loaded TiO<sub>2</sub> nanopowders were obtained. In all obtained samples, TiO<sub>2</sub> was in the anatase phase with an average particle size of 20 nm.

### 2.4.3 Preparation Au grating substrate

Blu-ray Recordable discs (BD-Rs, LTH type, TAIYO YUDEN) were used as diffraction grating substrates ( $\Lambda = 320$  nm). BD-Rs were cut into rectangles (2.5 cm  $\times$  4.0 cm) and soaked in nitric acid for 20 min to remove the dye layer deposited on the polycarbonate grating side. The grating substrate was cleaned sequentially by using first a commercial detergent, then water, then distilled water, and finally DI water. After cleaning, the BD-Rs were coated with a 150 nm Au film via vacuum evaporation as shown in Figure 2.2.



**Figure 2.2** Au vacuum evaporator.

#### 2.4.4 Indium Tin Oxide (ITO) glass substrate cleaning

ITO glasses with a sheet resistance ( $R_s$ ) of 10  $\Omega$ /sq were prepared with the size of 25 mm x 33 mm. After that, they were cleaned by dishwashing liquid, tap water, distilled water and DI water respectively in an ultrasonic bath for 20 min each. Then, they were dried in an oven at 60°C for 3 h. Finally, ITO glasses were cleaned in the Ultraviolet Ozone cleaning for 30 min.

#### 2.4.5 Fabrication and characterization of dye/TiO<sub>2</sub> films and dye/Au-loaded TiO<sub>2</sub> films

TiO<sub>2</sub> or Au-loaded TiO<sub>2</sub> nanopowders obtained from the modified sol–gel method were coated onto the Au films by electrophoretic deposition as shown in Figure 2.3. A voltage of 1.7 V was applied between a BD-R/Au cathode and an ITO anode for 300 s in 25 mM of TiO<sub>2</sub> or Au-loaded TiO<sub>2</sub> nanopowders dispersed in water.

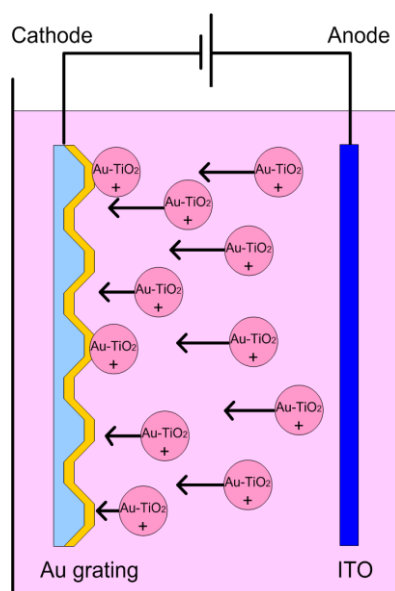


**Figure 2.3** Preparation of Au-TiO<sub>2</sub> film by electrophoretic deposition method.

After the deposition of TiO<sub>2</sub> or Au-loaded TiO<sub>2</sub>, BD-R/Au/TiO<sub>2</sub> or BD-R/Au/Au-loaded TiO<sub>2</sub> substrates were annealed at 100°C for 3 h under ambient conditions. For the dye, 5,10,15,20-Tetrakis (1-methyl-4-pyridinio) porphyrin tetra(p-toluenesulfonate) (TMPyP, Sigma-Aldrich) and sodium copper chlorophyllin (SCC, Sigma-Aldrich) were coated using a layer-by-layer (LbL) dip coating technique [57, 58]. As shown in Figure 2.4, BD-R/Au/TiO<sub>2</sub> or BD-R/Au/Au-loaded TiO<sub>2</sub> substrates were soaked first in SCC (0.25 mg mg/1) and then in TMPyP (0.25 mg mg/1) for 15 min each; this cycle was repeated until 20 bilayers were formed. Each layer was rinsed twice with DI water for 2 min.

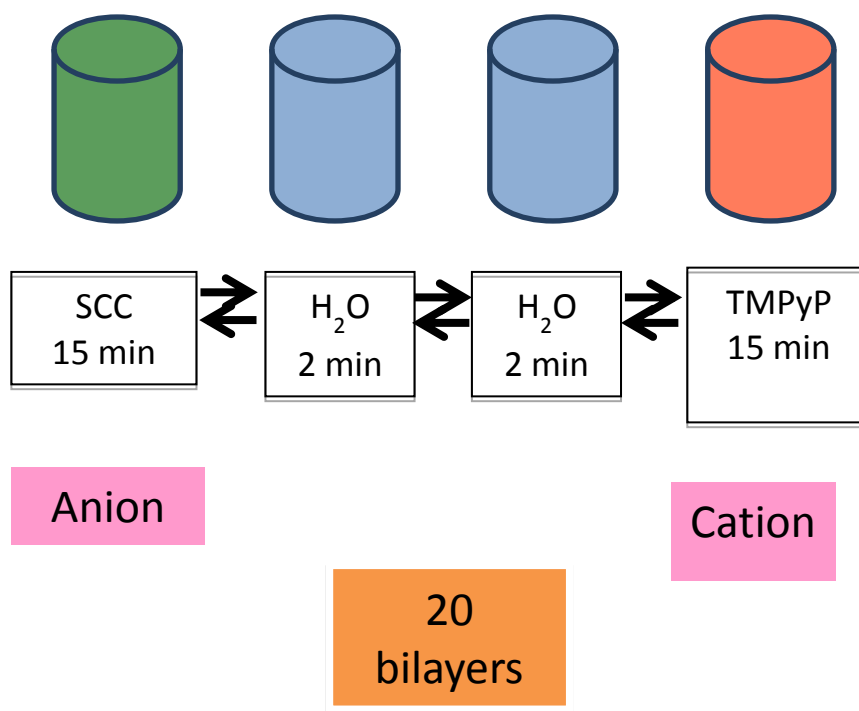


**Figure 2.4** Preparation of Au-TiO<sub>2</sub> film by electrophoretic deposition method.

Ferrous sulfate heptahydrate ( $\text{FeSO}_4 \cdot 7\text{H}_2\text{O}$ , 0.1 M, Sigma-Aldrich) and sodium sulfate ( $\text{Na}_2\text{SO}_4$ , 1 M, Sigma-Aldrich) were used as the electrolyte. An ITO glass substrate with a sheet resistance of  $10 \Omega/\text{sq}$  was used as the cathode. A schematic diagram of the fabricated DSSCs is shown in Figure 2.5.

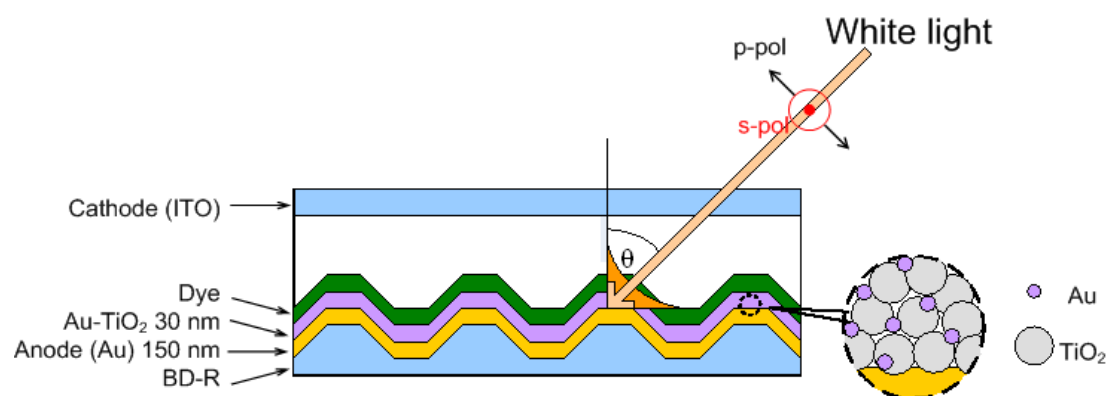


**Figure 2.5** Scheme of fabricated dye-sensitized solar cells (DSSCs).

## 2.5 Results and discussion

### 2.5.1 Surface morphology of the fabricated thin film on Au grating substrate

Figure 2.6 shows AFM image of BD-R grating and the fabricated 1.0 mol% Au-TiO<sub>2</sub> thin film on Au grating substrate. From the results, it could be confirmed that Au-TiO<sub>2</sub> thin film could be deposited on Au grating substrate by using electrophoretic deposition method. Moreover, grating structure of the substrates still remains after the deposition of Au-TiO<sub>2</sub>.

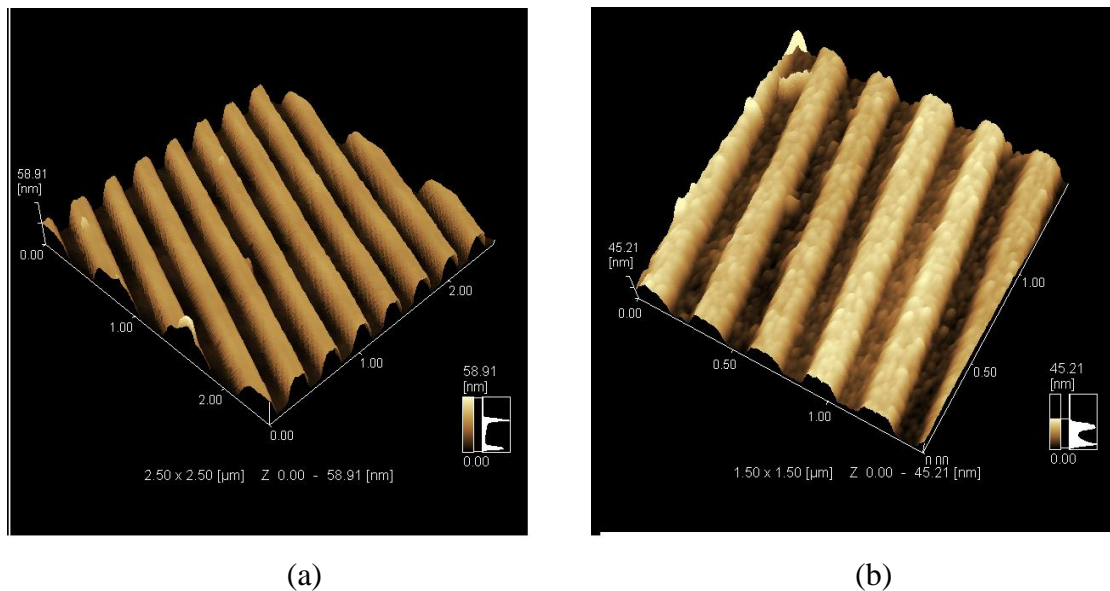


**Figure 2.6** AFM image of (a) BD-R grating and (b) the fabricated 1.0 at% Au-TiO<sub>2</sub> thin film on Au grating substrate (Film thickness = 30 nm).



## 2.5.2 White light-SPR measurements

SPR reflectivity curves for the BD-R grating/Au (*ca.* 150 nm)/Au-TiO<sub>2</sub> film (*ca.* 30 nm)/20 bilayers of SCC-TMPyP LbL film/electrolyte/ITO substrate structure were measured as a function of wavelength. Incident angles were fixed at 20–50°. As shown in Figure 2.7, SPR dip angles shift to longer wavelengths with increasing incident angle. These results show that the SP phenomena of the samples can be observed and that enhanced electric fields could be obtained on the fabricated grating surface. The SPR dips for incident angles of 25–30° corresponded to the absorption peak of TMPyP-SCC LbL at 640 nm [17].

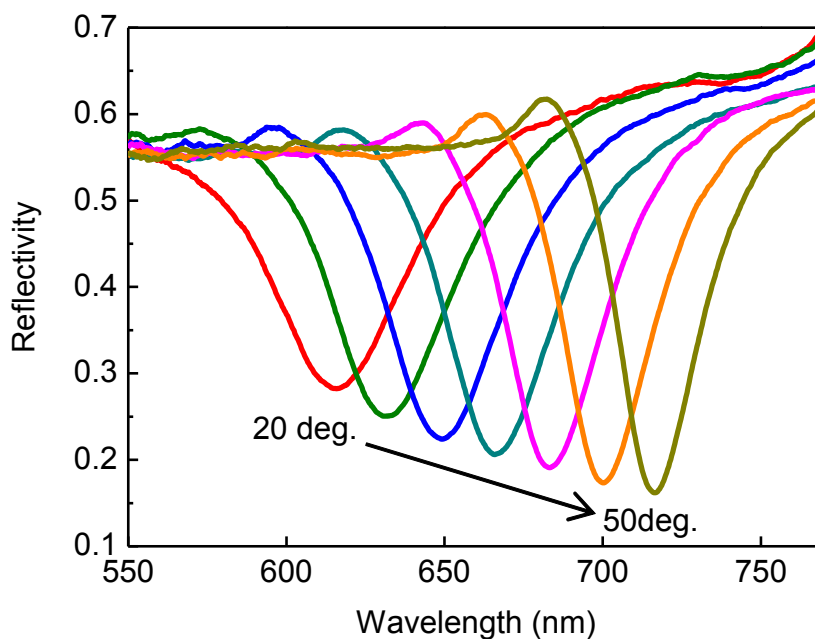


**Figure 2.7** SPR reflectivity curves for the fabricated DSSC measured at fixed incident angles of 20–50°.

### 2.5.3 Short-circuit photocurrent measurements

The effect of surface plasmon excitation on the short-circuit photocurrent was studied by irradiating visible light (490–740 nm, xenon lamp) with the light intensity of  $15.5 \text{ mW/cm}^2$  on the fabricated DSSCs. Figure 2.8 shows measurements of the short-circuit photocurrent with grating-coupled propagating SP (p-polarized light (p-pol.)) excitation and without grating-coupled propagating SP (s-polarized light (s-pol.)) excitation. After turning on the light, the photocurrent increased and then remained stable. As seen in the figure, irradiation with visible light results in a higher photocurrent when grating-coupled propagating SP excitation is present than when it is not.

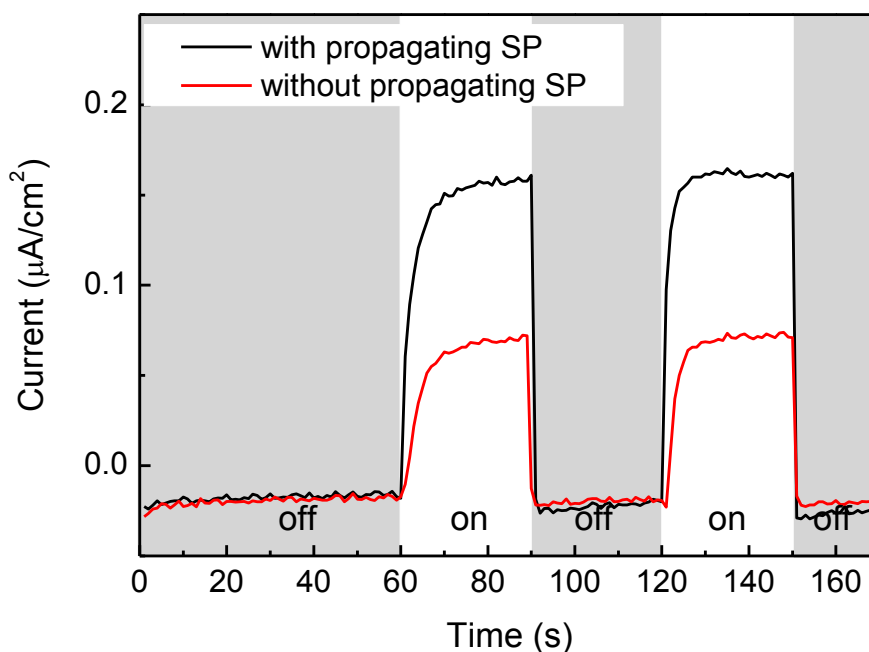


**Figure 2.8** Short-circuit photocurrent properties of the DSSC composed of Au grating/Au-TiO<sub>2</sub>/TMPyP-SCC LbL (20 bilayers)/electrolyte/ITO substrate upon irradiation of visible light with surface plasmon excitation (p-pol.) and without SP excitation (s-pol.).

To further study the effects of Au-loaded TiO<sub>2</sub>, the short-circuit photocurrents of DSSCs with unloaded TiO<sub>2</sub> and Au-loaded TiO<sub>2</sub> were compared at incident angles of 0–35° with and without grating-coupled propagating SP excitation. The thickness of both unloaded TiO<sub>2</sub> and Au-loaded TiO<sub>2</sub> layers were controlled to be *ca.* 30 nm. Figures 2.9, 2.10 and 2.11 show the relationship between the short-circuit photocurrent of DSSCs with 0–1.0 mol% Au-loaded TiO<sub>2</sub> and the incident visible light angles with and without grating-coupled propagating SP. The results showed that the short-circuit photocurrents of fabricated DSSCs with Au-loaded TiO<sub>2</sub> thin films were higher than that of fabricated DSSCs with unloaded TiO<sub>2</sub> thin films. Moreover, it was found that the photocurrent increased when the amounts of Au increased from 0.25 mol% up to 1.00 mol%. This clearly indicates that the Au-loaded TiO<sub>2</sub> enhances the photocurrent of the DSSC. Furthermore, the highest photocurrent was obtained at 25° in all DSSCs; this corresponded to the overlap between the grating-coupled propagating SPR excitation wavelength and the absorption peak wavelength of the dye. In each case, grating-coupled propagating SP further increased the values of the photocurrents beyond the effects of Au-loading TiO<sub>2</sub>. The short-circuit photocurrent of DSSCs with unloaded TiO<sub>2</sub>, 0.25 mol% Au-loaded TiO<sub>2</sub>, 1.0 mol% Au-loaded TiO<sub>2</sub> are shown in Table 2.3, 2.4 and 2.5, respectively.

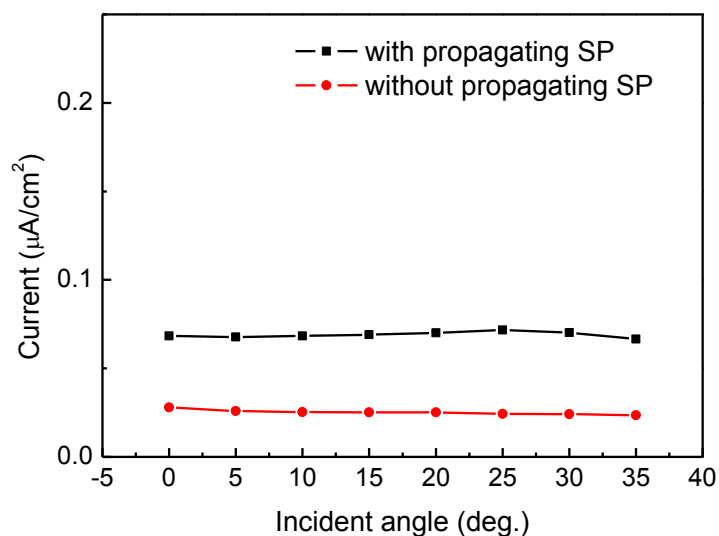


**Figure 2.9** Short-circuit photocurrents of the DSSC composed of the Au grating/Au-TiO<sub>2</sub>/TMPyP-SCC LbL (20 bilayers)/ electrolyte/ITO substrate upon irradiation with visible light at various incident angles with SP excitation (p-pol.) and without SP excitation (s-pol.) by using unloaded TiO<sub>2</sub> at incident angles of 0–35°.

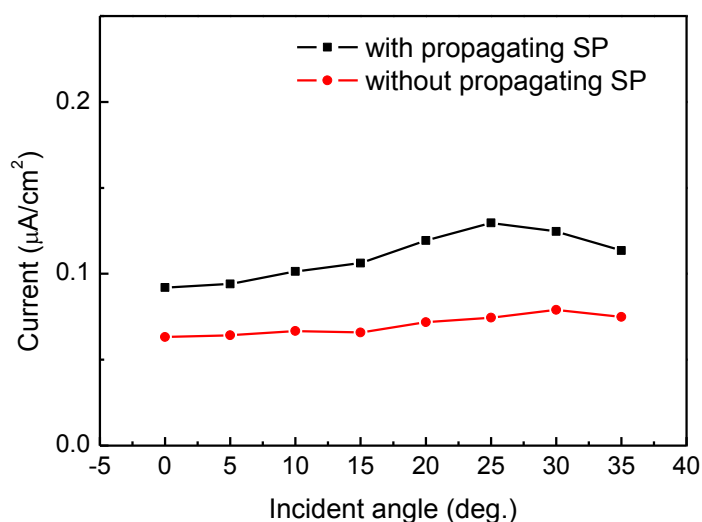


**Figure 2.10** Short-circuit photocurrents of the DSSC composed of the Au grating/Au-TiO<sub>2</sub>/TMPyP-SCC LbL (20 bilayers)/ electrolyte/ITO substrate upon irradiation with visible light at various incident angles with SP excitation (p-pol.) and without SP excitation (s-pol.) by using 0.25 mol% Au-TiO<sub>2</sub> at incident angles of 0–35°.

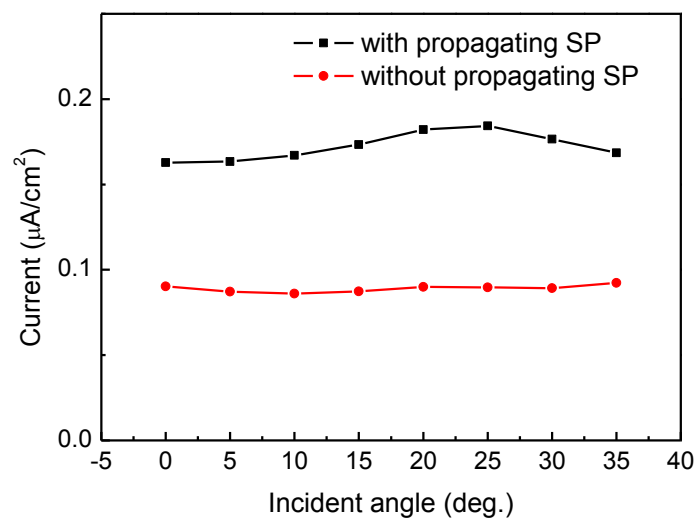


**Figure 2.11** Short-circuit photocurrents of the DSSC composed of the Au grating/Au-TiO<sub>2</sub>/TMPyP-SCC LbL (20 bilayers)/ electrolyte/ITO substrate upon irradiation with visible light at various incident angles with SP excitation (p-pol.) and without SP excitation (s-pol.) by using 1.00 mol% Au-TiO<sub>2</sub> at incident angles of 0–35°.

**Table 2.3** Short-circuit photocurrents of the DSSC composed of the Au grating/TiO<sub>2</sub>/TMPyP-SCC LbL (20 bilayers)/electrolyte/ITO substrate upon irradiation with visible light at various incident angles with SP excitation (p-pol.) and without SP excitation (s-pol.).

Incident angle (deg.)	Current ( $\mu\text{A}/\text{cm}^2$ )	
	Without propagating SP	With propagating SP
0	0.028	0.068
5	0.026	0.068
10	0.025	0.068
15	0.025	0.069
20	0.025	0.07
25	0.024	0.071
30	0.024	0.07
35	0.024	0.067

**Table 2.4** Short-circuit photocurrents of the DSSC composed of the Au grating/0.25 mol% Au-TiO<sub>2</sub>/TMPyP-SCC LbL (20 bilayers)/electrolyte/ITO substrate upon irradiation with visible light at various incident angles with SP excitation (p-pol.) and without SP excitation (s-pol.).

Incident angle (deg.)	Current ( $\mu\text{A}/\text{cm}^2$ )	
	Without propagating SP	With propagating SP
0	0.063	0.092
5	0.064	0.094
10	0.067	0.101
15	0.066	0.106
20	0.072	0.112
25	0.074	0.130
30	0.079	0.125
35	0.075	0.114

**Table 2.5** Short-circuit photocurrents of the DSSC composed of the Au grating/1.00 mol% Au-TiO<sub>2</sub>/TMPyP-SCC LbL (20 bilayers)/electrolyte/ITO substrate upon irradiation with visible light at various incident angles with SP excitation (p-pol.) and without SP excitation (s-pol.).

Incident angle (deg.)	Current ( $\mu\text{A}/\text{cm}^2$ )	
	Without propagating SP	With propagating SP
0	0.090	0.163
5	0.087	0.163
10	0.086	0.167
15	0.087	0.173
20	0.090	0.182
25	0.090	0.184
30	0.089	0.177
35	0.092	0.168



#### **2.5.4 The enhancement of short-circuit photocurrent**

The enhancement of short-circuit photocurrent by the excitation of SP with Au loading was studied. Figure 2.12 shows the enhanced photocurrent factor—i.e., the ratio of the current in each sample to the current with unloaded TiO<sub>2</sub> without propagating SP excitation—as a function of the incident light angle, as summarized in Table 2.6. The results showed that the photocurrent of unloaded TiO<sub>2</sub> with grating-coupled propagating SP excitation increased by more than a factor of 2 as compared to that of TiO<sub>2</sub> without the SP excitation. This corresponds well with our previous results [17]. For 1.0 mol% Au-loaded TiO<sub>2</sub> without grating-coupled propagating SP, an enhancement factor of more than 3 could be obtained as compared to that of unloaded TiO<sub>2</sub> without grating-coupled propagating SP. Larger amounts of Au loading could result in a stronger enhancement. Moreover, when the 1.0 mol% Au-loaded TiO<sub>2</sub> was combined with grating-coupled SP excitation, an enhancement factor of more than 7 at 25° was obtained. This large enhancement is caused by the strong field enhancement of SP excitation due to interactions between the grating-coupled propagating SP excitation and Au nanoparticles on TiO<sub>2</sub>. SP excitation could generate more excitons in the active layer leading to electron injection into the conduction band of TiO<sub>2</sub> [18, 54]. Besides the effect of SP excitation on the grating-Au loaded TiO<sub>2</sub>, the loaded Au could also increase light scattering that could generate more photon absorption at the active layer [53, 55]. Therefore, the largest increase in photocurrent was obtained by combining propagating SP with Au-loaded TiO<sub>2</sub>.

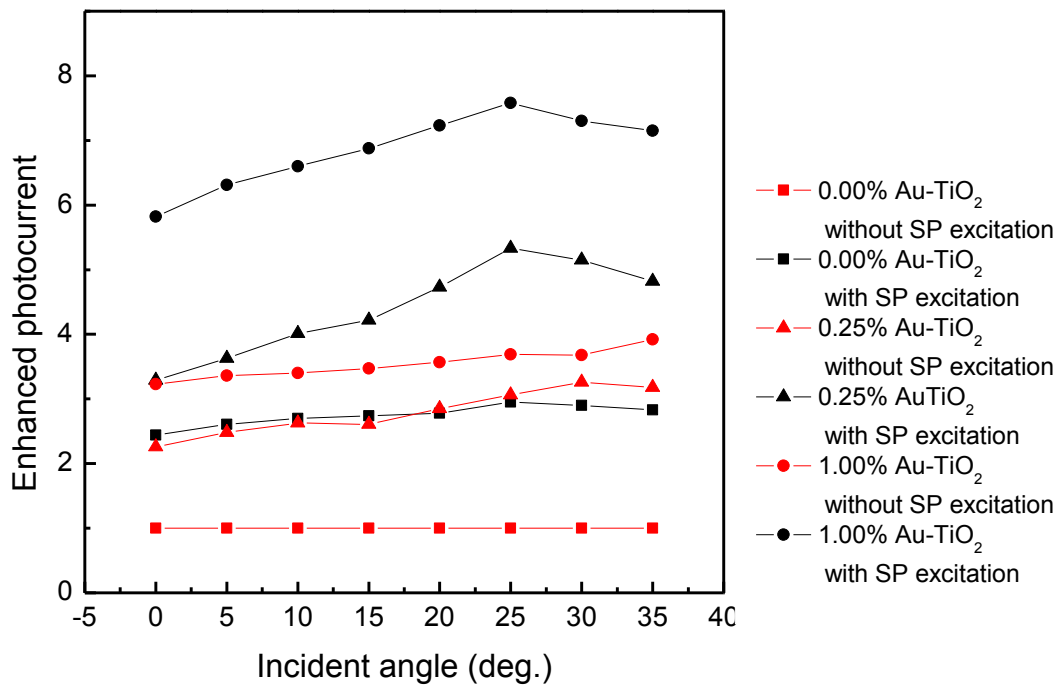


**Figure 2.12** Enhanced photocurrent factor as a function of the incident light angle. Here the enhancement factor is the ratio of the measured current in each sample to the current with unloaded TiO<sub>2</sub> and without propagating SP excitation.

**Table 2.6** Enhanced photocurrent factor, as a function of the incident light angle, of the fabricated DSSC.

Incident angle (deg.)	Enhanced photocurrent factor					
	Unloaded TiO <sub>2</sub>		0.25 mol% Au-TiO <sub>2</sub>		1.00 mol% Au-TiO <sub>2</sub>	
	Without propagating SP	With propagating SP	Without propagating SP	With propagating SP	Without propagating SP	With propagating SP
0	1.00	2.43	2.25	3.29	3.21	5.82
5	1.00	2.62	2.46	3.62	3.35	6.27
10	1.00	2.72	2.68	4.04	3.44	6.68
15	1.00	2.76	2.64	4.24	3.48	6.92
20	1.00	2.80	2.88	4.48	3.60	7.28
25	1.00	2.96	3.08	5.42	3.75	7.67
30	1.00	2.92	3.29	5.21	3.71	7.38
35	1.00	2.79	3.13	4.75	3.83	7.00

## 2.6 Conclusions

DSSCs composed of the Au grating/Au-loaded TiO<sub>2</sub>/TMPyP-SCC LbL (20 bilayers)/ electrolyte/ITO substrates were fabricated. Au-loaded TiO<sub>2</sub> films were deposited by electrophoretic deposition. TMPyP and SCC were used as photo-absorbing dyes and were prepared by LbL deposition. The fabricated cells were irradiated with visible light at various incident angles with SP excitation (p-pol.) and without surface plasmon excitation (s-pol.). The results show that up to a 7.5-fold increase in the short-circuit photocurrent can be obtained by combining Au-loaded TiO<sub>2</sub> with grating-coupled surface plasmon excitation in the cells.

## REFERENCE

- [1] A. Fujishima, T. N. Rao, and D. A. Tryk, "Titanium dioxide photocatalysis," *Journal of Photochemistry and Photobiology C: Photochemistry Reviews*, vol. 1, no. 1, pp. 1–21, 2000.
- [2] K. Pirkanniemi and M. Sillanpää, "Heterogeneous water phase catalysis as an environmental application: a review," *Chemosphere*, vol. 48, no. 10, pp. 1047–1060, 2002.
- [3] Y. Hu, H. L. Tsai, and C. L. Huang, "Effect of brookite phase on the anatase–rutile transition in titania nanoparticles," *Journal of the European Ceramic Society*, vol. 23, no. 5, pp. 691–696, 2003.
- [4] V. Samuel, R. Pasricha, and V. Ravi, "Synthesis of nanocrystalline rutile," *Ceramics International*, vol. 31, no. 4, pp. 555–557, 2005.
- [5] B. O'Regan and M. Gratzel, "A low-cost, high-efficiency solar cell based on dye-sensitized colloidal TiO<sub>2</sub> films," *Nature*, vol. 353, no. 6346, pp. 737–740, 1991.
- [6] K. G. Deepa, P. Lekha, and S. Sindhu, "Efficiency enhancement in DSSC using metal nanoparticles: A size dependent study," *Solar Energy*, vol. 86, no. 1, pp. 326–330, 2012.
- [7] H. A. P. Atwater, Albert, "Plasmonics for improved photovoltaic devices," *Nature Materials*, vol. 9, no. 3, pp. 205–213, 2010.

- [8] V. E. Ferry, J. N. Munday, and H. A. Atwater, "design considerations for plasmonic photovoltaics," *Advanced Materials*, vol. 22, no. 43, pp. 4794–4808, 2010.
- [9] B. Sebo, N. Huang, Y. Liu, Q. Tai, L. Liang, H. Hu, S. Xu, and X.-Z. Zhao, "Dye-sensitized solar cells enhanced by optical absorption, mediated by TiO<sub>2</sub> nanofibers and plasmonics Ag nanoparticles," *Electrochimica Acta*, vol. 112, no. 0, pp. 458–464, 2013.
- [10] H. M. N. Bandara, R. M. G. Rajapakse, K. Murakami, G. R. R. A. Kumara, and G. Anuradha Sepalage, "Dye-sensitized solar cell based on optically transparent TiO<sub>2</sub> nanocrystalline electrode prepared by atomized spray pyrolysis technique," *Electrochimica Acta*, vol. 56, no. 25, pp. 9159–9161, 2011.
- [11] C. Jiang, W. L. Koh, M. Y. Leung, W. Hong, Y. Li, and J. Zhang, "Influences of alcoholic solvents on spray pyrolysis deposition of TiO<sub>2</sub> blocking layer films for solid-state dye-sensitized solar cells," *Journal of Solid State Chemistry*, vol. 198, no. 0, pp. 197–202, 2013.
- [12] C. Jiang, M. Y. Leung, W. L. Koh, and Y. Li, "Influences of deposition and post-annealing temperatures on properties of TiO<sub>2</sub> blocking layer prepared by spray pyrolysis for solid-state dye-sensitized solar cells," *Thin Solid Films*, vol. 519, no. 22, pp. 7850–7854, 2011.
- [13] M. Okuya, K. Nakade, and S. Kaneko, "Porous TiO<sub>2</sub> thin films synthesized by a spray pyrolysis deposition (SPD) technique and their application to dye-sensitized solar cells," *Solar Energy Materials and Solar Cells*, vol. 70, no. 4, pp. 425–435, 2002.
- [14] O. Carp, C. L. Huisman, and A. Reller, "Photoinduced reactivity of titanium dioxide," *Progress in Solid State Chemistry*, vol. 32, no. 1–2, pp. 33–177, 2004.

- [15] I. K. Ding, J. Zhu, W. Cai, S.-J. Moon, N. Cai, P. Wang, S. M. Zakeeruddin, M. Grätzel, M. L. Brongersma, Y. Cui, and M. D. McGehee, "plasmonic dye-sensitized solar cells," *Advanced Energy Materials*, vol. 1, no. 1, pp. 52–57, 2011.
- [16] V. E. Ferry, L. A. Sweatlock, D. Pacifici, and H. A. Atwater, "Plasmonic nanostructure design for efficient light coupling into solar cells," *Nano Letters*, vol. 8, no. 12, pp. 4391–4397, 2008.
- [17] A. Baba, K. Wakatsuki, K. Shinbo, K. Kato, and F. Kaneko, "Increased short-circuit current in grating-coupled surface plasmon resonance field-enhanced dye-sensitized solar cells," *Journal of Materials Chemistry*, vol. 21, pp. 16436–16441, 2011.
- [18] S. Muduli, O. Game, V. Dhas, K. Vijayamohanan, K. A. Bogle, N. Valanoor, and S. B. Ogale, "TiO<sub>2</sub>-Au plasmonic nanocomposite for enhanced dye-sensitized solar cell (DSSC) performance," *Solar Energy*, vol. 86, no. 5, pp. 1428–1434, 2012.
- [19] G. Sahu, S. W. Gordon, and M. A. Tarr, "Synthesis and application of core-shell Au-TiO<sub>2</sub> nanowire photoanode materials for dye sensitized solar cells," *RSC Advances*, vol. 2, no. 2, pp. 573–582, 2012.
- [20] L. Wu, F. Li, Y. Xu, J. W. Zhang, D. Zhang, G. Li, and H. Li, "Plasmon-induced photoelectrocatalytic activity of Au nanoparticles enhanced TiO<sub>2</sub> nanotube arrays electrodes for environmental remediation," *Applied Catalysis B: Environmental*, vol. 164, pp. 217–224, 2015.
- [21] Z. Han, Z. Zhao, Z. Du, L. Zhao, and X. Cong, "A novel anode material of TiCl<sub>4</sub> treatment on Ag/TiO<sub>2</sub> in DSSC," *Materials Letters*, vol. 136, pp. 424–426, 2014.

- [22] Y. Liu, H. Yu, H. Wang, S. Chen, and X. Quan, "Efficient H<sub>2</sub> production over Au/graphene/TiO<sub>2</sub> induced by surface plasmon resonance of Au and band-gap excitation of TiO<sub>2</sub>," *Materials Research Bulletin*, vol. 59, pp. 111–116, 2014.
- [23] H. Dong, Z. Wu, Y. Gao, A. El-Shafei, S. Ning, J. Xi, B. Jiao, and X. Hou, "Silver-loaded anatase nanotubes dispersed plasmonic composite photoanode for dye-sensitized solar cells," *Organic Electronics*, vol. 15, no. 11, pp. 2847–2854, 2014.
- [24] J. H. Lee and Y. S. Yang, "Effect of HCl concentration and reaction time on the change in the crystalline state of TiO<sub>2</sub> prepared from aqueous TiCl<sub>4</sub> solution by precipitation," *Journal of the European Ceramic Society*, vol. 25, no. 16, pp. 3573–3578, 2005.
- [25] A. Sandoval, A. Aguilar, C. Louis, A. Traverse, and R. Zanella, "Bimetallic Au–Ag/TiO<sub>2</sub> catalyst prepared by deposition–precipitation: High activity and stability in CO oxidation," *Journal of Catalysis*, vol. 281, no. 1, pp. 40–49, 2011.
- [26] H. Wang, P. Liu, X. Cheng, A. Shui, and L. Zeng, "Effect of surfactants on synthesis of TiO<sub>2</sub> nano-particles by homogeneous precipitation method," *Powder Technology*, vol. 188, no. 1, pp. 52–54, 2008.
- [27] S. S. Kalanur, S. H. Lee, Y. J. Hwang, and O.-S. Joo, "Enhanced photoanode properties of CdS nanoparticle sensitized TiO<sub>2</sub> nanotube arrays by solvothermal synthesis," *Journal of Photochemistry and Photobiology A: Chemistry*, vol. 259, pp. 1–9, 2013.
- [28] M. Kang, S.-Y. Lee, C.-H. Chung, S. M. Cho, G. Y. Han, B.-W. Kim, and K. J. Yoon, "Characterization of a TiO<sub>2</sub> photocatalyst synthesized by the solvothermal method and its catalytic performance for CHCl<sub>3</sub> decomposition," *Journal of*



*Photochemistry and Photobiology A: Chemistry*, vol. 144, no. 2–3, pp. 185–191, 2001.

- [29] Y. Lee, J. Chae, and M. Kang, "Comparison of the photovoltaic efficiency on DSSC for nanometer sized TiO<sub>2</sub> using a conventional sol–gel and solvothermal methods," *Journal of Industrial and Engineering Chemistry*, vol. 16, no. 4, pp. 609–614, 2010.
- [30] Y. Zhang, H. Zheng, G. Liu, and V. Battaglia, "Synthesis and electrochemical studies of a layered spheric TiO<sub>2</sub> through low temperature solvothermal method," *Electrochimica Acta*, vol. 54, no. 16, pp. 4079–4083, 2009.
- [31] D. Crişan, N. Drăgan, M. Răileanu, M. Crişan, A. Ianculescu, D. Luca, A. Năstută, and D. Mardare, "Structural study of sol–gel Au/TiO<sub>2</sub> films from nanopowders," *Applied Surface Science*, vol. 257, no. 9, pp. 4227–4231, 2011.
- [32] J. N. Hart, D. Menzies, Y.-B. Cheng, G. P. Simon, and L. Spiccia, "TiO<sub>2</sub> sol–gel blocking layers for dye-sensitized solar cells," *Comptes Rendus Chimie*, vol. 9, no. 5–6, pp. 622–626, 2006.
- [33] M. Hočevar, U. O. Krašovec, M. Bokalič, M. Topič, W. Veurman, H. Brandt, and A. Hinsch, "Sol-gel based TiO<sub>2</sub> paste applied in screen-printed dye-sensitized solar cells and modules," *Journal of Industrial and Engineering Chemistry*, vol. 19, no. 25, pp. 1464–1469, 2013.
- [34] C. M. Malengreaux, A. Timmermans, S. L. Pirard, S. D. Lambert, J.-P. Pirard, D. Poelman, and B. Heinrichs, "Optimized deposition of TiO<sub>2</sub> thin films produced by a non-aqueous sol–gel method and quantification of their photocatalytic activity," *Chemical Engineering Journal*, vol. 195–196, pp. 347–358, 2012.

- [35] S. Šegota, L. Čurković, D. Ljubas, V. Svetličić, I. F. Houra, and N. Tomašić, "Synthesis, characterization and photocatalytic properties of sol–gel TiO<sub>2</sub> films," *Ceramics International*, vol. 37, no. 4, pp. 1153–1160, 2011.
- [36] J. N. Hart, R. Cervini, Y. B. Cheng, G. P. Simon, and L. Spiccia, "Formation of anatase TiO<sub>2</sub> by microwave processing," *Solar Energy Materials and Solar Cells*, vol. 84, no. 1–4, pp. 135–143, 2004.
- [37] J. N. Hart, D. Menzies, Y.-B. Cheng, G. P. Simon, and L. Spiccia, "A comparison of microwave and conventional heat treatments of nanocrystalline TiO<sub>2</sub>," *Solar Energy Materials and Solar Cells*, vol. 91, no. 1, pp. 6–16, 2007.
- [38] S. Uchida, M. Tomiha, N. Masaki, A. Miyazawa, and H. Takizawa, "Preparation of TiO<sub>2</sub> nanocrystalline electrode for dye-sensitized solar cells by 28GHz microwave irradiation," *Solar Energy Materials and Solar Cells*, vol. 81, no. 1, pp. 135–139, 2004.
- [39] C. Suresh, V. Biju, P. Mukundan, and K. G. K. Warriar, "Anatase to rutile transformation in sol-gel titania by modification of precursor," *Polyhedron*, vol. 17, no. 18, pp. 3131–3135, 1998.
- [40] Q. Zhang, L. Gao, and J. Guo, "Effect of hydrolysis conditions on morphology and crystallization of nanosized TiO<sub>2</sub> powder," *Journal of the European Ceramic Society*, vol. 20, no. 12, pp. 2153–2158, 2000.
- [41] N. Wetchakun, B. Incessungvorn, K. Wetchakun, and S. Phanichphant, "Influence of calcination temperature on anatase to rutile phase transformation in TiO<sub>2</sub> nanoparticles synthesized by the modified sol–gel method," *Materials Letters*, vol. 82, pp. 195–198, 2012.

- [42] N. Wetchakun and S. Phanichphant, "Effect of temperature on the degree of anatase–rutile transformation in titanium dioxide nanoparticles synthesized by the modified sol–gel method," *Current Applied Physics*, vol. 8, no. 3–4, pp. 343–346, 2008.
- [43] H. Ninsonti, W. Chomkitichai, A. Baba, N. Wetchakun, W. Kangwansupamonkon, S. Phanichphant, K. Shinbo, K. Kato, and F. Kaneko, "Au-loaded titanium dioxide nanoparticles synthesized by modified sol-gel/impregnation methods and their application to dye-sensitized solar cells," *International Journal of Photoenergy*, vol. 2014, pp. 1–8, 2014.
- [44] M. Pan, N. Huang, X. Zhao, J. Fu, and X. Zhong, "Enhanced Efficiency of Dye-Sensitized Solar Cell by High Surface Area Anatase-TiO<sub>2</sub>-Modified P25 Paste," *Journal of Nanomaterials*, vol. 2013, pp. 1–6, 2013.
- [45] V. Dhas, S. Muduli, S. Agarkar, A. Rana, B. Hannoyer, R. Banerjee, and S. Ogale, "Enhanced DSSC performance with high surface area thin anatase TiO<sub>2</sub> nanoleaves," *Solar Energy*, vol. 85, no. 6, pp. 1213–1219, 2011.
- [46] T. Kawawaki, Y. Takahashi, and T. Tatsuma, "Enhancement of Dye-Sensitized Photocurrents by Gold Nanoparticles: Effects of Plasmon Coupling," *The Journal of Physical Chemistry C*, vol. 117, no. 11, pp. 5901–5907, 2013/03/21 2013.
- [47] C.-S. Chou, R.-Y. Yang, C.-K. Yeh, and Y.-J. Lin, "Preparation of TiO<sub>2</sub>/Nano-metal composite particles and their applications in dye-sensitized solar cells," *Powder Technology*, vol. 194, no. 1–2, pp. 95–105, 2009.
- [48] C.-H. Huang, Y.-T. Yang, and R.-A. Doong, "Microwave-assisted hydrothermal synthesis of mesoporous anatase TiO<sub>2</sub> via sol–gel process for dye-sensitized

- solar cells," *Microporous and Mesoporous Materials*, vol. 142, no. 2–3, pp. 473–480, 2011.
- [49] M. Ghaffari, M. B. Cosar, H. I. Yavuz, M. Ozenbas, and A. K. Okyay, "Effect of Au nano-particles on TiO<sub>2</sub> nanorod electrode in dye-sensitized solar cells," *Electrochimica Acta*, vol. 76, pp. 446–452, 2012.
- [50] H. S. Jung and J.-K. Lee, "Dye sensitized solar cells for economically viable photovoltaic systems," *The Journal of Physical Chemistry Letters*, vol. 4, no. 10, pp. 1682–1693, 2013.
- [51] F. J. Beck, A. Polman, and K. R. Catchpole, "Tunable light trapping for solar cells using localized surface plasmons," *Journal of Applied Physics*, vol. 105, no. 11, pp. 114310–114310–7, 2009.
- [52] J. Li, X. Chen, N. Ai, J. Hao, Q. Chen, S. Strauf, and Y. Shi, "Silver nanoparticle doped TiO<sub>2</sub> nanofiber dye sensitized solar cells," *Chemical Physics Letters*, vol. 514, no. 1–3, pp. 141–145, 2011.
- [53] D. Derkacs, W. V. Chen, P. M. Matheu, S. H. Lim, P. K. L. Yu, and E. T. Yu, "Nanoparticle-induced light scattering for improved performance of quantum-well solar cells," *Applied Physics Letters*, vol. 93, no. 9, pp. 091107–1–091107–3, 2008.
- [54] D. M. Schaadt, B. Feng, and E. T. Yu, "Enhanced semiconductor optical absorption via surface plasmon excitation in metal nanoparticles," *Applied Physics Letters*, vol. 86, no. 6, pp. 063106–1–063106–3, 2005.
- [55] S. H. Lim, W. Mar, P. Matheu, D. Derkacs, and E. T. Yu, "Photocurrent spectroscopy of optical absorption enhancement in silicon photodiodes via

scattering from surface plasmon polaritons in gold nanoparticles," *Journal of Applied Physics*, vol. 101, no. 10, pp. 104309–1–104309–7, 2007.

- [56] N. Wetchakun, "Effect of transition metal ion doping on the photocatalytic activity of titanium dioxide", Ph.D. Dissertation, Chiang Mai University, Chiang Mai, 2008.
- [57] A. Baba, T. Matsuzawa, S. Sriwichai, Y. Ohdaira, K. Shinbo, K. Kato, S. Phanichphant, and F. Kaneko, "Enhanced photocurrent generation in nanostructured chromophore/carbon nanotube hybrid layer-by-layer multilayers," *Journal of Physical Chemistry C*, vol. 114, pp. 14716–14721, 2010.
- [58] A. Baba, Y. Kanetsuna, S. Sriwichai, Y. Ohdaira, K. Shinbo, K. Kato, S. Phanichphant, and F. Kaneko, "Nanostructured carbon nanotubes/copper phthalocyanine hybrid multilayers prepared using layer-by-layer self-assembly approach," *Thin Solid Films*, vol. 518, pp. 2200–2205, 2010.

# CHAPTER 1

## Introduction

Dye-sensitized solar cells have been attracted attention and widely studies due to the high energy-conversion efficiency and high potential of low manufacture costs [1–4]. At the present time many studies on dye-sensitized solar cells (DSSCs) have been reported [5–8]. Titanium dioxide ( $\text{TiO}_2$ ) is one of the most efficient for dye-sensitized solar cells (DSSCs) due to its chemical stability, nontoxicity, good electrical properties and inexpensiveness [5–8].

It was previously reported that the short-circuit photocurrent in organic solar cells could be increased by using grating-coupled surface plasmon (SP) excitations, in which a blu-ray disc recordable (BD-R) is used as a grating substrate [2, 9]. The increased optical field by the SP excitation was used to enhance the photovoltaic properties of DSSCs because the active thin film can absorb more light, and it could generate more photocarriers, resulting in an increased photocurrent for the DSSCs [10–12]. Grating-coupled SP excitations, which propagate adjacent to the grating metallic surface have been widely used in various applications [13–17]. Therefore, the use of grating-structured Ag on DSSCs should enhance the photovoltaic properties of these systems [18, 19].

The use of Au- $\text{TiO}_2$  on a metallic grating to enhance the photocurrent of photoanodes was also reported [17]. Metal nanoparticles have been known as potential sensitizers in photovoltaics. Metal nanoparticles have very high absorption and scattering cross sections [20]. Varying size and shape of metal nanoparticles could be modified throughout the visible region to the near infrared. Metal particles could enhance photovoltaic performance at least three different ways [20]. In the first case, the local near field enhancement related with surface plasmon excitation is used to increase charge carrier generation. A second case uses the high scattering property of metal nanoparticles at the surface plasmon resonance wavelengths to re-direct light into a

solar cell substrate. The third case is to use metal nanoparticles as the light harvesting part inducing charge separation in a photovoltaic cell [20].

In Chapter 2,  $\text{TiO}_2$  and Au-loaded  $\text{TiO}_2$  nanoparticles were synthesized by the modified sol-gel technique and coupling the modified sol-gel with impregnation technique respectively. The preparation of  $\text{TiO}_2$  by the modified sol-gel method using cellophane membrane was performed to decrease the diffusion rates of reactants in hydrolysis and condensation steps. This synthesis technique had many advantages such as excellent reproducibility, excellent ability to acquire  $\text{TiO}_2$  in nano-sized scale and excellent fabrication for high purity products [21, 22]. The obtained nanoparticles were used to enhance DSSCs performance. Dye/Au-loaded  $\text{TiO}_2$  films were fabricated on an Au grating surface to couple with surface plasmon resonance (SPR) to further enhance the photocurrent in DSSCs.

In Chapter 3, the fabrication of a grating structure consisting of a solid-state electrolyte layer on a dye- $\text{TiO}_2$  film formed by the nanoimprint technique using a polydimethylsiloxane (PDMS) stamp was studied. The application of this grating in solid-state DSSCs is also described. The PDMS grating pattern was imprinted from a BD-R. A silver electrode was deposited on the patterned solid-state electrolyte layers. Surface plasmon resonance (SPR) excitation was observed in the fabricated solar cells by irradiation with white light at the imprinted grating surface. The photoelectric conversion properties were measured to study the effect of the two types of SPR excitations, i.e., the propagating surface plasmon on the Ag grating surface and the localized surface plasmon from the Au nanoparticles on  $\text{TiO}_2$ .

## 1.1 Titanium dioxide (TiO<sub>2</sub>) [23, 24]

Titanium dioxide (TiO<sub>2</sub>) exists in nature in three crystallographic phases: rutile, anatase, and brookite, with the anatase the most commonly employed in photo-catalytic applications. Anatase is the polymorph of TiO<sub>2</sub> with less thermodynamically stable, although from energy calculations this phase appears as the more likely phase when the grain size is around 10 nm. The crystalline structure can be described in terms of TiO<sub>6</sub> octahedral chains differing by the distortion of each octahedron and the assembly pattern of octahedral chains. The Ti-Ti distances in the anatase structure are greater than in rutile, whereas Ti-O distances are shorter. These structural differences cause different mass densities and lead to a different electronic structure of the bands. Anatase phase is 9% less dense than rutile, presenting more pronounced localization of the Ti 3*d* states, and therefore, a narrower 3*d* band can be found in the anatase phase. Also the O 2*p*-Ti 3*d* hybridization is different in the two structures (more covalent mixing in the rutile), with anatase exhibiting a valence and conduction band with more pronounced O 2*p*-Ti 3*d* characters, respectively. These different structural features are presumably responsible for the difference in the mobility of charge carriers. Although the anatase-TiO<sub>2</sub> presents the higher photoactivities reported, commercial Degussa P25, which has a mixture of anatase and rutile in a ratio 80:20, is one of the best TiO<sub>2</sub> photo-catalysts and frequently used as a reference. The anatase-rutile coexistence would lead to a synergetic effect between the two phases that improves the photoactivity of TiO<sub>2</sub>, as has been reported by several authors for anatase-rutile mixtures prepared by different methods. This junction effect has been also described for the mixture anatase-brookite, which presents a high activity in gas-phase methanol photo-oxidation.



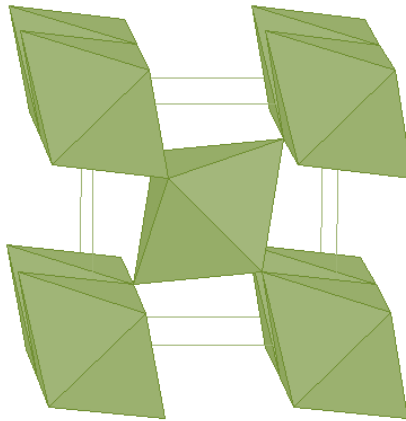


**Figure 1.1** The crystal structure of rutile TiO<sub>2</sub> [24].

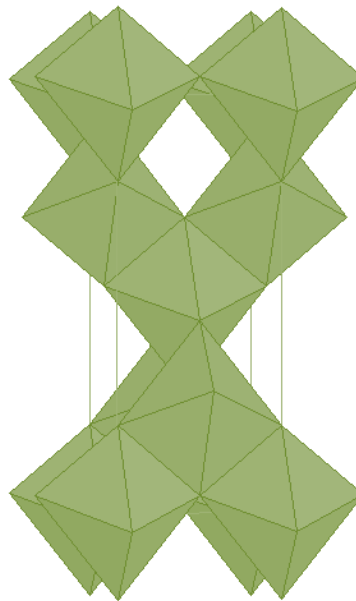


**Figure 1.2** The crystal structure of anatase TiO<sub>2</sub> [24].

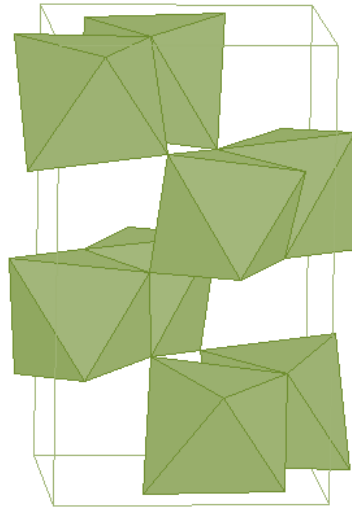


**Figure 1.3** The crystal structure of brookite TiO<sub>2</sub> [24].

**Table 1.1** Crystal structure properties of TiO<sub>2</sub> [24, 25].

		Crystal structure		
		Rutile	Anatase	Brookite
<b>System</b>		Tetragonal	Tetragonal	Rhombohedral
<b>Space group</b>		D <sub>4h</sub> <sup>14</sup> -P4 <sub>2</sub> /mm	D <sub>4h</sub> <sup>19</sup> -I4 <sub>1</sub> /amd	D <sub>2h</sub> <sup>15</sup> -Pbca
<b>Lattice constants (nm)</b>	<b>a</b>	0.4584	0.3733	0.5436
	<b>b</b>	-	-	0.09166
	<b>c</b>	0.2953	0.937	0.5135
	<b>c/a</b>	0.644	2.51	0.944
<b>Density (kg/m<sup>3</sup>)</b>		4240	3830	4170
<b>Band gap (eV)</b>		3.0 (indirect)	3.2 (indirect)	-

## 1.2 Dye-sensitized solar cells (DSSCs)

In 1991, O'Regan and Grätzel first introduced a high conversion efficiency DSSCs [26]. After that, many studies on dye-sensitized solar cells (DSSCs) have been reported due to their high efficiency property and low cost of materials [1, 11, 27–32]. In the active layer of DSSCs, a monolayer of organic dye molecules covered with covalent bond on anatase TiO<sub>2</sub> film is generally used [33]. To improve light harvesting by light scattering and localized surface plasmon properties of DSSCs, metal nanoparticles were used [28]. Metal nanoparticles have the scattering property which could increase its probability of exciting dye molecule. More electrons to be injected into TiO<sub>2</sub> conduction band due to the increased absorption in the dye. Therefore, the photocurrent of the device could be enhanced [28]. Localized surface plasmon excitation is a collective oscillation of electron in metal particles by incident light excitation. It could enhance the electric field on photoanode of DSSCs in order to increase the optical absorption. Therefore it has been widely used to improve the DSSCs performance [1, 11, 27, 28]. Moreover, metal nanoparticle could perform as electron acceptor from the photo-excited metal oxide. Therefore, electron transfer rate could be improved and the increasing of photocurrent was obtained [1, 3, 34].

### 1.2.1 Dye-sensitized solar cells (DSSCs) system [35]

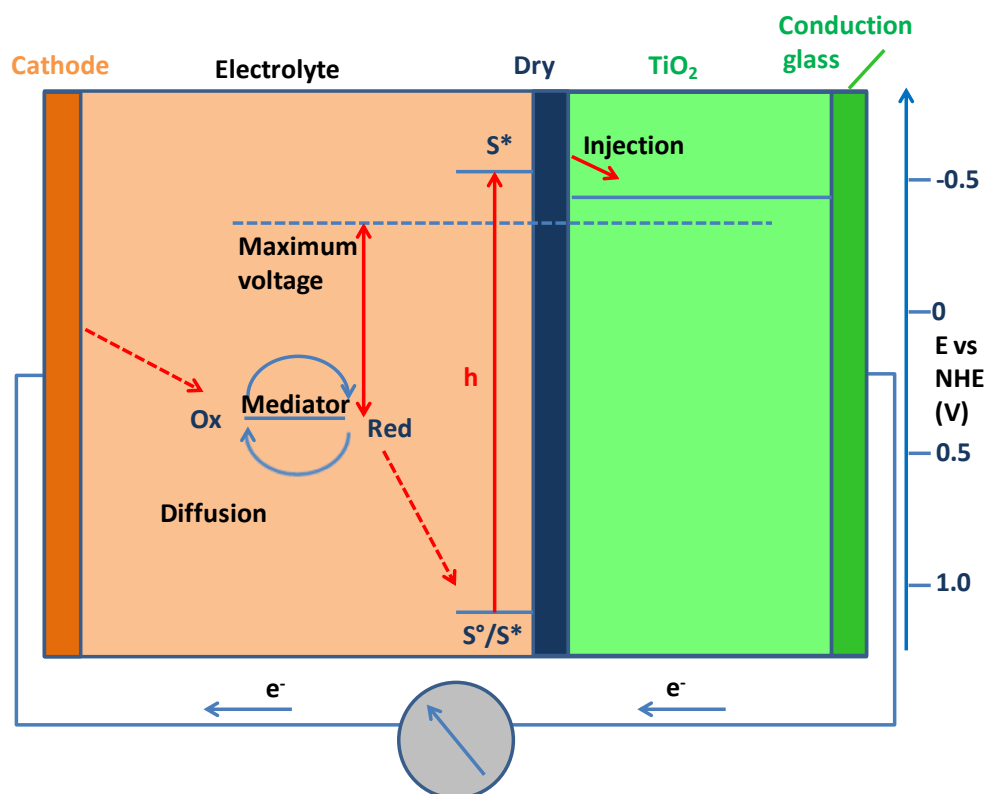


**Figure 1.4** Theory of process and energy level scheme of the dye-sensitized  $\text{TiO}_2$  solar cell [35].

Figure 1.4 shows a scheme of the DSSC system. Photoexcitation of the sensitizer (S) is followed by electron injection into the conduction band of an oxide semiconductor film. The dye molecule is regenerated by the redox system, which itself is regenerated at the counter-electrode by electrons passed through the load. Potentials are referred to the normal hydrogen electrode (NHE). The open circuit voltage of the solar cell corresponds to the difference between the redox potential of the mediator and the Fermi level of the nanocrystalline film indicated with a dashed line. The energy levels drawn for the sensitizer and the redox mediator match the redox potentials of the doubly deprotonated  $\text{N}_3$  sensitizer ground state and the iodide/triiodide couple.

For dye-sensitized solar cells (DSSCs) photo anode, various kind of wide band gap metal oxide nanoparticles film such as  $\text{TiO}_2$ ,  $\text{ZnO}$ ,  $\text{SnO}_2$  and  $\text{Nb}_2\text{O}_5$  have been used.  $\text{TiO}_2$  film is the most popular material that is positioned in contact with a redox couple of iodine and tri-iodide electrolyte. A monolayer of the dye sensitizer is formed on the surface of the  $\text{TiO}_2$  film. When DSSCs is exposed to the light, electron of dye will be excited and will be injected to the conduction band of the  $\text{TiO}_2$ . The original state of the dye is then restored by electron donation from the redox couple of iodine and tri-iodide electrolyte. The regeneration of the sensitizer by iodide intercepts the recapture of the conduction band electron by the oxidized dye. The iodide is regenerated in turn by the reduction of triiodide at the counter-electrode the circuit being completed via electron migration through the external load. The voltage generated under irradiation corresponds to the difference between the Fermi level of the electron in the solid and the redox potential of the electrolyte. Overall the device generates electric power from light without suffering any lasting chemical transformation. The first laboratory embodiment of the dye-sensitized solar cell dates back to 1988 [36]. The photo-anode was a titanium sheet covered with a high surface area “fractal”  $\text{TiO}_2$  film that was produced by a sol-gel method. The roughness factor of the film was about 150. The surface of the fractal film was derivatized with the yellow ruthenium dye  $\text{RuL}_3$  ( $\text{L} = 2,2\text{-bipyridyl-4,4,-dicarboxylate}$ ). A cylindrical platinum wire mesh electrode served as a counter-electrode. The beaker was filled with slightly acidic (pH ca. 4.5) aqueous electrolyte containing bromide and small amounts of bromine. The open circuit voltage of the cell was 1V under illumination with a halogen spotlight. The device converted more than 60% of the incident photons to electric current at the absorption maximum of the sensitizer near 470 nm and the overall conversion efficiency in full sunlight was between 1 and 2%.

## **1.2.2 Type of DSSCs [35, 37–53]**

### **(1) Liquid electrolyte based DSSCs [37]**

The nano-structuring of TiO<sub>2</sub> led to significant enhancement in the surface area of the interface resulting in an enhancement of the photo-current density in the device. Under the action of light the dyes undergo an excitonic splitting with the formation of a free electron/free hole pair, whereby the electrons are injected into the TiO<sub>2</sub> at an particularly rapid timescale (around 10 ps) and the holes are transported (relatively slowly) through the liquid electrolyte to the counter-electrode. The procedure involves the re-reduction of dyes, which are oxidized after losing an electron; however the charged state of dye is quickly replenished by the uptake of an electron from redox electrolyte leading to charge transport and overall chemical balance of the system. The recombination of charge carriers involved in the process is normally low, typically at a few milliseconds, leading to an efficient charge separation.

Despite the low cost methods of processing used for DSSCs fabrication, such as screen printing, spraying, doctor blading, etc., the technology has not come up to the initial cost-reduction expectations, at the commercial level; this is due to a multitude of engineering issues, such as encapsulation and sealing of the device, loss of iodine from the liquid electrolyte, degradation because of atmospheric moisture/ oxygen ingress etc. On the other hand, the stability of the dyes themselves, as used in the devices, has been found to be reasonably good. The dyes N719 (hydrophilic), Z907 (hydrophobic), Y123 (organic), generally used for DSSC devices have been found to be commercially scalable and substantially stable.

Although an excellent progress has been made towards acceptable stable performance of the devices documented by stability tests both indoors and outdoors, however, there are still barriers for the longevity of the DSSC modules at a commercial level. These arise mainly from the liquid electrolyte component, which limits the device's prospects for market penetration.

## **(2) Quasi solid state DSSCs [37]**

The electrolytes are one of the key components, which can greatly affect the conversion efficiencies of the DSSCs. Alternative approaches of using polymer electrolytes were reported earlier to overcome scale up challenges inherent with the liquid electrolyte based devices [35, 38, 39]. Ever since, different approaches were attempted with the use of ionic liquids or polymer gel electrolytes (PGEs). By using PAN-VA (poly(acrylonitrile-co-vinyl acetate)) co-polymers, the highest conversion efficiencies up to 10.5% were reported [40]. This was achieved by improving the efficiency of the gelators. The devices with PAN-VA co-polymers were proved to be very stable. PGEs, a potential alternative to liquid and solid electrolytes, have high ionic conductivity and good stability. This is because the polymer matrix in PGEs can effectively trap the liquid solvent to inhibit evaporation and meanwhile provide channels for fast transport of redox couples [41, 42]. Therefore, photovoltaic performances of the DSSCs fabricated with some specialized PGEs were found to be comparable to those of solar cells based on liquid electrolytes. Although better sealing advantages are inherent, the performance of such quasi-solid state devices are still below that of liquid electrolyte based devices owing to their lower ionic conductivity and reduced pore penetration into the mesoporous TiO<sub>2</sub> matrix as compared to their liquid counterparts. Besides, there is a lack of reliable long term stability data available for such systems. Nevertheless, the recent laboratory developments are likely to generate more industrial interests in the future.

## **(3) Quantum dot sensitised solar cells [37, 43–46].**

Dyes (organic and inorganic) are another vital component of the DSSCs device which inherently suffer from the limitations of narrow absorption peaks mostly below 700 nm limiting, thus, the coverage of whole solar spectrum. The limitations of the dyes can be largely overcome by the use of inorganic quantum dots. The advantages of the quantum dots (QDs) such as easy tuning of bandgap, larger extinction coefficient with wider spectral coverage, high stability and the possibility of multiple exciton generation from the absorption of a single photon makes them a very attractive and promising candidate for a future DSSC technology [43–46].

#### **(4) Flexible DSSCs [37, 38, 47–50]**

Flexible solar cells have opened new and emerging applications in the mobile and wearable electronic industries. The performance of the flexible substrate based DSSCs is relatively poor compared to flexible thin film CIGS technology (EMPA world record at 20.4% on polyimide foil), which outperform them in terms of efficiency and long term stability including bending tests. Nevertheless, DSSC may have advantage as they can be produced on a flexible foil using lower processing temperature below 150 °C [38]. The urge for higher efficiency on flexible DSSCs has led to many different approaches in modifying the TiO<sub>2</sub> paste preparation conditions [47–50] and different post deposition treatments [48, 49] on photoanodes to improve the adhesion as well as necking between the TiO<sub>2</sub> particles. The maximum conversion efficiency for fully flexible metal substrate based DSSCs is so far 8.6% whereas that of DSSCs with polyethylene naphthalate (PEN) plastic substrates has reached 8.1% efficiency [37].

#### **(5) Solid state dye-sensitized solar cells (SS-DSSCs) [37, 51–54]**

Attempts have been going on over many years to find an alternative to the liquid electrolytes with an improved solid state analogue of liquid electrolyte DSSCs. These will have ease of fabrication, less complication in the sealing and encapsulation of the device, possibility for monolithic interconnection of the cells within the module, and therefore also increased performance and lowering of the cost. Some of the initial highlights of such a solid state DSSC were reported by Bach *et al.* in 1998 [52] and later by Snaith *et al.* [51, 54] the latter group successfully made a 5% solid-state DSSCs using mesoporous TiO<sub>2</sub> with spiro-MeOTAD as an organic hole-transporting material. These cells achieved an optimised performance (highest efficiency) for a TiO<sub>2</sub> layer thickness of up to 2 μm and had current densities, which were limited to less than 10 mA/cm<sup>-2</sup>. This was primarily because of the poor pore filling of the hole-transporting material into mesoporous TiO<sub>2</sub> which was limited to the thickness of about 2 μm. Further improvements in these devices were achieved by the sensitisation of TiO<sub>2</sub> with the Y123 dyes and the p-type doping in spiro-MeOTAD using FK102 for an improved hole conductivity [53].



The advantage of the solid-state DSSCs over the liquid DSSCs are obvious: less complications involved in the manufacturing equipment, easy possibility for producing monolithically interconnected modules, easier sealing and encapsulation of the modules (similar to the processes employed for other thin film solar cells). On one hand, the efficiency values reached for small-size individual solar cells can be considered to be satisfactory, and should basically provide a great commercialisation potential for this technology in the future, especially thanks to the fact that we have here a true solid-state device, on the other hand the stability and longevity of the device are yet to be ascertained. Critical issues to be addressed in these devices are the long-term stability of the organic spiro OMeTAD layer and that of the perovskites with the Pb-free compounds.

### **1.3 Surface plasmons [55–58]**

Surface plasmon polaritons (SPPs), are infrared or visible-frequency electromagnetic waves, which travel along a metal-dielectric or metal-air interface. The term "surface plasmon polariton" explains that the wave involves both charge motion in the metal ("surface plasmon") and electromagnetic waves in the air or dielectric ("polariton").

Nevertheless, coupling of photons into SPPs can be achieved using a coupling medium such as a prism or grating to match the photon and surface plasmon wave vectors. A grating-coupled surface plasmon is a grating coupler matches the wave vectors by increasing the parallel wave vector component by an amount related to the grating period as shown in Figure 1.5.

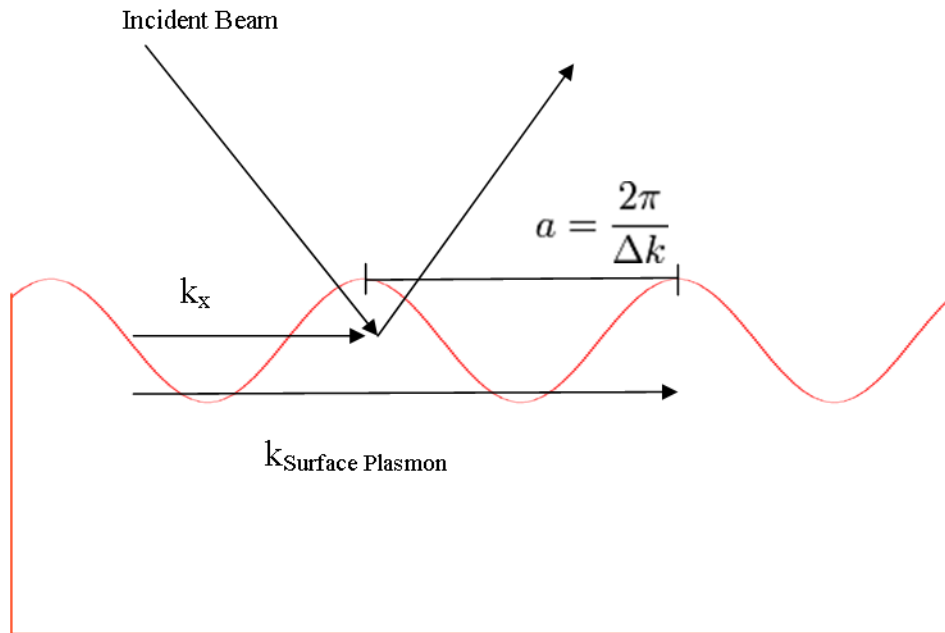


**Figure 1.5** grating-coupled surface plasmon [56].

The excitation of SPPs is frequently used in an experimental technique known as surface plasmon resonance (SPR). In SPR, the maximum excitation of surface plasmons are detected by monitoring the reflected power from a prism coupler as a function of incident angle or wavelength. This technique can be used to observe nanometer changes in thickness, density fluctuations, or molecular absorption.

Surface plasmons have attracted the attention of physicists, chemists, biologists and material scientists for widespread use in areas such as electronics, optical sensing, biomedicine, data storage and light generation. Recent developments in nanotechnology have generated new insights about control of various properties of nanomaterials that can support surface plasmons for specific applications. Localized surface plasmon resonance (LSPR) is an optical phenomena generated by a light wave trapped within conductive nanoparticles (NPs) smaller than the wavelength of light. The phenomenon is a result of the interactions between the incident light and surface electrons in a conduction band. This interaction produces coherent localized plasmon oscillations with a resonant frequency that strongly depends on the composition, size, geometry,

dielectric environment and particle–particle separation distance of NPs. Common materials used for NP production are noble metals such as Ag and Au, which due to the energy levels of d–d transitions exhibit LSPR in the visible range of the spectrum. Although, Ag exhibits the sharpest and strongest bands among all metals, Au is preferred for biological applications due to its inert nature and biocompatibility, and thiol-gold association for immobilization of biomolecules.

The interaction of NPs with light allows some photons to be absorbed and some to be scattered. NPs undergoing LSPR can have high molar extinction coefficients for absorption, with magnitude of up to about  $10^{11} \text{ M}^{-1} \text{ cm}^{-1}$ , and Rayleigh scattering that can be many orders of magnitude larger than without LSPR and. For example, a single 80-nm Ag nanosphere has been reported to scatter 445 nm light with a cross-section of  $3 \times 10^{-2} \mu\text{m}^2$ . This is six orders of magnitude greater than the cross-section of capture of a fluorescein molecule, and three orders of magnitude greater than the cross-section of the nanosphere of the same size filled with fluorescein. However, unlike fluorophores, plasmonic NPs do not photobleach or blink and thus can serve as intense and robust labels for biosensors, immunoassays, cellular imaging and surface-enhanced spectroscopies.

The extremely intense and highly localized electromagnetic (EM) fields induced by LSPR make NPs highly sensitive transducers of small changes in the local refractive index. These changes are exhibited in spectral shifts of extinction (absorption plus elastic light-scattering) and scattering spectra. For many organic molecules with a relatively high refractive index compared to solvent or air, binding to NPs results in a redshift. Additionally, strong EM fields enhance spectral information for surface-enhanced Raman spectroscopy. Figure A shows a schematic illustration of the LSPR excitation by metallic nanoparticles and the formation of an electric dipole on a metallic nanoparticle.

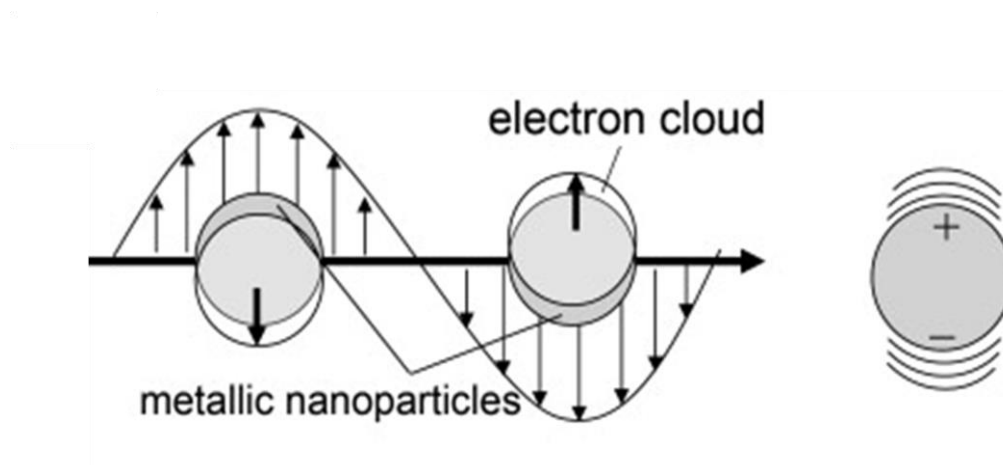


**Figure 1.6** schematic illustration of the LSPR excitation by metallic nanoparticles and the formation of an electric dipole on a metallic nanoparticle [58].

#### 1.4 Gold [20, 59, 60]

Gold is a chemical element with the symbol “Au” (from Latin: *aurum* "gold") and an atomic number of 79. It has been a valuable and highly sought-after precious metal for coinage, jewelry, and other arts since long before the beginning of recorded history. Besides its widespread monetary and symbolic functions, gold has many practical uses in dentistry, electronics, and other fields. It is useful because it is extremely malleable and ductile, highly resistant to corrosion in most other chemical reactions, and an excellent conductor of electricity.

**Table 1.2** Properties of gold [59, 60].

<b>Properties</b>	
<b>Name</b>	Gold
<b>Symbol</b>	Au
<b>Atomic number</b>	79
<b>Atomic Mass (amu)</b>	196.96655
<b>Melting Point °C</b>	1064.43
<b>Boiling Point °C</b>	2807.00
<b>Number of Protons/Electrons</b>	79
<b>Number of Neutrons</b>	118
<b>Classification</b>	Transition metal, Nobel metal
<b>Crystal Structure</b>	Face center cubic
<b>Density (at 293 K) (g/cm<sup>3</sup>)</b>	19.32
<b>Electron configuration</b>	[Xe] 4f <sup>14</sup> 5d <sup>10</sup> 6s <sup>1</sup>
<b>Atomic radius</b>	144 pm
<b>Covalent radius</b>	136±6 pm
<b>Van der Waals radius</b>	166 pm

Chemically, gold is a transition metal. Compared with other metals, pure gold is chemically least reactive, resisting individual acids but being attacked by the acid mixture aqua regia, so named because it dissolves gold. Gold also dissolves in alkaline solutions of cyanide, which have been used in mining. Gold dissolves in mercury, forming amalgam alloys. Gold is insoluble in nitric acid, which dissolves silver and base metals, a property that has long been used to confirm the presence of gold in items. The properties of gold are shown in Table 1.2

## 1.5 Preparation techniques of nanoparticles

### 1.5.1 Sol-gel method [23, 61–64]

Sol-gel techniques have long been known for the preparations of metal oxides and have been described in several texts. The process is typically used to prepare metal oxides via the hydrolysis of metal reactive precursors, usually alkoxides in an alcoholic solution, resulting in the corresponding hydroxide. Condensation of the hydroxide molecules by giving off water leads to the formation of a network of metal hydroxide. When hydroxide species undergo polymerization by condensation of the hydroxy network, gelation is achieved and a dense porous gel is obtained. The gel is a polymer of a three-dimensional skeleton surrounding interconnected pores. Removal of the solvents and appropriate drying of the gel is an important step that results in an ultra-fine powder of the metal hydroxide. Heat treatment of the hydroxide is a final step that leads to the corresponding ultrafine powder of the metal oxide. Depending on the heat treatment procedure, the final product may end up in the form of a nanometer scale powder, bulk material, or oxygen-deficient metal oxides.

The chemical and physical properties of the final product are primarily determined by the hydrolysis and drying steps. Hydrolysis of metal alkoxides ( $M(OR)_n$ ) involves nucleophilic reactions with water as follows:

The mechanism of this reaction involves the addition of a negatively charged  $HO^-$  group to the positively charged metal center ( $M^+$ ). The positively charged proton is then transferred to an alkoxy group followed by the removal of  $ROH$ . Condensation occurs when the hydroxide molecules bind together as they release water molecules and a gel/network of the hydroxide is obtained.

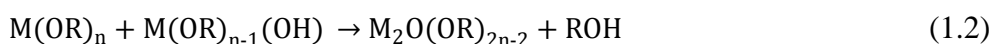
The reactionscheme is usually written as follows [63]:

1. Hydrolysis

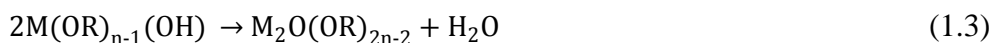


2. Condensation

Dehydration:



Dealcoholation:



The overall reaction is



The rates at which hydrolysis and condensation take place are important parameters that affect the properties of the final product. Slower and more controlled hydrolysis typically leads to smaller particle sizes and more unique properties. Hydrolysis and condensation rates depend on the electronegativity of the metal atom, the alkoxy group, solvent system, and the molecular structure of the metal alkoxide. Those metals with higher electronegativities undergo hydrolysis more slowly than those with lower electronegativities. For example, the hydrolysis rate of  $Ti(OEt)_4$  is about five orders of magnitude greater than that of  $Si(OEt)_4$ . Hence, the gelation times of silicon alkoxides are much longer (on the order of days) than those of titanium alkoxides (seconds or minutes). The sensitivity of metal alkoxides towards hydrolysis decreases as the OR group size increases. Smaller OR groups lead to higher reactivity of the corresponding alkoxide toward water and, in some cases, result in uncontrolled precipitation of the hydroxide.

Because alcohol interchange reactions are possible, the choice of solvents in sol-gel processes is very important. As an example, when silica gel was prepared from  $Si(OMe)_4$  and heated to  $600^\circ C$ , when ethanol was used as a solvent, the surface area was

300 m<sup>2</sup>/g with a mean pore diameter of 29 Å. However, when methanol was used, the surface area dropped to 170 m<sup>2</sup>/g and the mean pore diameter increased to 36Å.

The rate of hydrolysis also becomes slower as the coordination number around the metal center in the alkoxide increases. Therefore, alkoxides that tend to form oligomers usually show slower rates of hydrolysis and, hence, are easier to control and handle. n-Butoxide (O-n-Bu) is often preferred as a precursor to different oxides, including TiO<sub>2</sub> and Al<sub>2</sub>O<sub>3</sub>, because it is the largest alkoxy group that does not prevent oligomerization.

Careful handling in dry atmospheres is required to avoid rapid hydrolysis and uncontrolled precipitation because most metal alkoxides are highly reactive towards water. For alkoxides that have low rates of hydrolysis, acid or base catalysts can be used to enhance the process. The relatively negative alkoxides are protonated by acids creating a better leaving group and eliminating the need for proton transfer in the transition state. Alternatively, bases provide better nucleophiles (OH<sup>-</sup>) for hydrolysis, however; deprotonation of metal hydroxide groups enhances their condensation rates. Developments in the areas of solvent removal and drying have facilitated the production of nanoscale metal oxides with novel properties. When drying is achieved by evaporation under normal conditions, the gel network shrinks as a result of capillary pressure that occurs and the hydroxide product obtained is referred to as xerogel. However, if supercritical drying is applied using a high-pressure autoclave reactor at temperatures higher than the critical temperatures of solvents, less shrinkage of the gel network occurs, as there is no capillary pressure and no liquid-vapor interface, which allows the pore structure to remain largely intact. The hydroxide product obtained in this manner is referred to as an aerogel. Aerogel powders usually demonstrate higher porosities and larger surface areas as compared with analogous xerogel powders. Aerogel processing has been very useful in producing highly divided powders of different metal oxides.

Sol-gel processes have several advantages over other techniques for the synthesis of nanoscale metal oxides. Because the process begins with a relatively homogeneous mixture, the resulting product is a uniform ultra-fine porous powder. Sol-gel processing



also has the advantage that it can also be scaled up to accommodate industrial-scale production.

### **1.5.2 Impregnation method [23, 64, 65]**

Impregnated catalysts are prepared by impregnating a metal salt on a support. The metal loading in the finished catalyst is typically 1-5%. When liquid is slowly added to a solid powder, the liquid is first absorbed in the pores and the powder will flow as if it is dry. When the pores have been filled the outside of the grains rather suddenly become wet, the grains will tend to stick together and the powder will form lumps instead of flowing freely. The situation when the pores have been filled but the outside of the grains is dry is called incipient wetness (glistening and quite sticky) and can easily be detected by shaking or stirring the powder. Catalysts are prepared by impregnation or by spraying a solution of a metal salt onto pellets of a porous support until incipient wetness. The pellets are then dried and calcined to transform the metal into insoluble form. The metal salt can be deposited homogeneously through the pellet or most of the metal may be deposited near the outside of the pellet. The distribution of the metal is controlled through the pH or through addition of chelating agents to the impregnation liquid.

Compared to precipitation, impregnation offers a number of advantages as follows:

- (1) The pellets are shaped before the metal is added.
- (2) The filtering and the wash of the catalyst are eliminated.
- (3) Small metal loadings are easily prepared.
- (4) Impregnation offers some control over the distribution of the metal in pellets.

And disadvantages as follows:

- (1) High metal loadings are not possible.
- (2) A good impregnation solution may be impossible to find.

## 1.6 Characterization techniques

In this research, several techniques were used for the characterization of the unloaded TiO<sub>2</sub>, Au-loaded TiO<sub>2</sub> and Ag-loaded TiO<sub>2</sub>. The phase and crystal structure were studied by X-ray diffractometry (XRD). The morphology and particle size of all samples was examined by scanning electron microscopy (SEM) and high resolution transmission electron microscopy (HRTEM). The specific surface area and the average particle diameter were investigated by The Brunauer, Emmett and Teller (BET) method.

### 1.6.1 Electron microscopy [64, 66]

Electron microscopy is an extremely important technique for the examination and analysis of both the surface and subsurface of nanostructured systems (SEM) as well as the bulk structure of thin samples, usually averaged through thickness (TEM and STEM). In many respects, electron optics may be regarded as analogous to light optics; the main differences may be summarized as follows. Firstly, the wavelength of accelerated electrons is very much smaller than the wavelength of visible or UV photons, which implies a much greater resolution for electron imaging. Secondly, electrons interact much more strongly with matter than photons, thus all optical paths in an electron microscope must usually be under a vacuum of at least  $10^{-4}$  Pa. However a major benefit for nanostructures is that even though the signal is derived from a small amount of material, it will be relatively strong compared to that derived using other incident radiations. Thirdly, electrons are charged particles and may thus be focused by magnetic or electric fields. Furthermore, this focused electron beam may be scanned relatively easily using electrostatic fields. Finally, there is therefore no change in  $n_r$  during passage through such a lens, so  $n_r$  may be taken as unity, which simplifies the optical formulae. However, in order to reduce lens aberrations when using electromagnetic lenses, the value of  $\alpha$  is kept very small and only rays close to the optic axis are employed.

### (1) Electron beam generation [64, 66]

The electron beam may be produced either by thermionic emission, where thermal energy is used to overcome the surface potential barrier (work function) of a solid source and so allow extraction of electrons from the conduction band of an emitter, or by field emission, in which an extremely high electric field is employed to reduce the surface potential barrier of an emitter. The finite width of the barrier allows quantum tunnelling of electrons out of the source at room temperature (cold field emission), although higher temperatures have been used more recently (Schottky or thermally assisted field emission), which requires a lower field strength.

A typical thermionic electron gun employs a tungsten cathode filament which is resistively heated to 2800K in a vacuum of  $10^{-4}$  Pa to give the electrons sufficient energy to overcome the work function of the metal. The emitted electrons are collimated and focused using a Wehnelt cylinder to a beam of typically 50 mm in diameter. The anode potential is typically 1–20 kV in the SEM and 100–200 kV in the TEM.

An important electron gun parameter is the brightness of the source, the current density per unit solid angle. Increased brightness allows either the use of higher currents, which improve sensitivity and image contrast, or smaller probe areas, which yield higher spatial resolution. The brightness may be increased by using a lanthanum hexaboride ( $\text{LaB}_6$ ) filament that possesses a lower work function than tungsten and a smaller source size ( $\sim 1$  mm), giving an order of magnitude increase in  $\beta$ . Alternatively, a field emission gun (FEG), which employs a high field strength surrounding a pointed tungsten cathode of radius  $100 \text{ \AA}$ , gives a source size as low as 5 nm and a brightness increase of  $10^4$  over a thermionic tungsten filament. Both sources possess a longer lifetime than tungsten filaments but require a higher vacuum in the gun region. These sources also give a much reduced energy spread of the emitted electrons, leading to improved resolution as a result of reduced chromatic aberration in spectroscopic analysis.

## (2) Electron-specimen interactions [64, 66]

Figure 1.7 (a) summarizes the various signals produced as a result of electron-specimen interactions in SEM and shows the calculated volumes and penetration depths which give rise to the different signals from thick specimens. The interaction volume is defined as the volume within which 95% of the electrons are brought to rest by scattering, and has a characteristic teardrop shape (as shown in the figure). The depth and lateral width of electron penetration in the specimen are roughly proportional to  $V^2$  and  $V^{3/2}$ , respectively, where  $V$  is the accelerating voltage. Materials of high (average) atomic number will exhibit reduced electron penetration depths and increased lateral spread relative to those of lower atomic number. For comparison, Figure 1.7 (b) shows the signals produced in thin specimens appropriate for TEM imaging. Besides the primary electrons, there are various types of emitted electrons which leave the surface of a bulk sample and may be used for imaging or analysis, as summarized in the following sections.

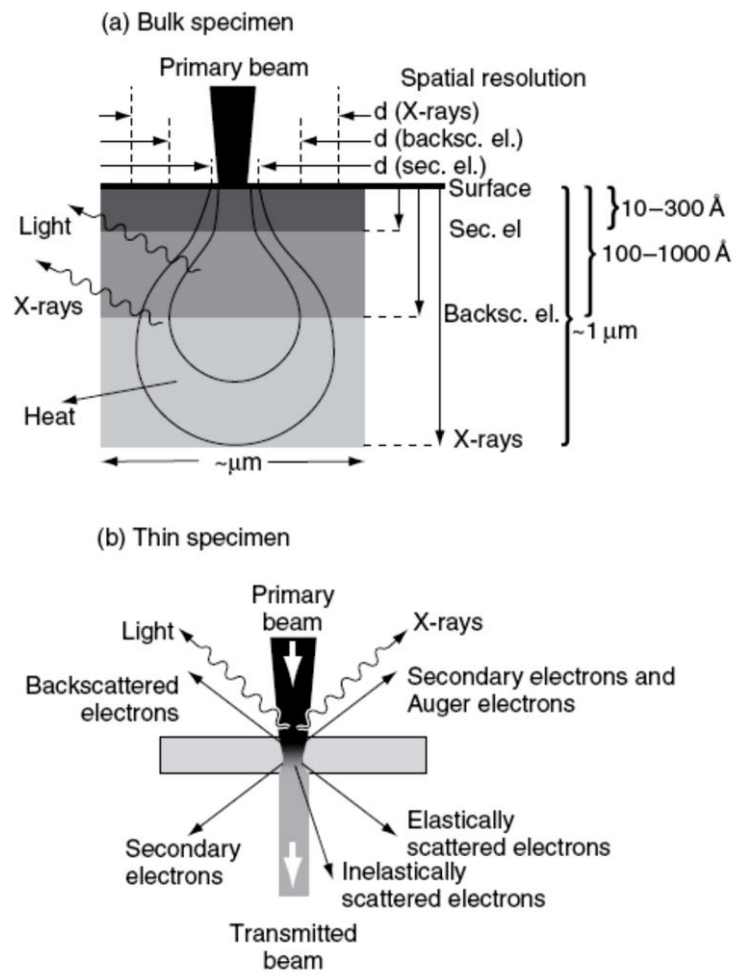


**Figure 1.7** Schematic diagram of the beam-specimen interaction in (a) a thick specimen and (b) a thin specimen [64].

### (3) Secondary electrons [64, 66]

The term ‘secondary electrons’ is used in general to describe any electrons that escape from the specimen with kinetic energies below about 50 eV. They are most likely to arise from ionized electrons previously associated with atoms close to the surface of the solid which have gained a small amount of kinetic energy and escaped. Alternatively they may be primary electrons which have lost nearly all their energy through scattering and have reached the surface. Secondary electrons are extremely abundant and the secondary electron yield,  $\delta$  (the number emitted per primary electron), is dependent on the accelerating voltage and can even exceed 1, hence they are extensively used for imaging in SEM.

#### **(4) Backscattered electrons [64, 66]**

Some primary electrons undergo large deflections and leave the surface with little change in their kinetic energy; these are termed backscattered electrons (BSE). The backscattered electron yield,  $\eta$ , is almost independent of accelerating voltage and is small compared with  $\delta$ , but backscattered electrons are also used for imaging in SEM as  $\eta$  is strongly dependent on  $Z$  (unlike  $\delta$ ) owing to the fact that they arise from Rutherford backscattering from the nucleus. Owing to this nuclear interaction, backscattered electron imaging can be used to differentiate phases of differing average atomic numbers.

#### **(5) Auger electrons and emitted X-rays [64, 66]**

Atoms which have undergone inner shell ionization and have been promoted into an excited state by the primary electron beam relax when electrons from higher energy levels drop into the vacant inner shells. This process results in the release of the excess energy between the electron energy levels involved in the transitions ( $\Delta E$ ), producing low-energy (100-1000 eV) Auger electrons, or X-rays, or visible photons of wavelength  $\lambda = hc/\Delta E$ . The Auger yield is small, except in the case of light elements, and is extremely useful for surface analysis. The energies and wavelengths of the emitted X-rays, which are characteristic of the atom involved, are used in elemental analysis.

#### **(6) Scanning electron microscopy [64, 66]**

The scanning electron microscope (SEM) is extremely useful for imaging surface and subsurface microstructure. The basic layout of SEM instrumentation is shown in Figure 1.8.

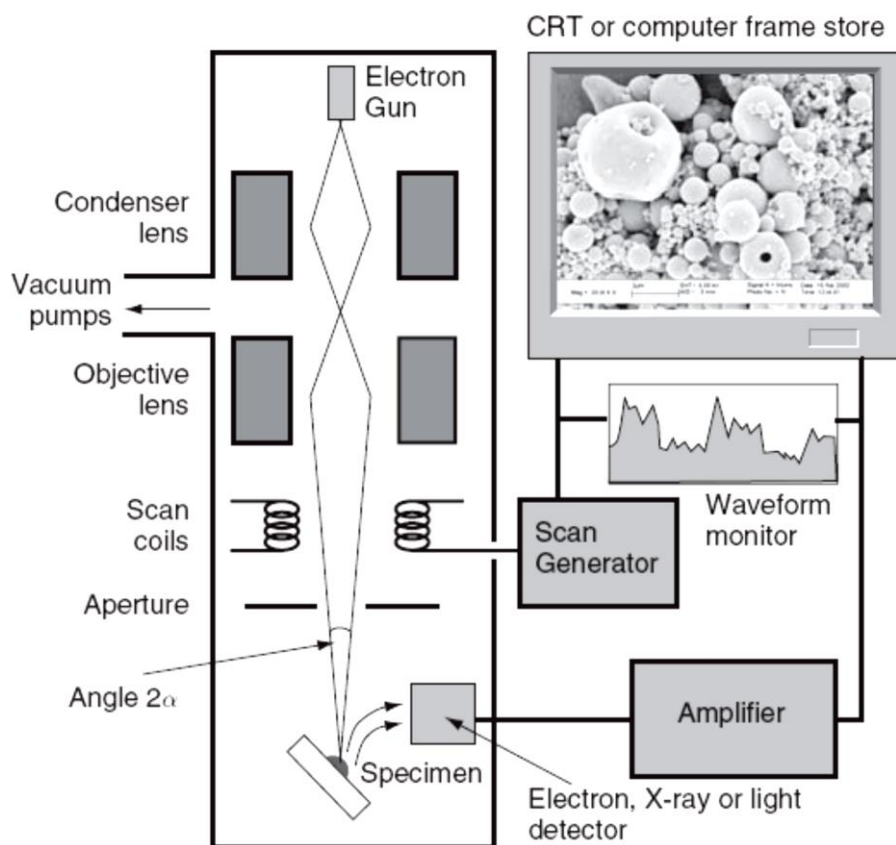


**Figure 1.8** Schematic diagram of the layout of a scanning electron microscope [64].

The electron gun usually consists of a tungsten or LaB<sub>6</sub> filament, however FEGs are becoming increasingly necessary for imaging nanostructures at high resolution. The accelerating voltage is usually between 1 and 30 kV. The lower voltages can be used with high-brightness LaB<sub>6</sub> and FEG sources and they are often employed to increase surface detail and obviate sample charging in non-conducting or poorly conducting samples.

In the SEM, two or more condenser lenses are used to demagnify the crossover produced by the gun, while the objective lens focuses the electron probe onto the specimen so that the final probe diameter lies between 2 and 10 nm. The objective aperture limits the angular spread  $\alpha$  of the electrons. The focused beam is scanned across the specimen surface in a two-dimensional raster, with the beam passing through the optic axis at the objective lens; meanwhile, an appropriate detector monitors the

secondary electrons or other signal, such as backscattered electrons or X-rays, as they are emitted from each point on the surface. Simultaneously, using the same scan generator, a beam is scanned across the recording monitor. The intensity of each pixel on the monitor is controlled by the amplified output of the selected detector and is therefore directly related to the emission intensity of the selected interaction at the corresponding point on the specimen surface. The magnification is simply the ratio of the monitor raster size to the specimen raster size and, as in field ion microscopy, it involves no lenses.

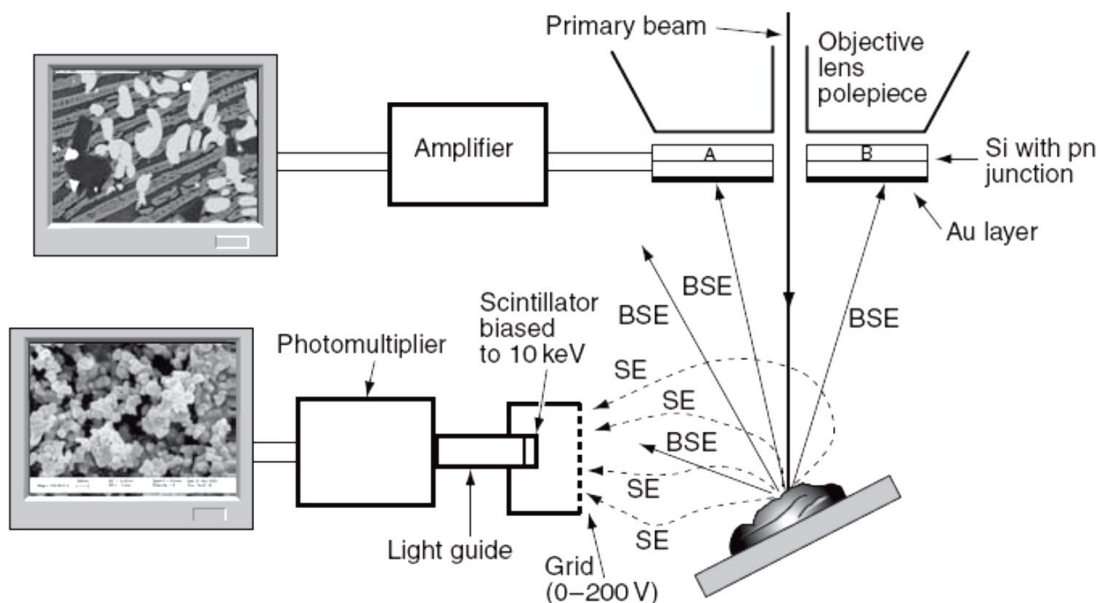


**Figure 1.9** Schematic diagram showing a secondary electron detector and a solid-state backscattered electron detector together with typical images [64].

During electron irradiation, a wide spectrum of low-energy secondary electrons are emitted from the surface of the specimen with a high emission cross section, giving images with a high signal-to-noise ratio. They are detected by a scintillator-photomultiplier system known as an Everhart-Thornley (BET) detector positioned to the side of the specimen chamber. Surrounding the scintillator is a grid (a Faraday cage) which has a small positive bias to attract the low-energy secondary electrons that are travelling in all directions away from the specimen surface. High-



energy backscattered electrons travelling directly towards the detector will also contribute to the image, however due to the small detector collection angle, this signal is relatively low. The ET detector will collect nearly all secondary electrons and therefore images appear to look down holes and over hills. However, the signal from sample areas in direct line-of-sight of the detector is slightly higher than the signal from ‘unseen’ parts of the specimen and consequently they will appear brighter, an effect known as shadowing contrast. The detector and a typical secondary electron image are shown in Figure 1.9.

The shape of the interaction volume relative to the specimen surface, and hence the secondary electron yield, depends on the angle of inclination  $\theta_{inc}$  between the beam and the specimen surface, varying as  $1/\cos\theta_{inc}$ . This inclination effect means that the edges of a spherical particle will appear brighter than the centre and, for studies of specimen topography, specimens are normally tilted 20–40° towards the detector to maximize the signal. Due to increased field strength at sharp edges and spikes on the specimen surface, the emission of secondary and backscattered electrons increases, and such features will appear bright, known as edge contrast. Consequently, owing to the surface specificity and the contrast effects mentioned above, the major use of secondary electron imaging is for topographic contrast. In general, topographic images obtained with secondary electrons have the same appearance as an object illuminated with diffuse light, in that there are no harsh shadows. Quantitative information on surface topography may be obtained using stereomicroscopy techniques in which two images are taken under identical magnification conditions at slightly different tilt angles (e.g., -5° and +5°). The images may be viewed using a special stereo viewer (which allows the brain to interpret them as a 3D picture). For quantitative work, the relative displacement or parallax between two features on the pair of tilted images allows their height separation to be determined.

## 1.7 Research objectives

-To study the synthesis of unloaded TiO<sub>2</sub>, Au-loaded and Ag-loaded TiO<sub>2</sub> nanoparticles by the modified sol-gel/impregnation methods.

-To study the physical and chemical characteristics of unloaded TiO<sub>2</sub>, Au-loaded and Ag-loaded TiO<sub>2</sub> nanoparticles

-To fabricate dye/Au-loaded TiO<sub>2</sub> films on a Au grating surface.

-To investigate the performance of dye/Au-loaded TiO<sub>2</sub> films on a Au grating surface.

-To fabricate solid-state electrolyte layer on a dye-TiO<sub>2</sub> film formed by the nanoimprint technique.

-To investigate the performance of solid-state electrolyte layer on a dye-TiO<sub>2</sub> film.

-To investigate the enhancement of grating-coupled surface plasmon and localized surface plasmon.

## REFERENCE

- [1] K. G. Deepa, P. Lekha, and S. Sindhu, "Efficiency enhancement in DSSC using metal nanoparticles: A size dependent study," *Solar Energy*, vol. 86, no. 1, pp. 326–330, 2012.
- [2] A. Baba, K. Wakatsuki, K. Shinbo, K. Kato, and F. Kaneko, "Increased short-circuit current in grating-coupled surface plasmon resonance field-enhanced dye-sensitized solar cells," *Journal of Materials Chemistry*, vol. 21, pp. 16436–16441, 2011.
- [3] S. Muduli, O. Game, V. Dhas, K. Vijayamohanan, K. A. Bogle, N. Valanoor, and S. B. Ogale, "TiO<sub>2</sub>–Au plasmonic nanocomposite for enhanced dye-sensitized solar cell (DSSC) performance," *Solar Energy*, vol. 86, no. 5, pp. 1428–1434, 2012.
- [4] S. Nakade, Y. Makimoto, W. Kubo, T. Kitamura, Y. Wada, and S. Yanagida, "Roles of electrolytes on charge recombination in dye-sensitized TiO<sub>2</sub> solar cells (2): The case of solar cells using cobalt complex redox couples," *The Journal of Physical Chemistry B*, vol. 109, no. 8, pp. 3488–3493, 2005.
- [5] A. Fujishima, T. N. Rao, and D. A. Tryk, "Titanium dioxide photocatalysis," *Journal of Photochemistry and Photobiology C: Photochemistry Reviews*, vol. 1, no. 1, pp. 1–21, 2000.
- [6] K. Pirkanniemi and M. Sillanpää, "Heterogeneous water phase catalysis as an environmental application: a review," *Chemosphere*, vol. 48, no. 10, pp. 1047–1060, 2002.
- [7] Y. Hu, H. L. Tsai, and C. L. Huang, "Effect of brookite phase on the anatase–rutile transition in titania nanoparticles," *Journal of the European Ceramic Society*, vol. 23, no. 5, pp. 691–696, 2003.

- [8] V. Samuel, R. Pasricha, and V. Ravi, "Synthesis of nanocrystalline rutile," *Ceramics International*, vol. 31, no. 4, pp. 555–557, 2005.
- [9] A. Baba, N. Aoki, K. Shinbo, K. Kato, and F. Kaneko, "Grating-coupled surface plasmon enhanced short-circuit current in organic thin-film photovoltaic cells," *ACS Applied Materials & Interfaces*, vol. 3, no. 6, pp. 2080–2084, 2011.
- [10] H. A. Atwater and A. Polman, "Plasmonics for improved photovoltaic devices," *Nat Mater*, vol. 9, no. 3, pp. 205–213, 2010.
- [11] V. E. Ferry, J. N. Munday, and H. A. Atwater, "Design considerations for plasmonic photovoltaics," *Advanced Materials*, vol. 22, no. 43, pp. 4794–4808, 2010.
- [12] I. K. Ding, J. Zhu, W. Cai, S.-J. Moon, N. Cai, P. Wang, S. M. Zakeeruddin, M. Grätzel, M. L. Brongersma, Y. Cui, and M. D. McGehee, "Plasmonic dye-sensitized solar cells," *Advanced Energy Materials*, vol. 1, no. 1, pp. 52–57, 2011.
- [13] J. Homola, I. Koudela, and S. S. Yee, "Surface plasmon resonance sensors based on diffraction gratings and prism couplers: sensitivity comparison," *Sensors and Actuators B: Chemical*, vol. 54, no. 1–2, pp. 16–24, 1999.
- [14] W. Knoll, "Interfaces and thin films as seen by bound electromagnetic waves," *Annual Review of Physical Chemistry*, vol. 49, no. 1, pp. 569–638, 1998.
- [15] B. K. Singh and A. C. Hillier, "Surface plasmon resonance imaging of biomolecular interactions on a grating-based sensor array," *Analytical Chemistry*, vol. 78, no. 6, pp. 2009–2018, 2006.
- [16] B. K. Singh and A. C. Hillier, "Surface plasmon resonance enhanced transmission of light through gold-coated diffraction Gratings," *Analytical Chemistry*, vol. 80, no. 10, pp. 3803–3810, 2008.

- [17] B. Akira, K. Kenji, O. Tsutomu, O. Yasuo, S. Kazunari, K. Keizo, and K. Futao, "Multimode surface plasmon excitations on organic thin film/metallic diffraction grating," *Japanese Journal of Applied Physics*, vol. 49, no. 1S, p. 01AE02, 2010.
- [18] V. E. Ferry, L. A. Sweatlock, D. Pacifici, and H. A. Atwater, "Plasmonic nanostructure design for efficient light coupling into solar cells," *Nano Letters*, vol. 8, no. 12, pp. 4391–4397, 2008.
- [19] H. Ninsonti, A. Baba, W. Kangwansupamonkon, S. Phanichphant, K. Shinbo, K. Kato, F. Kaneko "Enhanced photocurrent properties of dye/Au-loaded TiO<sub>2</sub> films by grating-coupled surface plasmon excitation," *IEICE Transactions on Electronics*, vol. E96–C no. 3, pp. 385–388, 2013.
- [20] P. Reineck, G. P. Lee, D. Brick, M. Karg, P. Mulvaney, and U. Bach, "A solid-state plasmonic solar cell via metal nanoparticle self-assembly," *Advanced Materials*, vol. 24, no. 35, pp. 4750–4755, 2012.
- [21] N. Wetchakun, B. Incessungvorn, K. Wetchakun, and S. Phanichphant, "Influence of calcination temperature on anatase to rutile phase transformation in TiO<sub>2</sub> nanoparticles synthesized by the modified sol–gel method," *Materials Letters*, vol. 82, no. 0, pp. 195–198, 2012.
- [22] N. Wetchakun and S. Phanichphant, "Effect of temperature on the degree of anatase–rutile transformation in titanium dioxide nanoparticles synthesized by the modified sol–gel method," *Current Applied Physics*, vol. 8, no. 3–4, pp. 343–346, 2008.
- [23] J. A. Rodríguez and G. M. Fernández, *Synthesis, Properties and Applications of Oxide Nanomaterials*. Canada: John Wiley & Sons, Inc., 2007.

- [24] Online at: [http://en.wikipedia.org/wiki/Titanium\\_dioxide](http://en.wikipedia.org/wiki/Titanium_dioxide), October, 29<sup>th</sup> 2014.
- [25] U. Diebold, "The surface science of titanium dioxide," *Surface Science Reports*, vol. 48, no. 5–8, pp. 53–229, 2003.
- [26] B. O'Regan and M. Gratzel, "A low-cost, high-efficiency solar cell based on dye-sensitized colloidal TiO<sub>2</sub> films," *Nature*, vol. 353, no. 6346, pp. 737–740, 1991.
- [27] H. A. P. Atwater, Albert, "Plasmonics for improved photovoltaic devices," *Nat Mater*, vol. 9, no. 3, pp. 205–213, 2010.
- [28] B. Sebo, N. Huang, Y. Liu, Q. Tai, L. Liang, H. Hu, S. Xu, and X.-Z. Zhao, "Dye-sensitized solar cells enhanced by optical absorption, mediated by TiO<sub>2</sub> nanofibers and plasmonics Ag nanoparticles," *Electrochimica Acta*, vol. 112, pp. 458–464, 2013.
- [29] H. M. N. Bandara, R. M. G. Rajapakse, K. Murakami, G. R. R. A. Kumara, and G. Anuradha Sepalage, "Dye-sensitized solar cell based on optically transparent TiO<sub>2</sub> nanocrystalline electrode prepared by atomized spray pyrolysis technique," *Electrochimica Acta*, vol. 56, no. 25, pp. 9159–9161, 2011.
- [30] C. Jiang, W. L. Koh, M. Y. Leung, W. Hong, Y. Li, and J. Zhang, "Influences of alcoholic solvents on spray pyrolysis deposition of TiO<sub>2</sub> blocking layer films for solid-state dye-sensitized solar cells," *Journal of Solid State Chemistry*, vol. 198, pp. 197–202, 2013.
- [31] C. Jiang, M. Y. Leung, W. L. Koh, and Y. Li, "Influences of deposition and post-annealing temperatures on properties of TiO<sub>2</sub> blocking layer prepared by spray pyrolysis for solid-state dye-sensitized solar cells," *Thin Solid Films*, vol. 519, no. 22, pp. 7850–7854, 2011.

- [32] M. Okuya, K. Nakade, and S. Kaneko, "Porous TiO<sub>2</sub> thin films synthesized by a spray pyrolysis deposition (SPD) technique and their application to dye-sensitized solar cells," *Solar Energy Materials and Solar Cells*, vol. 70, no. 4, pp. 425–435, 2002.
- [33] O. Carp, C. L. Huisman, and A. Reller, "Photoinduced reactivity of titanium dioxide," *Progress in Solid State Chemistry*, vol. 32, no. 1–2, pp. 33–177, 2004.
- [34] G. Sahu, S. W. Gordon, and M. A. Tarr, "Synthesis and application of core-shell Au-TiO<sub>2</sub> nanowire photoanode materials for dye sensitized solar cells," *RSC Advances*, vol. 2, no. 2, pp. 573–582, 2012.
- [35] M. Grätzel, "Conversion of sunlight to electric power by nanocrystalline dye-sensitized solar cells," *Journal of Photochemistry and Photobiology A: Chemistry*, vol. 164, no. 1–3, pp. 3–14, 2004.
- [36] N. Vlachopoulos, P. Liska, J. Augustynski, and M. Graetzel, "Very efficient visible light energy harvesting and conversion by spectral sensitization of high surface area polycrystalline titanium dioxide films," *Journal of the American Chemical Society*, vol. 110, no. 4, pp. 1216–1220, 1988.
- [37] H. M. Upadhyaya, S. Senthilarasu, M.-H. Hsu, and D. K. Kumar, "Recent progress and the status of dye-sensitised solar cell (DSSC) technology with state-of-the-art conversion efficiencies," *Solar Energy Materials and Solar Cells*, vol. 119, pp. 291–295, 2013.
- [38] S. A. Haque, E. Palomares, H. M. Upadhyaya, L. Otley, R. J. Potter, A. B. Holmes, and J. R. Durrant, "Flexible dye sensitised nanocrystalline semiconductor solar cells," *Chemical Communications*, no. 24, pp. 3008–3009, 2003.
- [39] V. C. Nogueira, C. Longo, A. F. Nogueira, M. A. Soto-Oviedo, and M.-A. D. Paoli, "Solid-state dye-sensitized solar cell: Improved performance and stability

- using a plasticized polymer electrolyte," *Journal of Photochemistry and Photobiology A: Chemistry*, vol. 181, no. 2–3, pp. 226–232, 2006.
- [40] C.-L. Chen, T.-W. Chang, H. Teng, C.-G. Wu, C.-Y. Chen, Y.-M. Yang, and Y.-L. Lee, "Highly efficient gel-state dye-sensitized solar cells prepared using poly(acrylonitrile-co-vinyl acetate) based polymer electrolytes," *Physical Chemistry Chemical Physics*, vol. 15, no. 10, pp. 3640–3645, 2013.
- [41] J. Kang, W. Li, X. Wang, Y. Lin, X. Li, X. Xiao, and S. Fang, "Gel polymer electrolytes based on a novel quaternary ammonium salt for dye-sensitized solar cells," *Journal of Applied Electrochemistry*, vol. 34, no. 3, pp. 301–304, 2004.
- [42] A. F. Nogueira, J. R. Durrant, and M. A. De Paoli, "Dye-sensitized nanocrystalline solar cells employing a polymer electrolyte," *Advanced Materials*, vol. 13, no. 11, pp. 826–830, 2001.
- [43] T.-L. Li, Y.-L. Lee, and H. Teng, "High-performance quantum dot-sensitized solar cells based on sensitization with CuInS<sub>2</sub> quantum dots/CdS heterostructure," *Energy & Environmental Science*, vol. 5, no. 1, pp. 5315–5324, 2012.
- [44] J.-H. Im, C.-R. Lee, J.-W. Lee, S.-W. Park, and N.-G. Park, "6.5% efficient perovskite quantum-dot-sensitized solar cell," *Nanoscale*, vol. 3, no. 10, pp. 4088–4093, 2011.
- [45] P. K. Santra and P. V. Kamat, "Mn-doped quantum dot sensitized solar cells: a strategy to boost efficiency over 5%," *Journal of the American Chemical Society*, vol. 134, no. 5, pp. 2508–2511, 2012.
- [46] S. D. Sung, I. Lim, P. Kang, C. Lee, and W. I. Lee, "Design and development of highly efficient PbS quantum dot-sensitized solar cells working in an aqueous polysulfide electrolyte," *Chemical Communications*, vol. 49, no. 54, pp. 6054–6056, 2013.



- [47] L. Grinis, S. Kotlyar, S. Rühle, J. Grinblat, and A. Zaban, "Conformal nano-sized inorganic coatings on mesoporous TiO<sub>2</sub> films for low-temperature dye-sensitized solar cell fabrication," *Advanced Functional Materials*, vol. 20, no. 2, pp. 282–288, 2010.
- [48] S. Senthilarasu, T. A. N. Peiris, J. García-Cañadas, and K. G. U. Wijayantha, "Preparation of nanocrystalline TiO<sub>2</sub> electrodes for flexible dye-sensitized solar cells: Influence of mechanical compression," *The Journal of Physical Chemistry C*, vol. 116, no. 36, pp. 19053–19061, 2012.
- [49] H. M. Upadhyaya, N. Hirata, S. A. Haque, M.-A. de Paoli, and J. R. Durrant, "Kinetic competition in flexible dye sensitised solar cells employing a series of polymer electrolytes," *Chemical Communications*, no. 8, pp. 877–879, 2006.
- [50] H. C. Weerasinghe, P. M. Sirimanne, G. P. Simon, and Y.-B. Cheng, "Cold isostatic pressing technique for producing highly efficient flexible dye-sensitised solar cells on plastic substrates," *Progress in Photovoltaics: Research and Applications*, vol. 20, no. 3, pp. 321–332, 2012.
- [51] H. J. Snaith, A. J. Moule, C. Klein, K. Meerholz, R. H. Friend, and M. Grätzel, "Efficiency enhancements in solid-state hybrid solar cells via reduced charge recombination and increased light capture," *Nano Letters*, vol. 7, no. 11, pp. 3372–3376, 2007.
- [52] U. Bach, D. Lupo, P. Comte, J. E. Moser, F. Weissortel, J. Salbeck, H. Spreitzer, and M. Gratzel, "Solid-state dye-sensitized mesoporous TiO<sub>2</sub> solar cells with high photon-to-electron conversion efficiencies," *Nature*, vol. 395, no. 6702, pp. 583–585, 1998.

- [53] J. Burschka, A. Dualeh, F. Kessler, E. Baranoff, N.-L. Cevey-Ha, C. Yi, M. K. Nazeeruddin, and M. Grätzel, "Tris(2-(1H-pyrazol-1-yl)pyridine)cobalt(III) as p-type dopant for organic semiconductors and its application in highly efficient solid-state dye-sensitized solar cells," *Journal of the American Chemical Society*, vol. 133, no. 45, pp. 18042-18045, 2011.
- [54] H. J. Snaith and L. Schmidt-Mende, "advances in liquid-electrolyte and solid-state dye-sensitized solar cells," *Advanced Materials*, vol. 19, no. 20, pp. 3187–3200, 2007.
- [55] E. Petryayeva and U. J. Krull, "Localized surface plasmon resonance: Nanostructures, bioassays and biosensing-A review," *Analytica Chimica Acta*, vol. 706, no. 1, pp. 8–24, 2011.
- [56] Online at: [http://en.wikipedia.org/wiki/Surface\\_plasmon\\_polariton](http://en.wikipedia.org/wiki/Surface_plasmon_polariton), October, 29<sup>th</sup> 2014.
- [57] S. Zeng, D. Baillargeat, H.-P. Ho, and K.-T. Yong, "Nanomaterials enhanced surface plasmon resonance for biological and chemical sensing applications," *Chemical Society Reviews*, vol. 43, no. 10, pp. 3426–3452, 2014.
- [58] K. Ueno and H. Misawa, "Surface plasmon-enhanced photochemical reactions," *Journal of Photochemistry and Photobiology C: Photochemistry Reviews*, vol. 15, no. 0, pp. 31–52, 2013.
- [59] Online at: <http://en.wikipedia.org/wiki/Gold>, October, 29<sup>th</sup> 2014.
- [60] Online at: <http://www.chemicalelements.com/elements/au.html>, October, 29<sup>th</sup> 2014.
- [61] Y. S. Lee, *Self-Assembly and Nanotechnology-A Force Balance Approach*. Canada: Wiley & Sons, Inc, 2008.

- [62] M. G. Ali, *Principles of Nanotechnology*. Chicago: University of Chicago Press.
- [63] C. Su, B. Y. Hong, and C. M. Tseng, "Sol–gel preparation and photocatalysis of titanium dioxide," *Catalysis Today*, vol. 96, no. 3, pp. 119–126, 2004.
- [64] R. W. Kelsall, I. W. Hamley, and M. Geoghegan, *Nanoscale Science And Technology*. Canada: John Wiley & Sons, Inc., 2007.
- [65] D. J. Shaw, *Introduction to Colloid and Surface Chemistry*. Elsevier Science Ltd: Oxford, 1992.
- [66] D. Minoli, *Nanotechnology Applications to Telecommunications and Networking*. Canada: John Wiley and Sons, 2006.

## CHAPTER 3

### **Enhanced photocurrent generation at a spiro-OMeTAD/AuNPs-TiO<sub>2</sub> interface with grating-coupled surface plasmon excitation**

Dye-sensitized solar cells (DSSCs) have attracted attention due to their low fabrication cost and relatively high efficiency [1–3]. One major problem in liquid-based DSSCs is solvent evaporation and leakage [4]. Recently, solid-state hole-transporting materials, such as spiro-OMeTAD (2,2',7,7'-tetrakis-(N,N-di-p-methoxyphenylamine) 9,9'-spirobifluorene), have been studied as a good strategy to replace liquid electrolytes for improving DSSCs [5]. Solid-state dye-sensitized solar cells (ss-DSSCs) prepared using spiro-OMeTAD have exhibited good stability under elevated temperature light soaking and have attained high efficiencies [6].

It was previously reported that the short-circuit photocurrent in organic solar cells could be increased by using grating-coupled surface plasmon (SP) excitations, in which a blu-ray disc recordable (BD-R) is used as a grating substrate [2, 7]. The increased optical field by the SP excitation was used to enhance the photovoltaic properties of DSSCs because the active thin film can absorb more light, and it could generate more photocarriers, resulting in an increased photocurrent for the DSSCs [8-10]. Grating-coupled SP excitations, which propagate adjacent to the grating metallic surface, have been widely used in various applications [11–15]. Therefore, the use of grating-structured Ag on DSSCs should enhance the photovoltaic properties of these systems [16, 17].

The use of Au-TiO<sub>2</sub> on a metallic grating to enhance the photocurrent of photoanodes also reported [17]. Au is known to be the most effective catalyst among various kind of metal nanoparticles that could especially improve dye sensitized solar cells by surface plasmon resonance effect [18, 19]. Metal nanoparticles such as gold nanoparticles (AuNPs) could enhance the optical absorption, electron transfer, light

scattering, and localized SP excitation [1, 3, 10, 20–23]. Hence, metal nanoparticles have been employed to enhance the efficiency of DSSCs.

In this Chapter, the fabrication of a grating structure consisting of a solid-state electrolyte layer on a dye-TiO<sub>2</sub> film formed by the nanoimprint technique using a polydimethylsiloxane (PDMS) stamp was studied. The application of this grating in solid-state DSSCs is also described. The PDMS grating pattern was imprinted from a BD-R. A silver electrode was deposited on the patterned solid-state electrolyte layers. Surface plasmon resonance (SPR) excitation was observed in the fabricated solar cells by irradiation with white light at the imprinted grating surface. The photoelectric conversion properties were measured to study the effect of the two types of SPR excitations, i.e., the propagating surface plasmon on the Ag grating surface and the localized surface plasmon from the Au nanoparticles on TiO<sub>2</sub>.

### **3.1 Literature review**

Nogueira *et al.* [4] reported that dye sensitized solar cells (DSSC) were the consequence of a combination of several different materials: optically transparent electrodes, nanoparticulated semiconductors, coordination compounds, inorganic salts, solvents and metallic catalysts. Each material showed a specific task toward the overall purpose of harvesting solar light and transforming it into electricity. To develop the efficiency and increase the technological perspectives of DSSC, there was a tendency to substitute some of these materials by polymers. Poly(ethylene terephthalate) based electrodes can replace glass electrodes, improving the flexibility and impact resistance of a DSSC. If the cell was not appropriately sealed, liquid electrolytes were volatile and possibly will leak. Their replacement by polymeric electrolytes solved both troubles with the further advantage that they perform as a binder for the electrodes. More lately, essentially conducting polymers have been used as hole conducting materials in DSSC, with talented results.

Reineck *et al.* [24] reported on the fabrication and performance analysis of such a solid-state plasmonic solar cell. Au and Ag nanoparticle mono layers on a TiO<sub>2</sub>-coated substrates using the organic hole conductor Spiro-OMeTAD were fabricated. Au NPs were prepared using the Turkevich citrate reduction method. Ag particles were prepared using a modified borohydride reduction procedure of silver nitrate. Preparation of TiO<sub>2</sub> on FTO-coated glass using the spray pyrolysis method was studied. Au and Ag solution was pipetted onto TiO<sub>2</sub> substrate. The fabricated solar cells were fabricated from the Au and Ag nanoparticle mono layers on TiO<sub>2</sub>-coated substrates. It was found that, photocurrent was generated by the excitation of Au or Ag nanoparticles coated on TiO<sub>2</sub>, while holes were transported through a hole conducting material (Spiro-OMeTAD) to the counter electrode. The nanoparticle films were created via a fast and scalable, electrostatic self-assembly method yielding well-defined interparticle distances. These optically homogeneous films absorb up to 37% of the incident photons at the respective surface plasmon resonance wavelengths. The spectral photocurrent response of the solar cells closely follows the absorption spectrum of the metal nanoparticle layers. The photocurrents were sustainable for at least 20 h demonstrating that the charge separation process was regenerative.

Turkevich method for gold nanoparticle synthesis revisited was reported by Kimling *et al.* [25]. The growth of gold nanoparticles by reduction by citrate and ascorbic acid had been examined in detail to investigate the parameter space of reaction conditions. It was found that gold particles could be formed in a wide range of sizes, from 9 to 120 nm, with defined size distribution, following the earlier work of Turkevich [26]. The reaction was initiated thermally or in comparison by UV irradiation, which results in similar final products. The kinetics of the extinction spectra showed the multiple steps of primary and secondary clustering leading to polycrystallites. The results showed that the organize of the easy Turkevich method by the reduction conditions was sufficient to define particles in shape and size.

Size evaluation of gold nanoparticles by UV–vis spectroscopy was studied by Amendola *et al.* [27]. They reported a technique for the estimation of the average size of gold nanoparticles based on the fitting of their UV–vis spectra by the Mie model for spheres. The technique gave good results using a calibration of the dumping frequency of the surface plasmon resonance and accounting for the presence of nonspherical AuNP in solution by the Gans model for spheroids. It had been effectively useful to free and functionalized gold nanoparticles in various solvents with diameters in the 4–25 nm range. Even though the differences among samples, they found an accuracy of about 6% on the nanoparticles average size with respect to sizes studied by transmission electron microscopy (TEM). Furthermore, the fitting model provided other information not obtainable from TEM like the concentration of AuNPs in the sample and the fraction of nonspherical nanoparticles, which was mostly helpful for measuring aggregation processes.

The pore filling of spiro-OMeTAD (2,2',7,7'-tetrakis-(*N,N*-di-*p*-methoxyphenylamine)9,9'-spirobifluorene) in mesoporous TiO<sub>2</sub> films was quantified for the first time using XPS depth profiling and UV–vis absorption spectroscopy by Ding *et al.* [28]. It was revealed that spiro-OMeTAD could penetrate the whole depth of the film, and its concentration was steady throughout the film. They found that in a 2.5- $\mu$ m-thick film, the volume of the pores was 60–65% filled. The pores become less filled when thicker films were used. Such filling fraction was much higher than the solution concentration since the excess solution on top of the film could act as a reservoir during the spin coating process. Lastly, they demonstrated that by using a lower spin coating speed and higher spiro-OMeTAD solution concentration, they could increase the filling fraction and consequently the efficiency of the device.

A simple strategy was presented by Docampo *et al.* [29] to determine the pore-filling fraction of the hole-conductor 2,2'-7,7'-tetrakis-*N,N*-di-*p*-methoxyphenylamine-9,9'-spirobifluorene (spiro-OMeTAD) into mesoporous photoanodes in solid-state dye-sensitized solar cells (ss-DSCs). Based on refractive index determination by the film's reflectance spectra and using effective medium approximations the volume fractions of the component materials could be extracted, consequently the pore-filling fraction quantified. This non-destructive method could be used with entire films and did not

require detailed model assumptions. Pore-filling fractions of up to 80% are estimated for optimized solid-state DSSCs photoanodes, which was higher than that earlier estimated by indirect methods. Furthermore, transport and recombination lifetimes as a function of the pore-filling fraction were determined using photovoltage and photocurrent decay measurements. While extended electron lifetimes were observed with increasing pore-filling fractions, no trend was found in the transport kinetics. The data suggested that a pore-filling fraction of greater than 60% was necessary to achieve optimized performance in ss-DSSCs. This degree of pore-filling was even achieved in 5  $\mu\text{m}$  thick mesoporous photoanodes. It was concluded that pore-filling was not a limiting factor in the fabrication of “thick” ss-DSSCs with spiro-OMeTAD as the hole-conductor.

Yoon *et al.* [30] reported a process for fabricating  $\text{TiO}_2$  nano-patterns using nanoimprint lithography and a sol–gel method. An ethanol-based  $\text{TiO}_2$  sol was prepared using tetrabutylorthotitanate as a precursor and used as an imprint resin. A replicated polydimethylsiloxane (PDMS) mold was used as an imprint stamp. During the imprinting procedure at 5 atm and  $200^\circ\text{C}$  for 1 h, the  $\text{TiO}_2$  sol changed to a  $\text{TiO}_2$  gel by absorbing the solvent into the PDMS mold. After imprinting, a  $\text{TiO}_2$  gel pattern was formed on an oxidized Si wafer. After subsequent annealing, it confirmed that patterns of the master template were transferred to  $\text{TiO}_2$  patterns by scanning electron microscopy. Furthermore, transmission electron microscopy and X-ray diffraction showed that the  $\text{TiO}_2$  gel patterns had been converted to an inorganic polycrystalline  $\text{TiO}_2$  pattern.



### 3.2 Materials

**Table 3.1** Chemical, molecular weight, purity and company.

<b>Chemical</b>	<b>Molecular weight</b>	<b>Purity</b>	<b>Company</b>
Ethanol absolute (C <sub>2</sub> H <sub>5</sub> OH)	46.08	100% v/v	Ajax
Ammonia (NH <sub>3</sub> )	17	25% v/v	Merck
Ethanol absolute (C <sub>2</sub> H <sub>5</sub> OH)	46.08	100% v/v	Ajax
Formic acid (HCOOH)	46.02	90%	Ajax
Gold chloride hydrate (H(AuCl <sub>4</sub> ).H <sub>2</sub> O)	393.83	49% of gold	Electron Microscopy Science
Nitric acid (HNO <sub>3</sub> )	63.01	65% v/v	Merck
Oxalic acid (C <sub>2</sub> H <sub>2</sub> O <sub>4</sub> ·2H <sub>2</sub> O)	126.07	98%	Aldrich
Perchloric acid(HClO <sub>4</sub> )	100.47	70%	Ajax

**Table 3.1 (cont.)** Chemical, molecular weight, purity and company.

<b>Chemical</b>	<b>Molecular weight</b>	<b>Purity</b>	<b>Company</b>
Ethanol absolute (C <sub>2</sub> H <sub>5</sub> OH)	46.08	100% v/v	Ajax
1-Octadecanethiol ((CH <sub>3</sub> (CH <sub>2</sub> ) <sub>17</sub> SH),	286.56	98%	Aldrich
5,10,15,20-Tetrakis (1- methyl-4-pyridinio) porphyrin tetra(p- toluenesulfonate) (C <sub>72</sub> H <sub>66</sub> N <sub>8</sub> O <sub>12</sub> S <sub>4</sub> , TMPyP)	1363.60	97%	Aldrich
Sodium copper chlorophyllin (C <sub>34</sub> H <sub>31</sub> CuN <sub>4</sub> Na <sub>3</sub> O <sub>6</sub> , SCC)	724.15	99%	Aldrich
Ferrous sulfate heptahydrate (FeSO <sub>4</sub> .7H <sub>2</sub> O)	278.01	99.99%	Aldrich
sodium sulfate (Na <sub>2</sub> SO <sub>4</sub> )	142.04	99.99%	Aldrich

### 3.3 Instruments

**Table 3.2** Instruments, model and company.

<b>Instruments</b>	<b>Model</b>	<b>Company</b>
Ultrasonic bath	D-78224 Transonic Digitals	Elma
Oven	Memmert 70	Memmert
Atomic force microscope (AFM)	SPM-9600	SHIMADZU
Potentiostat set	HZ-5000	Hokuto Denko Ltd.
Solar simulator (AM1.5)	HAL-C100	Asahi Spectra
Scanning electron microscope (SEM)	JSM6335F	JEOL
UV-vis spectrophotometer (UV-vis)	V-650	Jasco
Spin coater	1H-D3	Misaka
UV/Ozone Cleaning Equipment	ASM401N	ASUMI GIKEN Limited
Imprint machine	AH-1T	AS ONE

## **3.4 Experimental**

### **3.4.1 Preparation of 1 mM gold nanoparticles**

1 mM gold nanoparticles were prepared by citrate reduction method [25, 27]. Briefly,  $\text{HAuCl}_4$  (2 mM, 10 mL) and trisodium citrate (5 mM, 10 mL) were separately heated to 100°C and consecutively mixed together under vigorous stirring. The solution were further kept heating at 100°C and stirring for 15 min. Then, the solution was cooled down to room temperature before using. The average size of gold nanoparticles were estimated to be ca. 20 nm from our previous study and UV-vis absorption measurement as the peak position was related to the average size of those particles [17, 25, 27].

### **3.4.2 Preparation of BD-Rs grating master template**

Blu-ray Recordable discs (BD-Rs, LTH type, TAIYO YUDEN) were used as diffraction grating substrates ( $\Lambda = 320$  nm). BD-Rs were cut into rectangles (2.5 cm  $\times$  4.0 cm) and soaked in nitric acid for 20 min to remove the dye layer deposited on the polycarbonate grating side. The grating substrate was cleaned sequentially by using first a commercial detergent, then water, then distilled water, and finally DI water. Figure 3.1 shows AFM image of BD-Rs grating master template.

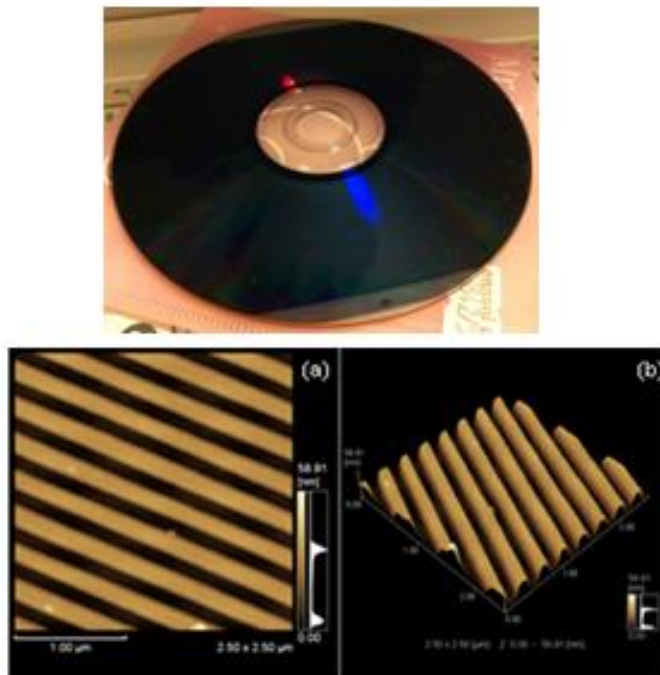


**Figure 3.1** AFM image of BD-Rs grating master template.

### **3.4.3 Preparation of PDMS grating mold**

Sylgard 184 silicone elastomer base and silicone elastomer curing agent were mixed in a ratio of 10 parts base to 1 curing by weight. Then, the silicone elastomer mixture was stirred for 5 min. All bubbles in the silicone elastomer mixture were removed before pouring into the BD-R grating master template. All bubbles were removed again and it was heated at 79°C for 3 h. Finally, BD-R was removed to get PDMS grating mold as shown in Figure 3.2.

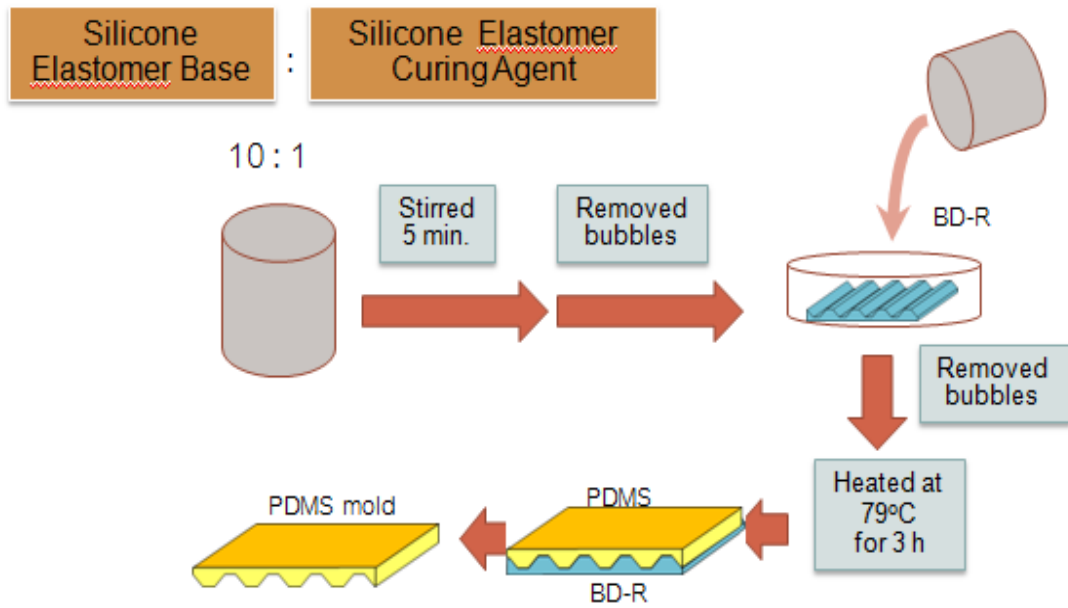


**Figure 3.2** Scheme of PDMS grating mold preparation.

#### 3.4.4 Indium Tin Oxide (ITO) glass substrate cleaning

ITO glasses with a sheet resistance ( $R_s$ ) of  $10 \Omega/\text{sq}$  were prepared with the size of 25 mm x 33 mm. After that, they were cleaned by commercial detergent, tap water, distilled water and DI water respectively in an ultrasonic bath for 20 min each. Then, they were dried in an oven at  $60^\circ\text{C}$  for 3 h. Finally, ITO glasses were cleaned in the Ultraviolet Ozone cleaning for 30 min.

#### 3.4.5 Fabrication of the grating pattern on the solid-state electrolyte/ $\text{TiO}_2$ or solid-state electrolyte/Au- $\text{TiO}_2$ films

$\text{TiO}_2$  gel was deposited on ITO substrates to form a compact  $\text{TiO}_2$  layer.  $\text{Ti}(\text{OCH}_2\text{CH}_2\text{CH}_2\text{CH}_3)_4$  in  $\text{EtOH}/\text{HNO}_3$  was heated at  $125^\circ\text{C}$  for 5 min.  $\text{TiO}_2$  gel was then spin coated on the ITO substrate. For the porous  $\text{TiO}_2$  layer,  $\text{TiO}_2$  (commercial Degussa P25- $\text{TiO}_2$ ) was deposited by the squeegee technique with subsequent calcination at  $450^\circ\text{C}$  for 30 min. For the porous Au- $\text{TiO}_2$  layer, deposited P25- $\text{TiO}_2$  film was immersed in 1 mM gold nanoparticles dispersion solution for 30 min. And then, it

was calcined at 450°C for 30 min. Localized surface plasmon absorption was observed at around 550 nm in the Au-TiO<sub>2</sub> film on ITO substrate by UV-vis spectroscopy. The TiO<sub>2</sub> or Au-TiO<sub>2</sub> on the ITO substrate samples were then immersed in 0.5 mM di-tetrabutylammonium *cis*-bis(isothiocyanato)bis(2,2'-bipyridyl-4,4'-dicarboxylato) ruthenium(II) (N-719) (Sigma-Aldrich) for 12 h and the solid-state electrolyte, spiro-OMeTAD (EMD Chemicals; Merck), was spin coated on the N-719/TiO<sub>2</sub>. Spiro-OMeTAD (dissolved in chlorobenzene at a concentration of 225 mg/mL) was mixed with 4-*tert*-butylpyridine (tBP) and lithium bis(trifluoromethylsulfonyl)imide salt (Li-TFSI) as an ionic dopant before spin coating. The grating pattern was then fabricated on the spiro-OMeTAD layer by the nanoimprinting technique using a PDMS mold as a template at 125°C for 30 min. The grating pattern was stable after immersion in a dye solution, and this technique is therefore applicable for fabricating DSSC photoanodes. The procedure for fabricating the grating pattern on the spiro-OMeTAD layer by the nanoimprinting technique is represented in Figure 3.3. The silver electrode was then deposited by the vacuum evaporation method on the spiro-OMeTAD layer as shown in Figure 3.4.

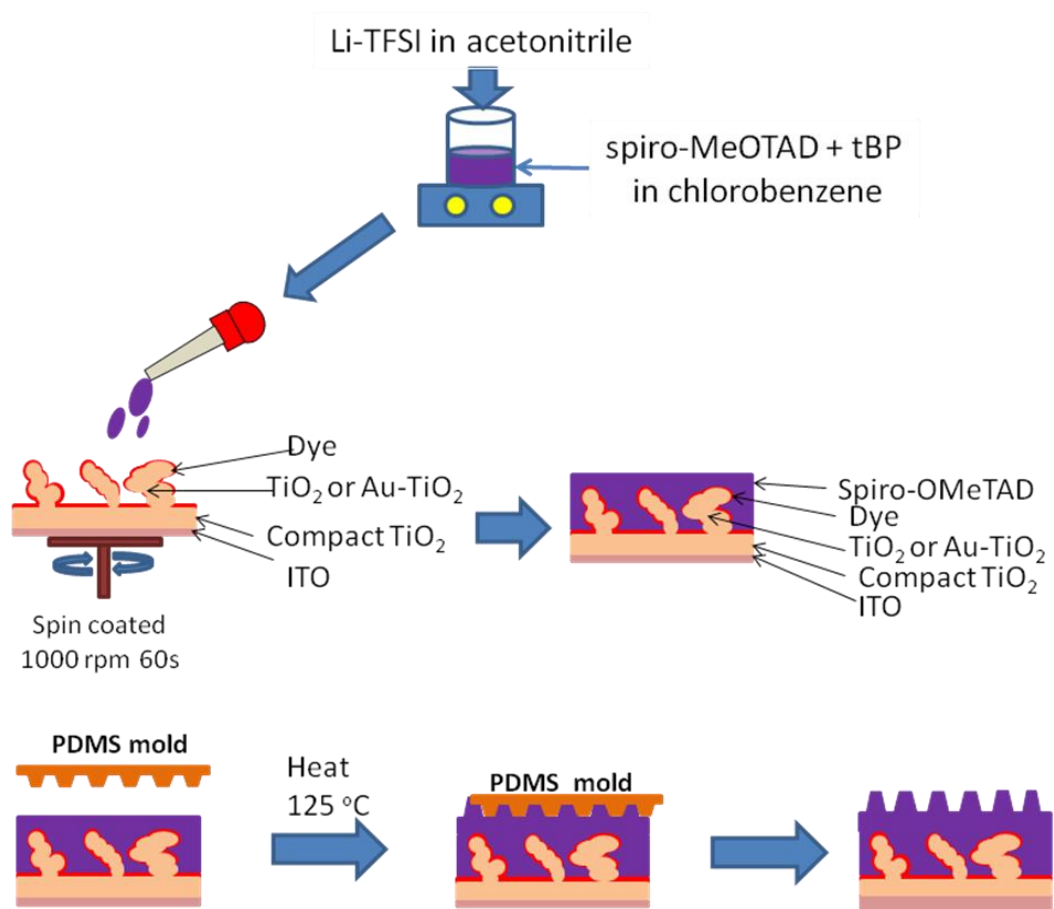


**Figure 3.3** Schematic illustration for fabricating the grating pattern of Ag/spiro-OMeTAD.





**Figure 3.4** The silver electrode deposited by the vacuum evaporation method on the spiro-OMeTAD layer.

### **3.4.6 Surface plasmon resonance measurements**

SPR-reflectivity scan measurements of Ag/spiro-OMeTAD (imprinted grating)/N-719/TiO<sub>2</sub>/ITO-glass, as shown in Figure 3.5, were conducted by mounting the prepared cells on a goniometer. A halogen lamp was used as the white light source for the SP excitation. P-polarized light was collimated by objectives and irradiated on the grating samples. A monochromator was used to detect the reflected zero-order light after it passed through a pin hole and an optical fiber. The SPR excitation experiments were conducted at a fixed incident angle as a function of the wavelength.

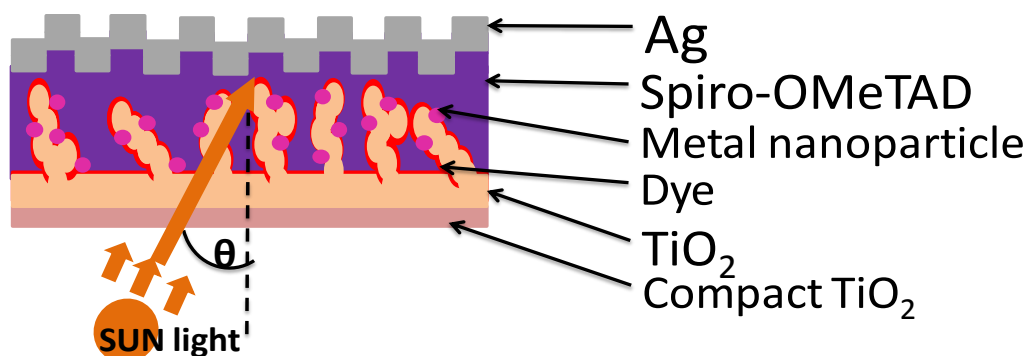


**Figure 3.5** Fabricated dye-sensitized solar cells (DSSCs).

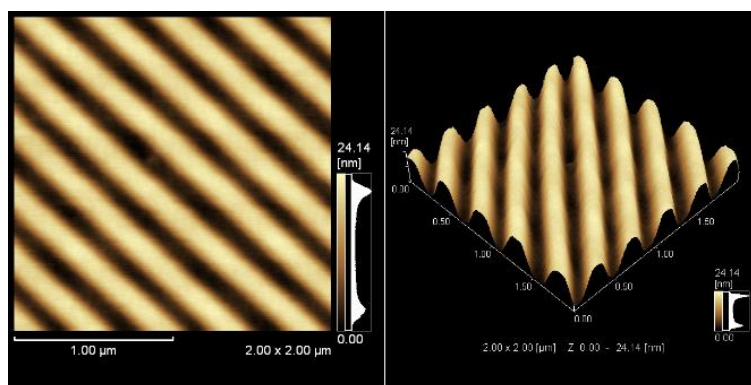
### 3.4.7 Characterization of the fabricated solid-state dye-sensitized solar cells

Photocurrent properties were studied by irradiation with a solar simulator (HAL-C100, 75 mW/cm<sup>2</sup> compact xenon light source, ASAHI SPECTRA) on the fabricated solid-state DSSCs. The light was irradiated at an incident angle of 0°.

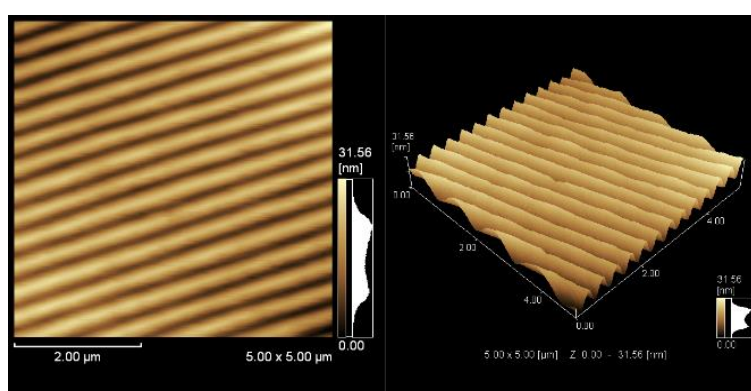
## 3.5 Results and discussion

### 3.5.1 Atomic force microscopy images of the imprinted grating pattern

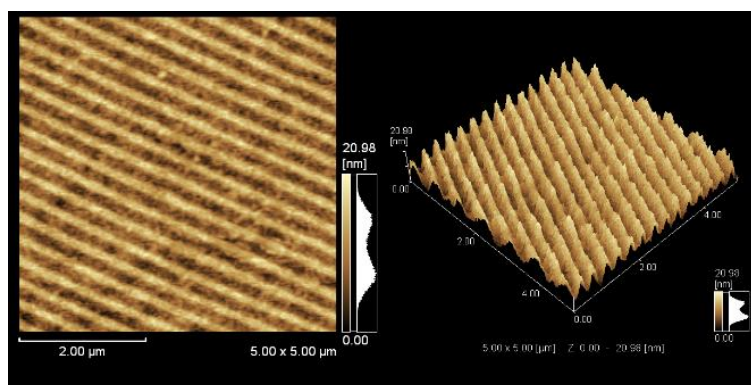
An atomic force microscopy (AFM) of grating patterned PDMS mold is shown in Figure 3.6(a). The grating height of grating patterned PDMS mold was approximately 20 nm with the grating pitch approximately 320 nm. AFM image of imprinted spiro-OMeTAD on the N-719/TiO<sub>2</sub>/ITO/glass substrate is shown in Figure 3.6(b). It can be seen that the grating pattern was created on the spiro-OMe-TAD layer with a grating height of approximately 12 nm. Even after the deposition of the silver layer (approximately 150 nm) on the spiro-OMeTAD layer, the grating pattern was visible on the silver surface, although the grating height decreased to approximately 10 nm (Figure 3.6(c)). Moreover, it was found that the grating pitch of Ag grating was approximately 320 nm.



(a)



(b)



(c)

**Figure 3.6** AFM images of grating patterned PDMS mold (a), imprinted spiro-OMeTAD on the N-719/TiO<sub>2</sub>/ITO/glass substrate (b), and Ag/spiro-OMeTAD on the N-719/TiO<sub>2</sub>/ITO/glass substrate (c).

### 3.5.2 White light-SPR measurements

SPR reflectivity curves for the fabricated Ag/spiro-OMeTAD/N-719/TiO<sub>2</sub>/ITO-glass substrate structure as a function of the wavelength at each fixed incident angle upon irradiation with white light are shown in Figure 3.7. The light was irradiated from the side of the glass substrates. Reflectivity dips can be observed at each incident angle. This result indicates that the propagating surface plasmon can certainly be excited at the Ag/spiro-OMeTAD/dye interface, which is useful to confine and enhance the irradiated light in the photoelectric conversion layer. Although the SPR reflectivity curve was not obtained at an incident angle of 0° due to current experimental configuration, the SPR dip wavelength at 0° is roughly estimated to be around 400 nm where the absorption of N-719 dye corresponded.

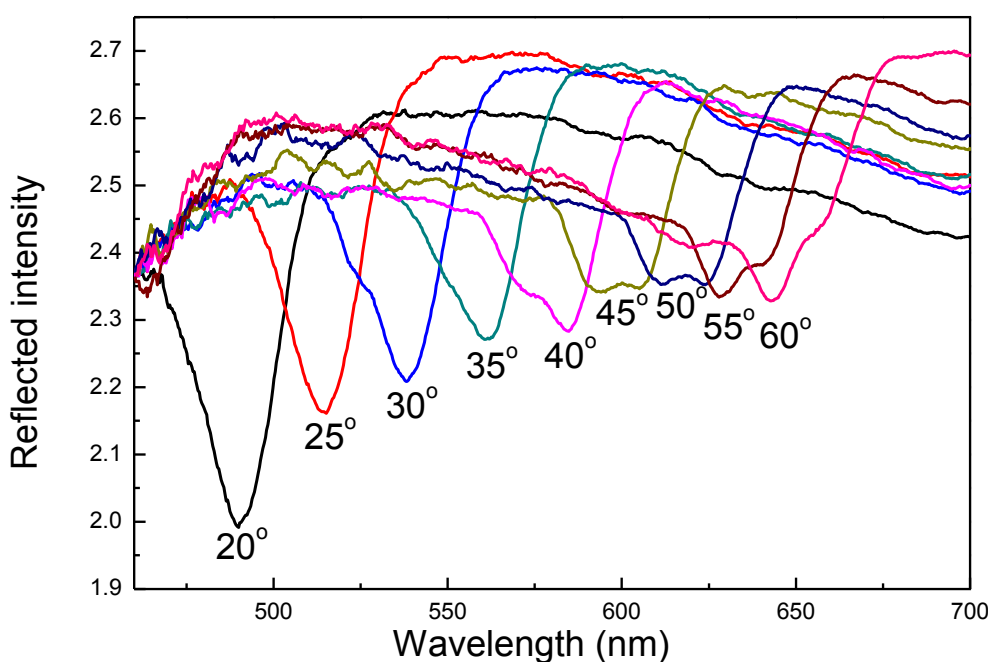


**Figure 3.7** SPR reflectivity curves for the Ag/spiro-OMeTAD (imprinted grating)/N-719/TiO<sub>2</sub>/ITO-glass measured at fixed incident angles of 20°–60°.

### 3.5.3 Short-circuit photocurrent measurements

To study the effect of the propagating grating-coupled SP excitation, current density vs. voltage (J–V) curves for Ag/spiro-OMeTAD (imprinted grating)/N-719/TiO<sub>2</sub>/ITO-glass and Ag/spiro-OMeTAD (without imprinting)/N-719/TiO<sub>2</sub>/ITO-glass were measured, and the results are shown in Figure 3.8. Photovoltaic performance was calculated from these J–V curves, and the results are shown in Table 3.3. The open circuit voltage ( $V_{oc}$ ) of TiO<sub>2</sub> with the imprinted Ag grating was almost equal to the  $V_{oc}$  of TiO<sub>2</sub> with flat Ag (without imprinting), but the short-circuit current density ( $J_{sc}$ ) was higher. Therefore, the efficiency ( $\eta$ ) of TiO<sub>2</sub> with the imprinted Ag grating was higher than the photoefficiency of TiO<sub>2</sub> with flat Ag (without imprinting). This result confirms that the propagating surface plasmon of the grating structure increased the photocarriers in the dye, and hence the current density of the fabricated solid-state DSSCs.

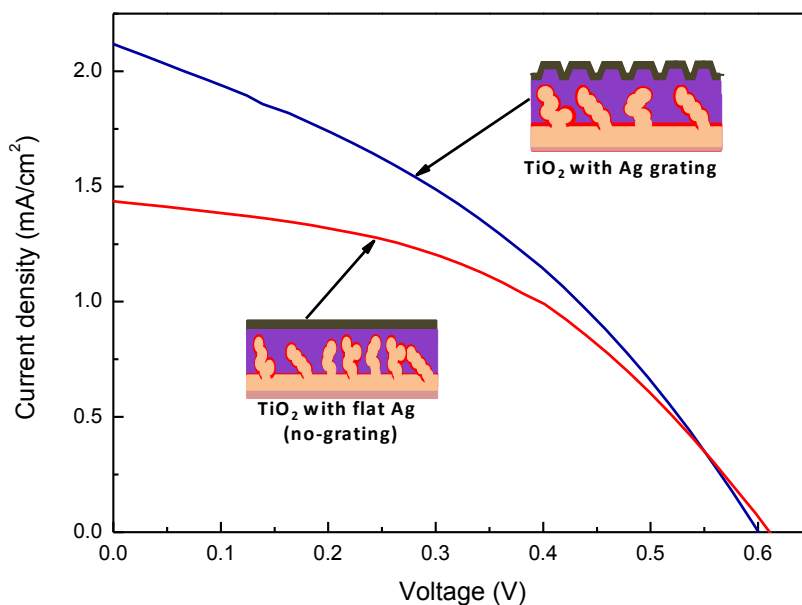


**Figure 3.8** Current density vs. voltage (J–V) curves for Ag/spiro-OMeTAD (imprinted grating)/N-719/TiO<sub>2</sub>/ITO-glass and Ag/spiro-OMeTAD (without imprinting)/N-719/TiO<sub>2</sub>/ITO-glass.

**Table 3.3** Photovoltaic performance of Ag/spiro-OMeTAD (imprinted grating)/N-719/TiO<sub>2</sub>/ITO-glass and Ag/spiro-OMeTAD (without imprinting)/N-719/TiO<sub>2</sub>/ITO-glass.

	$V_{oc}$ (V)	$J_{sc}$ (mA/cm <sup>2</sup> )	$\eta$ (%)	$FF$
TiO <sub>2</sub> with imprinted grating	0.60	2.11	0.62	0.37
TiO <sub>2</sub> without imprinting	0.61	1.44	0.53	0.45

To further enhance the short-circuit photocurrent, Au-TiO<sub>2</sub> was then used on the grating structure. The short-circuit photocurrent properties of all samples were studied by solar light irradiation. The short-circuit photocurrent properties of Ag/spiro-OMeTAD (imprinted grating)/N-719/Au-TiO<sub>2</sub>/ITO-glass, Ag/spiro-OMeTAD (imprinted grating)/N-719/TiO<sub>2</sub>/ITO-glass, and Ag/spiro-OMeTAD (without imprinting)/N-719/TiO<sub>2</sub>/ITO-glass are shown in Figure 3.9. The results show that the photocurrent increased when the Ag grating structure on spiro-OMeTAD was used. Moreover, the photocurrent further increased when the Au-TiO<sub>2</sub> was used instead of TiO<sub>2</sub> (without Au loading). The results show that a combination of the propagating surface plasmon of the grating structure and the localized surface plasmon of Au leads to an increase in the photoelectric conversion properties. As shown in the figure, the cell with Au-TiO<sub>2</sub> showed slow response for the increase of the photocurrent. The mechanism for this is not clear yet, however, one possibility is due to the formation of an electric double layer on Au nanoparticles. It is known that the TiO<sub>2</sub> surface in solid-state DSSCs is negatively charged under light irradiation by the injected electrons and the electric double layer is formed on the surface of TiO<sub>2</sub> or the electrode [31]. The formation of the electric double layer is known to be slow process in the solid-state DSSCs [32]. In the case of Au-TiO<sub>2</sub>, the Au nanoparticles act as the enhancement of

electric field, at the same time, the bare Au nanoparticles facilitate the charge recombination, which causes the decrease of the photocurrent. The electric double layer gradually forms on the Au nanoparticles, hence the photocurrent should gradually increase as the electric double layer prevent the charge recombination at the Au nanoparticles interfaces.

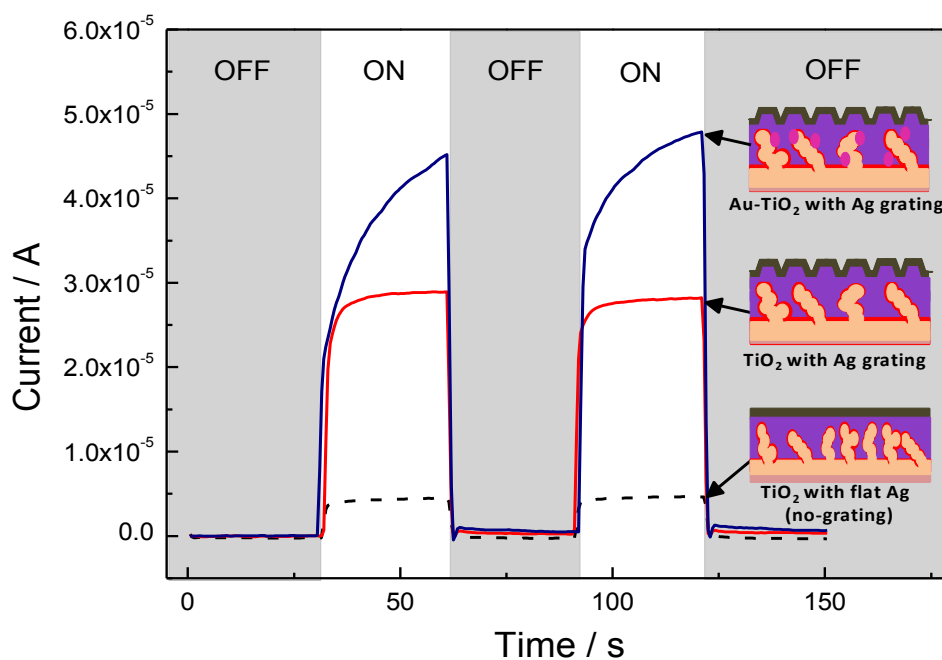


**Figure 3.9** Short-circuit photocurrent properties upon irradiation with solar light: Ag/spiro-OMeTAD (imprinted grating)/N-719/Au-TiO<sub>2</sub>/ITO-glass, Ag/spiro-OMeTAD (imprinted grating)/N-719/TiO<sub>2</sub>/ITO-glass, and Ag/spiro-OMeTAD (without imprinting)/N-719/TiO<sub>2</sub>/ITO- glass.

### 3.6 Conclusions

The fabrication of a grating structure formed by a solid-state electrolyte layer on a dye-TiO<sub>2</sub> film by the nanoimprinting technique using a polydimethylsiloxane (PDMS) stamp and its application in photoelectric conversion devices are described. The PDMS grating pattern is imprinted from blu-ray disc recordable. A silver electrode was deposited on the patterned solid-state electrolyte layers. Surface plasmon resonance (SPR) excitation was observed in the fabricated solar cells by irradiation with white light. The photoelectric conversion properties were measured to study the effect of the two types of SPR excitations, i.e., the propagating surface plasmon on the Ag grating surface and the localized surface plasmon from the Au nanoparticles on TiO<sub>2</sub>.



## REFERENCE

- [1] K. G. Deepa, P. Lekha, and S. Sindhu, "Efficiency enhancement in DSSC using metal nanoparticles: A size dependent study," *Solar Energy*, vol. 86, no. 1, pp. 326–330, 2012.
- [2] A. Baba, K. Wakatsuki, K. Shinbo, K. Kato, and F. Kaneko, "Increased short-circuit current in grating-coupled surface plasmon resonance field-enhanced dye-sensitized solar cells," *Journal of Materials Chemistry*, vol. 21, pp. 16436–16441, 2011.
- [3] S. Muduli, O. Game, V. Dhas, K. Vijayamohanan, K. A. Bogle, N. Valanoor, and S. B. Ogale, "TiO<sub>2</sub>–Au plasmonic nanocomposite for enhanced dye-sensitized solar cell (DSSC) performance," *Solar Energy*, vol. 86, no. 5, pp. 1428–1434, 2012.
- [4] A. F. Nogueira, C. Longo, and M. A. De Paoli, "Polymers in dye sensitized solar cells: overview and perspectives," *Coordination Chemistry Reviews*, vol. 248, no. 13–14, pp. 1455–1468, 2004.
- [5] H. J. Snaith and L. Schmidt-Mende, "Advances in liquid-electrolyte and solid-state dye-sensitized solar cells," *Advanced Materials*, vol. 19, no. 20, pp. 3187–3200, 2007.
- [6] H. J. Snaith, A. J. Moule, C. Klein, K. Meerholz, R. H. Friend, and M. Grätzel, "Efficiency enhancements in solid-state hybrid solar cells via reduced charge recombination and increased light capture," *Nano Letters*, vol. 7, no. 11, pp. 3372–3376, 2007.

- [7] A. Baba, N. Aoki, K. Shinbo, K. Kato, and F. Kaneko, "Grating-coupled surface plasmon enhanced short-circuit current in organic thin-film photovoltaic cells," *ACS Applied Materials & Interfaces*, vol. 3, no. 6, pp. 2080–2084, 2011.
- [8] H. A. Atwater and A. Polman, "Plasmonics for improved photovoltaic devices," *Nature Materials*, vol. 9, no. 3, pp. 205–213, 2010.
- [9] V. E. Ferry, J. N. Munday, and H. A. Atwater, "Design considerations for plasmonic photovoltaics," *Advanced Materials*, vol. 22, no. 43, pp. 4794–4808, 2010.
- [10] I. K. Ding, J. Zhu, W. Cai, S.-J. Moon, N. Cai, P. Wang, S. M. Zakeeruddin, M. Grätzel, M. L. Brongersma, Y. Cui, and M. D. McGehee, "Plasmonic dye-sensitized solar cells," *Advanced Energy Materials*, vol. 1, no. 1, pp. 52–57, 2011.
- [11] J. Homola, I. Koudela, and S. S. Yee, "Surface plasmon resonance sensors based on diffraction gratings and prism couplers: sensitivity comparison," *Sensors and Actuators B: Chemical*, vol. 54, no. 1–2, pp. 16–24, 1999.
- [12] W. Knoll, "Interfaces and thin films as seen by bound electromagnetic waves," *Annual Review of Physical Chemistry*, vol. 49, no. 1, pp. 569–638, 1998.
- [13] B. K. Singh and A. C. Hillier, "Surface Plasmon Resonance Imaging of Biomolecular Interactions on a Grating-Based Sensor Array," *Analytical Chemistry*, vol. 78, no. 6, pp. 2009–2018, 2006.
- [14] B. K. Singh and A. C. Hillier, "surface plasmon resonance enhanced transmission of light through gold-coated diffraction gratings," *Analytical Chemistry*, vol. 80, no. 10, pp. 3803–3810, 2008.

- [15] B. Akira, K. Kenji, O. Tsutomu, O. Yasuo, S. Kazunari, K. Keizo, and K. Futao, "Multimode surface plasmon excitations on organic thin film/metallic diffraction grating," *Japanese Journal of Applied Physics*, vol. 49, no. 1S, p. 01AE02–1–4, 2010.
- [16] V. E. Ferry, L. A. Sweatlock, D. Pacifici, and H. A. Atwater, "Plasmonic nanostructure design for efficient light coupling into solar cells," *Nano Letters*, vol. 8, no. 12, pp. 4391–4397, 2008.
- [17] H. Ninsonti, A. Baba , W. Kangwansupamonkon, S. Phanichphant, K. Shinbo, K. Kato, F. Kaneko "Enhanced photocurrent properties of dye/Au-loaded TiO<sub>2</sub> films by grating-coupled surface plasmon excitation," *IEICE Transactions on Electronics*, vol. E96–C, no. 3, pp. 385–388, 2013.
- [18] Y. Liu, H. Yu, H. Wang, S. Chen, and X. Quan, "Efficient H<sub>2</sub> production over Au/graphene/TiO<sub>2</sub> induced by surface plasmon resonance of Au and band-gap excitation of TiO<sub>2</sub>," *Materials Research Bulletin*, vol. 59, pp. 111–116, 2014.
- [19] H. Dong, Z. Wu, Y. Gao, A. El-Shafei, S. Ning, J. Xi, B. Jiao, and X. Hou, "Silver-loaded anatase nanotubes dispersed plasmonic composite photoanode for dye-sensitized solar cells," *Organic Electronics*, vol. 15, no. 11, pp. 2847–2854, 2014.
- [20] R. A. Pala, J. White, E. Barnard, J. Liu, and M. L. Brongersma, "Design of plasmonic thin-film solar cells with broadband absorption enhancements," *Advanced Materials*, vol. 21, no. 34, pp. 3504–3509, 2009.
- [21] D. M. Schaadt, B. Feng, and E. T. Yu, "Enhanced semiconductor optical absorption via surface plasmon excitation in metal nanoparticles," *Applied Physics Letters*, vol. 86, no. 6, pp. 063106–1–063106–3, 2005.

- [22] D. Derkacs, W. V. Chen, P. M. Matheu, S. H. Lim, P. K. L. Yu, and E. T. Yu, "Nanoparticle-induced light scattering for improved performance of quantum-well solar cells," *Applied Physics Letters*, vol. 93, no. 9, pp. 091107–1–091107–3, 2008.
- [23] S. H. Lim, W. Mar, P. Matheu, D. Derkacs, and E. T. Yu, "Photocurrent spectroscopy of optical absorption enhancement in silicon photodiodes via scattering from surface plasmon polaritons in gold nanoparticles," *Journal of Applied Physics*, vol. 101, no. 10, pp. 104309–1–104309–7, 2007.
- [24] P. Reineck, G. P. Lee, D. Brick, M. Karg, P. Mulvaney, and U. Bach, "A solid-state plasmonic solar cell via metal nanoparticle self-assembly," *Advanced Materials*, vol. 24, no. 35, pp. 4750–4755, 2012.
- [25] J. Kimling, M. Maier, B. Okenve, V. Kotaidis, H. Ballot, and A. Plech, "Turkevich method for gold nanoparticle synthesis revisited," *The Journal of Physical Chemistry B*, vol. 110, no. 32, pp. 15700–15707, 2006.
- [26] J. Turkevich, P. C. Stevenson, and J. Hillier, "A study of the nucleation and growth processes in the synthesis of colloidal gold," *Discussions of the Faraday Society*, vol. 11, pp. 55–75, 1951.
- [27] V. Amendola and M. Meneghetti, "Size evaluation of gold nanoparticles by UV–vis spectroscopy," *The Journal of Physical Chemistry C*, vol. 113, no. 11, pp. 4277–4285, 2009.
- [28] I. K. Ding, N. Tétreault, J. Brillet, B. E. Hardin, E. H. Smith, S. J. Rosenthal, F. Sauvage, M. Grätzel, and M. D. McGehee, "Pore-filling of spiro-OMeTAD in solid-state dye sensitized solar cells: quantification, mechanism, and consequences for device performance," *Advanced Functional Materials*, vol. 19, no. 15, pp. 2431–2436, 2009.

- [29] P. Docampo, A. Hey, S. Guldin, R. Gunning, U. Steiner, and H. J. Snaith, "Pore filling of spiro-OMeTAD in solid-state dye-sensitized solar cells determined via optical reflectometry," *Advanced Functional Materials*, vol. 22, no. 23, pp. 5010-5019, 2012.
- [30] K.-m. Yoon, K.-y. Yang, and H. Lee, "Fabrication of polycrystalline TiO<sub>2</sub> nanopatterns by TiO<sub>2</sub> sol base imprint lithography," *Thin Solid Films*, vol. 518, no. 1, pp. 126–129, 2009.
- [31] S. Nakade, Y. Makimoto, W. Kubo, T. Kitamura, Y. Wada, and S. Yanagida, "Roles of electrolytes on charge recombination in dye-sensitized TiO<sub>2</sub> solar cells (2): The case of solar cells using cobalt complex redox couples," *The Journal of Physical Chemistry B*, vol. 109, no. 8, pp. 3488–3493, 2005.
- [32] Y. Saito, N. Fukuri, R. Senadeera, T. Kitamura, Y. Wada, and S. Yanagida, "Solid state dye sensitized solar cells using in situ polymerized PEDOTs as hole conductor," *Electrochemistry Communications*, vol. 6, no. 1, pp. 71–74, 2004.

## CHAPTER 4

### Conclusions

This research reported the enhancement of photocurrent properties at dye/gold nanoparticles loaded TiO<sub>2</sub> thin films on metallic gratings was studied. Enhanced photocurrent properties of dye/Au-loaded TiO<sub>2</sub> films by grating-coupled surface plasmon excitation was mentioned in Chapter 2 and enhanced photocurrent generation at a spiro-OMeTAD/AuNPs-TiO<sub>2</sub> interface with grating-coupled surface plasmon excitation was mentioned in Chapter 3.

In Chapter 2, DSSC was improved by using an effect of Au-loaded titanium dioxide (Au-loaded TiO<sub>2</sub>). The Au-loaded TiO<sub>2</sub> nanopowders were synthesized by the modified sol-gel method together with the impregnation method. Anatase phase of TiO<sub>2</sub> was obtained in all samples with an average particle size of 20 nm. For the enhancement of DSSCs study, DSSCs composed of the Au grating/Au-loaded TiO<sub>2</sub>/TMPyP-SCC LbL (20 bilayers)/electrolyte/ITO substrates were fabricated. Au-loaded TiO<sub>2</sub> films were deposited by electrophoretic deposition. TMPyP and SCC were used as photo-absorbing dyes and were prepared by LbL deposition. The fabricated cells were irradiated with visible light at various incident angles with SP excitation (p-pol.) and without surface plasmon excitation (s-pol.).

SPR reflectivity curves for the BD-R grating/Au (*ca.* 150 nm)/Au-TiO<sub>2</sub> film (*ca.* 30 nm)/20 bilayers of SCC-TMPyP LbL film/electrolyte/ITO substrate structure were measured as a function of wavelength. It was found that SPR dip angles shift to longer wavelengths with increasing incident angle. These results show that the SP phenomena of the samples could be observed and that enhanced electric fields could be obtained on the fabricated grating surface.

The effect of surface plasmon excitation on the short-circuit photocurrent was studied by irradiating visible light on the fabricated DSSCs. After turning on the light,

the photocurrent increased and then remained stable. The results showed that irradiation with visible light results in a higher photocurrent when grating-coupled propagating SP excitation is present than when it is not.

To further study the effects of Au-loaded TiO<sub>2</sub>, the short-circuit photocurrents of DSSCs with unloaded TiO<sub>2</sub> and Au-loaded TiO<sub>2</sub> were compared at incident angles of 0–35° with and without grating-coupled propagating SP excitation. The short-circuit photocurrents of fabricated DSSCs with Au-loaded TiO<sub>2</sub> thin films were higher than that of fabricated DSSCs with unloaded TiO<sub>2</sub> thin films. Moreover, it was found that the photocurrent increased when the amounts of Au increased from 0.25 mol% up to 1.00 mol%. This clearly indicates that the Au-loaded TiO<sub>2</sub> enhances the photocurrent of the DSSC. Furthermore, the highest photocurrent was obtained at 25° in all DSSCs; this corresponded to the overlap between the grating-coupled propagating SPR excitation wavelength and the absorption peak wavelength of the dye. In each case, grating-coupled propagating SP further increased the values of the photocurrents outside the effects of Au-loading TiO<sub>2</sub>. Moreover, the results showed that up to a 7.5-fold increase in the short-circuit photocurrent can be obtained by combining Au-loaded TiO<sub>2</sub> with grating-coupled surface plasmon excitation in the cells.

For further application on solid-state dye-sensitized solar cell (ss-DSSCs), in Chapter 3, enhanced photocurrent generation at a spiro-OMeTAD/AuNPs-TiO<sub>2</sub> interface with grating-coupled surface plasmon excitation was studied. A grating structure consisting of a solid-state electrolyte layer on a dye-TiO<sub>2</sub> film formed by the nanoimprint technique using a polydimethylsiloxane (PDMS) stamp was fabricated. The PDMS grating pattern is imprinted from blu-ray disc recordable. A silver electrode was deposited on the patterned solid-state electrolyte layers.

Surface plasmon resonance (SPR) excitation was observed in the fabricated solar cells by irradiation with white light. Reflectivity dips of the fabricated Ag/spiro-OMeTAD/N-719/TiO<sub>2</sub>/ITO-glass substrate structure could be observed at each

incident angle. This result indicates that the propagating surface plasmon could definitely be excited at the Ag/spiro-OMeTAD/dye interface, which is practical to confine and increase the irradiated light in the photoelectric conversion layer. The photoelectric conversion properties were measured to study the effect of the two types of SPR excitations, i.e., the propagating surface plasmon on the Ag grating surface and the localized surface plasmon from the Au nanoparticles on TiO<sub>2</sub>.

To further enhance the short-circuit photocurrent, Au-TiO<sub>2</sub> was then used on the grating structure. The short-circuit photocurrent properties of all samples were studied by solar light irradiation. The short-circuit photocurrent properties of Ag/spiro-OMeTAD (imprinted grating)/N-719/Au-TiO<sub>2</sub>/ITO-glass, Ag/spiro-OMeTAD (imprinted grating)/N-719/TiO<sub>2</sub>/ITO-glass, and Ag/spiro-OMeTAD (without imprinting)/N-719/TiO<sub>2</sub>/ITO-glass showed that the photocurrent increased when the Ag grating structure on spiro-OMeTAD was used. Moreover, the photocurrent further increased when the Au-TiO<sub>2</sub> was used instead of TiO<sub>2</sub> (without Au loading). The results show that the propagating surface plasmon of the grating structure and the localized surface plasmon of Au could increase in the photocurrent properties.

From Chapter 2 and 3 The results confirmed that a combination of the propagating surface plasmon of the grating structure and the localized surface plasmon of Au leads to an enhancement in the photoelectric conversion properties of the photoanode of DSSC.



## APPENDIX

### Instrument

#### A.1 Atomic force microscope



**Figure A.1** Atomic force microscope (AFM), SPM-9600, SHIMADZU.

## A.2 UV-vis spectrophotometer

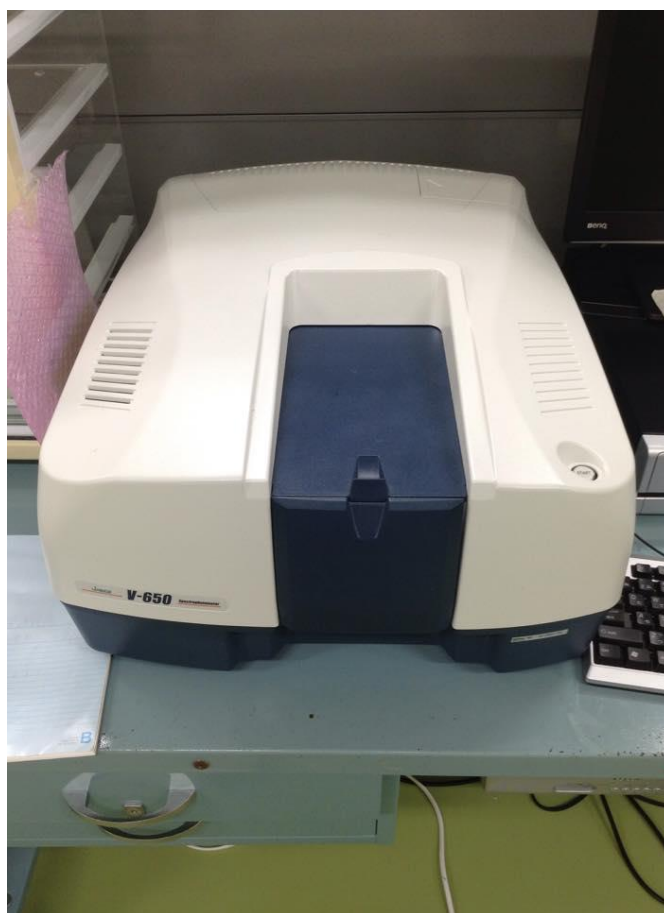


**Figure A.2** UV-vis spectrophotometer (UV-vis), V-650, Jasco.

### A.3 Solar simulator



**Figure A.3** Solar simulator (AM1.5), HAL-C100, Asahi Spectra.

#### A.4 Spin coater



**Figure A.4** Spin coater, 1H-D3, Misaka.

## CURRICULUM VITAE

Author's Name	Ms. Hathaithip Ninsonti	
Date/Year of Birth	9 September 1986	
Place of Birth	Chiang Mai	
Education	1999–2004	High school, Wattanothaipayap School, Chiang Mai, Thailand
	2005–2008	B.Sc. (Chemistry, 1 <sup>st</sup> Class Honors), Maejo University, Chiang Mai, Thailand
Scholarship	2005–2008	Human Resource Development in Science Project (Science Achievement Scholarship of Thailand, SAST)
	2008	Young Scientist and Technologist Program : YSTP, National Science and Technology Development Agency (NSTDA), Thailand
	2009–2010	Thailand Graduate Institute of Science and Technology Scholarship, National Science and Technology Development Agency (NSTDA), Thailand
	2010–2013	<i>The Royal Golden Jubilee Ph.D.</i> Program, Thailand Research Fund
	2013	Graduate School of Science and Technology, Niigata University

## Publications

- 1) H. Ninsonti, S. Sangsrichan, W. Kangwansupamonkon, S. Phanichphant and P. Pookmanee, "Hydrothermal synthesis of titanium dioxide (TiO<sub>2</sub>) micropowder," *Journal of Microscopy Society of Thailand*, vol. 23, pp. 91–94, 2009.
- 2) P. Pookmanee, H. Ninsonti, S. Sangsrichan, W. Kangwansupamonkon and S. Phanichphant, "Photocatalytic degradation of geosmin by titanium dioxide powder synthesized by the hydrothermal route" *Advanced Material Research*, vol. 93–94, pp. 161–164, 2010.
- 3) V. Kruefu, H. Ninsonti, N. Wetchakun, B. Inceesungvorn, P. Pookmanee, S. Phanichphant, "Photocatalytic degradation of phenol using Nb-loaded ZnO nanoparticles," *Engineering Journal*, vol. 16, pp. 91–99, 2012.
- 4) H. Ninsonti, W. Chomkitichai, A. Baba, W. Kangwansupamonkon, S. Phanichphant, K. shinbo, K. Kato and F. Kaneko, "Enhanced photocurrent properties of dye/Au-loaded TiO<sub>2</sub> films by grating-coupled surface plasmon excitation," *IEICE Transactions on Electronics*, vol. E96-C, pp. 385–388, 2013.
- 5) W. Chomkitichai, H. Ninsonti, C. Liewhiran, A. Wisitsoraat, S. Sriwichai, and S. Phanichphant, "Flame-made Pt-loaded TiO<sub>2</sub> thin films and their application as H<sub>2</sub> gas sensors," *Journal of Nanomaterials*, vol. 2013, pp. 1–8, 2013.

- 6) W. Chomkitichai, H. Ninsonti, A. Baba, S. Phanichphant, K. Shinbo, K. Kato, and F. Kaneko, "Multiple plasmonic effect on photocurrent generation of metal-loaded titanium dioxide composite/dye films on gold grating surface," *Surface and Interface Analysis*, vol. 46, pp. 607–612, 2014.
- 7) S. Nootchanat, H. Ninsonti, A. Baba, S. Ekgasit, C. Thammacharoen, K. Shinbo, K. Kato, and F. Kaneko, "Investigation of localized surface plasmon/grating-coupled surface plasmon enhanced photocurrent in TiO<sub>2</sub> thin films," *Physical Chemistry Chemical Physics*, vol. 16, pp. 24484–24492, 2014.
- 8) H. Ninsonti, W. Chomkitichai, A. Baba, N. Wetchakun, W. Kangwansupamonkon, S. Phanichphant, K. Shinbo, K. Kato and F. Kaneko Au-loaded titanium dioxide nanoparticles synthesized by modified sol-gel/impregnation methods and their application to dye-sensitized solar cells. *International Journal of Photoenergy*, vol. 2014, pp. 1–8, 2014.
- 9) H. Ninsonti, K. Hara, S. Nootchanat, W. Chomkitichai, A. Baba, W. Kangwansupamonkon, S. Phanichphant, K. Shinbo, K. Kato and F. Kaneko, "Enhanced photocurrent generation at spiro-OMeTAD/AuNPs-TiO<sub>2</sub> interface with grating-coupled surface plasmon excitation," *IEICE Trans. Fundamentals/Commun. /Electron./Inf. & Syst.*, vol. E85-A/B/C/D, 20xx

## Experience

- 1) Researched on “Au-loaded titanium dioxide nanoparticles synthesized by modified sol-gel/impregnation methods and their application to dye-sensitized solar cells” in the Graduate School of Science and Technology from November 2011 to October 2013 at Niigata University, Niigata, Japan.
- 2) Further study in the Double Degree Program between Chiang Mai University and Niigata University at the Graduate School of Science and Technology from December 2012 to December 2013 at Niigata University, Niigata, Japan.

## Awards

- 1) Outstanding oral presentation award, German-Thai Symposium on Nanoscience and Nanotechnology (GTSNN) 2011, 13–16 September 2011, Synchrotron Light Research Institute Conference Center, Nakhorn Ratchasima, Thailand
- 2) Oral Presentation, In recognition and appreciation certificate, RGJ Seminar Series LXXXIV : Research and Innovation in Chemistry for Sustainable and Development, 2010, Chiang Mai, Thailand
- 3) Excellent poster presentation award, Korea-Japan Joint Forum International Conference on Organic Materials for Electronics and Photonics 2012 (KJF2012), 29 August – 1 September 2012, Sendai, Japan



## Conferences

### International Conference Participation:

- 1) H. Ninsonti, S. Phanichphant and P. Pookmanee, Development Saa paper coated with titanium dioxide powders, Proceeding of the 34th Congress on Science and Technology of Thailand, 31 October – 2 November 2008, Bangkok, Thailand (Poster Presentation).
- 2) H. Ninsonti, K. Pingmuang, V. Kruefu, S. Phanichphant and P. Pookmanee, Degradation of phenol by titanium dioxide powders, Pure and Applied Chemistry International Conference, 14–16 January 2009, Phitsanulok, Thailand (Poster Presentation).
- 3) H. Ninsonti, S. Sangsrichan, W. Kangwansupamonkon, S. Phanichphant and P. Pookmanee, Hydrothermal synthesis of titanium dioxide (TiO<sub>2</sub>) micropowder, Proceedings of the 26th Annual Conference of the Microscopy Society of Thailand, 28–30 January 2009, Chiang Mai, Thailand, 207–208. (Poster Presentation).
- 4) H. Ninsonti, B. Inceesungvorn, N. Wetchakun, P. Pookmanee, W. Kangwansupamonkon and S. Phanichphant. Characterization of gold-doped titanium dioxide nanopowders for use as photocatalysts. Proceeding of NanoThailand 2010 International Conference 2010, 18–20 November 2010, Pathumthani, Thailand (Oral Presentation).

- 5) H. Ninsonti, S. Sriwichai, B. Inceesungvorn, N. Wetchakun, W. Kangwansupamonkon and S. Phanichphant. The enhancement of UV and visible light photocatalytic Activity of TiO<sub>2</sub> with gold by using the modified sol-gel coupled with the impregnation technique. RGJ Seminar Series LXXXIV : Research and Innovation in Chemistry for Sustainable and Development, 2010, Chiang Mai, Thailand (Oral Presentation).
- 6) H. Ninsonti, K. Boonpavanictchakul, S. Sriwichai, B. Inceesungvorn, N. Wetchakun, P. Pookmanee, W. Kangwansupamonkon and S. Phanichphant. Synthesis of Au-doped titanium dioxide nanoparticles by the modified sol-gel process for use as UV and visible light photocatalysts. German-Thai Symposium on Nanoscience and Nanotechnology (GTSNN) 2011, 13-16 September 2011, Synchrotron Light Research Institute Conference Center, Nakhorn Ratchasima, Thailand (Oral Presentation).
- 7) H. Ninsonti, W. Chomkitichai, A. Baba, W. Kangwansupamonkon, S. Phanichphant, K. shinbo, K. Kato and F. Kaneko. Enhanced photocurrent properties of dye/Au-loaded TiO<sub>2</sub> films by grating-coupled surface plasmon excitation. the 7th International Symposium on Organic Molecular Electronics (ISOME2012), 8–9 June 2012, Tokyo, Japan (Poster Presentation).

- 8) H. Ninsonti, W. Chomkitichai, A. Baba, W. Kangwansupamonkon, S. Phanichphant, K. shinbo, K. Kato and F. Kaneko. 2012 International Conference on Solid State Devices and Materials (SSDM 2012), 25–27 September 2012, Kyoto International Conference Center, Kyoto, Japan (Oral Presentation).
- 9) H. Ninsonti, W. Chomkitichai, A. Baba, W. Kangwansupamonkon, S. Phanichphant, K. shinbo, K. Kato and F. Kaneko. Enhanced photovoltaic properties in dye-sensitized solar cell using Au-loaded TiO<sub>2</sub>. KJF (Korea-Japan Joint Forum) International Conference on Organic Materials for Electronics and Photonics 2012 (KJF2012), 29 August – 1 September 2012, Sendai, Japan (Poster Presentation).
- 10) H. Ninsonti, W. Chomkitichai, A. Baba, W. Kangwansupamonkon, S. Phanichphant, K. shinbo, K. Kato and F. Kaneko. Photocurrent enhancement in dye-sensitized solar cells with Au-loaded TiO<sub>2</sub> on metallic grating surface. 2013 Niigata Graduate Research Forum, 10–15 January 2013, Niigata University, Niigata-shi, Japan (Oral Presentation).
- 11) H. Ninsonti, W. Chomkitichai, A. Baba, N. Wetchakun, W. Kangwansupamonkon, S. Phanichphant, K. shinbo, K. Kato and F. Kaneko. Improvement of dye-sensitized solar cell using Au-loaded TiO<sub>2</sub> synthesized by modified sol-gel/impregnation method. The 4<sup>th</sup> International Symposium on Organic Electronic Materials and

Related Nanotechnologies (EM-NANO 2013), 17–20 June 2013, Kanazawa, Japan (Poster Presentation).

12)H. Ninsonti, W. Chomkitichai, S. Nootchanat, C. Khantha, A. Baba, S. Phanichphant, K. shinbo, K. Kato and F. Kaneko. Fabrication of metal nanoparticles-loaded TiO<sub>2</sub> grating pattern by sol-gel nanoimprinting technique. Korea-Japan Joint Forum International Conference 2013 on Organic Materials for Electronics and Photonics (KJF 2013), 28–31 August 2013, Busan, Korea, (Poster Presentation).

11)H. Ninsonti, W. Chomkitichai, A. Baba, N. Wetchakun, W. Kangwansupamonkon, S. Phanichphant, K. shinbo, K. Kato and F. Kaneko. Modified sol-gel/impregnation synthesis of titanium dioxide nanoparticles and Ag-loaded titanium dioxide nanoparticles for dye-sensitized solar cells application, International Conference on Environment and Renewable Energy (ICERE 2015), 7–8 May 2014, Cité Internationale Universitaire de Paris, Paris, France (Poster Presentation).

12)H. Ninsonti, W. Chomkitichai, A. Baba, W. Kangwansupamonkon, S. Phanichphant, K. shinbo, K. Kato and F. Kaneko. Au-loaded TiO<sub>2</sub> nanopowders synthesized by the modified sol-gel method and their use in dye-sensitized solar cells, RGJ-Ph.D. Congress XV, 28–30 May 2014, Pattaya, Thailand (Poster Presentation).